NEU INSIGHTS AND DEVELOPMENT OF POTENTIAL THERAPEUTICS FOR PULMONARY FIBROSIS

A Dissertation

by

TEJAS RAJEEV KARHADKAR

Submitted to the Office of Graduate and Professional Studies of
Texas A&M University
in partial fulfillment of the requirements for the degree of

DOCTOR OF PHILOSOPHY

Chair of Committee,	Richard H. Gomer
Committee Members,	Michael Criscitiello
	Steve Lockless
	Jennifer Dulin
	Sally Ward
Intercollegiate Faculty Chair,	David Threadgill

December 2020

Major Subject: Genetics

ABSTRACT

Fibrosing diseases involve the formation of inappropriate scar tissue, but what drives fibrosis is unclear. Idiopathic pulmonary fibrosis involves the formation of excess scar tissue in the lungs. Sialidases (also called neuraminidases) are enzymes that desialylate glycoconjugates by cleaving terminal sialic acids from the glycoconjugates. Our lab previously found that a sialylated serum glycoprotein called serum amyloid P (SAP) inhibits fibrosis, and that sialidases attenuate SAP function. Mammals have four different sialidases, NEU1 – 4. In this dissertation, I show that extensive desialylation of glycoconjugates and upregulation of the sialidase NEU3 is observed in the fibrotic lesions in human and mouse lungs. NEU3 is upregulated in the bronchoalveolar lavage (BAL) fluid of the fibrotic mouse lungs in bleomycin-induced pulmonary fibrosis mouse model studies. Fibrosis-associated signals such as transforming growth factor-β1 (TGF-β1) and interleukin (IL)-6 upregulate NEU3 in a variety of human lung cells. Conversely, recombinant human NEU3 upregulates extracellular accumulation of active TGF-β1 and upregulates IL-6 in human peripheral blood mononuclear cells (PBMC). NEU3 also desialylates the human latency associated glyco-peptide (LAP) protein, which holds TGF-β1 in an inactive state, releasing active TGF-β1. Compared to wild-type mice, mice lacking NEU3 have significantly less bleomycin-induced pulmonary fibrosis, reduced TGF-β1 staining in the lungs after bleomycin-assault, and reduced protein, cells, and IL-6 levels in the lung fluid, providing genetic evidence for the role of NEU3 in pulmonary fibrosis in mice. Two small molecule sialidase inhibitors, DANA

and oseltamivir (Tamiflu), work well on viral and mouse sialidases, but relatively poorly on human sialidases. In the bleomycin-induced pulmonary fibrosis mouse model, daily intraperitoneal injections of either DANA or oseltamivir at 10 mg / kg, starting at day 10 after bleomycin insult, strongly attenuated pulmonary fibrosis at day 21. The currently studied NEU3 inhibitors have relatively poor efficacies; thus, we designed a new class of small molecule NEU3 inhibitors. Some of our designed inhibitors have nanomolar IC50 values for the inhibition of recombinant human NEU3 releasing active TGF-β1 from the recombinant human latent TGF-β1, and inhibition of the NUE3-induced accumulation of IL-6 in human PBMC. One of our small molecule inhibitors given as daily 0.1 mg/kg injections, and two inhibitors as daily 1 mg/ kg injections, starting at day 10 after bleomycin insult, strongly attenuated pulmonary fibrosis at day 21 in the bleomycin-induced fibrosis mouse model. All of these results suggest that a NEU3-to-fibrosis-to-NEU3 positive feedback loop helps to potentiate pulmonary fibrosis. NEU3 could be a suitable target to develop treatments for lung fibrosis and our NEU3 inhibitors might be effective as therapeutics for fibrosing diseases.

DEDICATION

I would like to dedicate this dissertation to my family, friends, and teachers who have always been supportive and encouraged me.

ACKNOWLEDGEMENTS

I want to take the opportunity to thank all the people who have played a role in my journey towards doctoral studies in IDP-Genetics and Department of Biology.

Above all, I thank my research advisor, Prof. Dr. Richard H. Gomer, for giving me this wonderful opportunity to work on the most exciting and challenging projects in his lab and providing all the resources and intellectual inputs. Richard always gave me the freedom to think independently and showed faith in my systematic approach to problem-solving. Equally important were the opportunities Richard provided me to participate in research paper & grant proposal writing, and to attend prestigious conferences. Putting everything together, I could not have asked for better training as a graduate student!

I express my sincere gratitude to my committee members, Dr. Criscitiello, Dr. Lockless, Dr. Dulin, and Dr. Ward. Their insightful feedback during my annual committee meetings and prelim was very important in providing the necessary direction for my project.

Dr. Darrell Pilling, I can’t thank you enough. Darrell and I worked together as a team throughout my Ph.D. on exciting projects involving mouse model systems. Darrell is among one of the finest immunologists I have met. Darrell’s approach towards

solving scientific problems is very impressive and served as a great source of motivation for me. I will cherish these exciting times throughout my life.

I am very much thankful to Prof. Dr. Dylan McCreedy of Department Biology, Texas A&M University, for being an important substitute for my dissertation defense. I am thankful to all the former and current lab mates for their support, suggestions, and kindness throughout my Ph.D. tenure.

A very big thanks to all my friends and colleagues. Thanks a lot for being enthusiastic and supportive friends and making my stay in College Station enjoyable.

A very special thanks to all the administrative staff and graduate student advisors from IDP – Genetics and Department of Biology, volunteer blood donors, and the staff of Beutel Health center. Their support, guidance and services made this Ph.D. training very easy process.

Finally, I would like to thank my parents for their unconditional love, concern, support and encouragement.

This dissertation would not have been possible without the foundations laid by everyone mentioned above. Thanks to all for making my time at Texas A&M University a great experience for life!

CONTRIBUTORS AND FUNDING SOURCES

This work was supervised by a dissertation committee consisting of Professor Gomer, Professor Lockless, and Prof. Dulin, of the Department of Biology, Professor Criscitiello, of the Department of Veterinary Pathobiology and Prof. Ward of the Department of Molecular and Cellular Medicine, Texas A&M University.

The *Neu3*$^{-/-}$ mouse strain used in Chapter 3 were provided by Dr. Jamey Marth and Dr. Douglas Heithoff from University of California Santa Barbara. The *Neu3*$^{-/-}$ mouse strain was originally generated by Dr. Takeo Miyagi and Dr. Kazunori Yamaguchi from Miyagi Cancer Center Research Institute, Japan.

The post-doctoral fellow Dr. Wensheng Chen from Gomer lab, Department of Biology, Texas A&M University contributed to part of the data for Figure 27 in chapter 3.

All other work conducted for the dissertation was completed by the student independently.

Funding Sources

Graduate study was supported by the National Institutes of Health (HL-118507 and HL-132919).

NOMENCLATURE

AMPCA	4-amino-1-methyl-2-piperidine carboxylic acid
BAL	Bronchoalveolar lavage
BSA	Bovine serum albumin
CRP	C – reactive protein
DAMP	Damage-associated molecular patterns
DANA	2-Deoxy-2,3-dehydro-n-acetyl-neuraminic acid
ECM	Extra cellular matrix
EMT	Epithelial-to-mesenchymal transition
ER	Endoplasmic reticulum
FDA	Food and Drug Administration
IL	Interleukin
IgG	Immunoglobulin
IC	Inhibition constant
ILD	Interstitial lung disease
IPF	Idiopathic pulmonary fibrosis
LAP	Latency associated peptide / Latency associated glycopeptide
LTBP	Latent TGF-β-binding protein
MP	Methyl picolinate
MALII	Maackia Amurensis Lectin II
PBMC	Peripheral blood mononuclear cells

PNA	Peanut Agglutinin
PBS	Phosphate buffered saline
PMN	Peripheral blood neutrophils
SAP	Serum amyloid P
SNA	Sambucus Nigra Lectin
TGF-β1	Transforming growth factor-β1
2AP	2-acetyl pyridine
4MU-NANA	2′-(4-methylumbelliferyl)-α-D-N-acetylneuraminic acid sodium salt hydrate

TABLE OF CONTENTS

Page

LIST OF FIGURES

Page

LIST OF TABLES

Page

1. INTRODUCTION

1.1. Overview

Fibrosis is a disease that involves an increased amount of scar tissue appearing in an internal organ. In a fibrosing disease, an insult or an injury to an internal organ initiates a uncontrolled wound repair mechanism which leads to a progressive increase in the deposition of scar tissue, eventually leading to organ failure and death [1, 2]. There are more than 60 different fibrosing diseases and it is estimated that approximately 45% of deaths in the western world are attributed to diseases where fibrosis was a significant factor [3-5]. One tissue that can develop fibrosis is the lung [5]. The lungs are directly exposed to external harmful environmental factors present in air, which can cause a recurring injury in the lungs, initiating a repeated wound healing response and eventually causing lung-fibrosis [6-9].

Interstitial lung disease (ILD) is a general term for a group of diseases that includes idiopathic pulmonary fibrosis (IPF). By definition, IPF is chronic inflammatory disorder which is characterized by the accumulation of scar tissue in the lungs [10]. With an incidence rate of 2 – 30 cases per 100,000 person-years, this translates to a population prevalence of ~3 million people worldwide [10, 11]. IPF has a survival rate of only 30% within five years after initial diagnosis, and has an incidence of 1 in 400 in patients older than 65 years [12]. Despite the high prevalence of IPF, there are only two FDA-approved therapeutics which slow down but do not reverse the progression of the disease

[13]. The limited knowledge of the underlying mechanism of IPF progression can be one reason for very few therapeutics option against IPF. Thus, there is a great need to understand the mechanisms behind IPF and its progression to create better therapeutic strategies.

In the process of finding therapeutics against pulmonary fibrosis, our lab has found that a serum protein called Serum Amyloid P (SAP) is important in regulating fibrosis-associated cell differentiation and thus, can attenuate fibrosis in mammals [14-16]. Further studies from our lab reported that the sialylated version of the SAP protein has the potential to attenuate fibrosis-associated cell differentiation [17]. When the monosaccharide known as sialic acid is present on SAP, it is called sialylated SAP, and when the sialic acid is removed from SAP, it is referred to as desialylated SAP. The process of removing sialic acid from SAP is performed by a group of enzymes called neuraminidases or sialidases.

Sialidases are widely distributed in nature from viruses, bacteria, protozoa, and mammals [18, 19]. Viruses such as influenza require sialidase to release the virus from the sialic acids on the outside of a host cell [20]. The bacterial respiratory pathogen *Pseudomonas aeruginosa* uses a sialidase to colonize the lungs [21]. The sialidase NanA from *Streptococcus pneumoniae* causes downregulation of tight junction protein expression in endothelial cells and allows bacterial invasion through the blood-brain barrier, which can then affect the central nervous system [22]. Mammals have four

sialidases, named NEU1, NEU2, NEU3, and NEU4. NEU1 is in the lysosome [23-25], NEU2 is a soluble, cytosolic enzyme, and NEU4 has 2 isoforms, one throughout the mitochondria, and the other on intracellular membranes [26-28]. NEU3 is in endosomes and on the extracellular side of the plasma membrane, and under some conditions, can be released from the membrane to the extracellular environment [29]. Sialidases are known to be associated with inflammation in mammals [30-36]. A recent study reported that sialidase NEU1 is upregulated in IPF [37]. In a study of human patients with IPF, 8 of 9 IPF patients had a high sialidase activity in the lung bronchoalveolar lavage (BAL) fluid, while the healthy controls showed no detectable sialidase activity [38]. These studies point towards a significant involvement of sialidases in progression of pulmonary fibrosis.

Here in this dissertation, I explored the role of sialidases in the progression of IPF using *in-vitro* human cell types study and *in-vivo* mouse model studies. I report my contributions to a possible mechanism that shows targeting sialidases could be an efficient strategy in controlling the progression and reversing pulmonary fibrosis. Further, I report my contributions in developing sialidase inhibitors as potential therapeutics for treating IPF. Before describing the experimental details and the data acquired, I will briefly introduce some terms that I have used throughout in my projects like sialidases, histopathology of IPF, and fibrosis-associated cytokine.

1.2. *Neu*raminidases, also called sialidases

In eukaryotic cells, some proteins undergo post-translational modification. One type of post-translational modification is adding a chain of sugar molecules onto specific amino acids in the protein sequence and this process is called glycosylation [39, 40]. The chain of sugar molecules formed on the protein is called a glycan structure and the modified protein is called a glycoconjugate [39, 41]. One of the steps in glycosylation is sialylation, in which the distal tips of glycan structures on a glycoconjugates are capped by the addition of a sugar called sialic acid [42-44]. In many cases, the addition of sialic acid on the distal tips of glycan structures makes a glycoconjugate fully functional and can alter a wide variety of physiological and pathological processes [41, 44-46]. Loss or removal of sialic acid from the tip of the glycan structure of a glycoconjugate can cause the glycoconjugate to completely lose its functional ability [44, 45, 47].

The removal of sialic acid from a glycoconjugate is an enzymatic process carried out by a group of enzymes called neuraminidases (also called sialidases). As mentioned above, sialidases are widely distributed in nature from viruses, bacteria, protozoa, and all mammals [18, 19]. Mammals have four sialidases, NEU1 – NEU4. In mammals, all these sialidases play an important role in catabolism of glycoconjugates, modulation of the sialylated content on cell membranes, skeletal muscle architecture central nervous system, and modulation of immune function [48-50]. Considering these important functions, a properly regulated distribution of sialidases is considered crucial [51, 52].

As mentioned above, many studies have shown that dysregulation of sialidase levels can cause severe pathological conditions like lymphomas, leukemias, and inflammation. NEU1 plays a key role in potentiating airway inflammation in asthma [53], and upregulated levels of NEU1 act as a novel modulator of inflammation in atherosclerosis [54]. NEU3 is upregulated in, and is important for the survival of, cancerous cells in colon [55], renal [56], ovarian [57], and prostate cancers [58]. Two studies also reported upregulation of some sialidases in IPF in mammals [37, 38].

1.3. Mammalian lungs and pathophysiology of IPF

The major function of mammalian lungs is to perform gas exchange. To carry out gas exchange properly, different cell types are required. Alveolar epithelial cells are crucial in forming small air sacs (called alveoli) that facilitate gas exchange [59]. The connecting space between the walls of these alveoli is called the interstitium of the lungs [60]. The alveoli and the interstitium together are supported by pulmonary fibroblasts. They play an important role in the repair and remodeling process after any injury to the lungs [61]. Another cell type in the lung is resident immune cells called alveolar macrophages, which play an important role in the clearance of any harmful agents encountered in the lungs [62]. Other than these cells, the lungs are also occupied by circulatory immune cells from blood collectively called peripheral blood mononuclear cells (PBMC) which consists of a mixture of different lymphocytes (T cells, B cells, and natural killer cells), dendritic cells, and monocytes [63]. The monocytes are attracted to the active site of a lung injury or insult and can differentiate into other cell types such as

macrophages or spindle-shaped fibroblast-like cells called fibrocytes, which are detected in pulmonary fibrosis [14, 64, 65].

The aforementioned cell types generate a cascade of signals as a part of the repair mechanism during a lung injury or in response to the intrusion of a harmful agent. As the result of an injury or on encountering a harmful agent, the aforementioned cell types get damaged or apoptotic [66, 67]. These damaged or dying cells release signals in the form of cell-to-cell membrane-bound signals, secreted proteins or some danger molecules known as damage-associated molecular patterns (DAMPS) to initiate a repair mechanism [68]. The repair signaling molecules are primarily secreted in the alveoli or in the supporting interstitium [69]. In response to these repair signals, the surrounding healthy or un-injured cell types initiate another signaling cascade or undergo a morphological change in an attempt to potentiate the repair process, which is a timely and regulated series of events in normal conditions [70, 71] . If this repair process is dysregulated, it becomes chronic and an active non-healing injury site [71]. In the case of an internal organ like lungs, the dysregulated chronic non-healing injury affects the architecture of the lungs, primarily by forming inappropriate scar tissue [5, 10]. The scar tissue in lungs is deposited in the interstitium space. The deposited scar tissue impedes gas exchange causing difficulty in breathing and eventually leads to IPF. The histopathological characterization of IPF is identified by features such as:

(i) Epithelial-to-mesenchymal transition (EMT), where the transition causes the alveolar epithelial cells to acquire mesenchymal features of invasion, migration, and production of extracellular matrix (ECM) [72, 73].

(ii) Differentiation of pulmonary fibroblasts to myofibroblasts which form fibroblastic foci and produce ECM components [74]. The formation of these fibroblastic foci leads to worsening lung compliance [11, 75].

(iii) Excessive deposition of extracellular matrix (ECM) components like hyaluronan, periostin, versican, fibulin, fibrillin, fibronectin, proteoglycans, and collagen [76-78], in the interstitium, which makes the lung tissue hard and stiff, eventually decreasing lung functionality [11, 79, 80].

(iv) Accumulation of abnormal levels of fibrosis-associated cytokines, secreted by immune cells locally at the active site of fibrosis or by non-immune lung cell types like mesenchymal cells, myofibroblasts, and epithelial cells [9, 81-83].

These are some of the primarily observed pathological and physiological characteristic features of IPF. A couple of the features, like the abnormal levels of fibrosis-associated cytokines, can have adverse effects on the surrounding healthy tissues also. Among all of the fibrosis-associated cytokines, transforming growth factor-β1 (TGF-β1) is a key driver of fibrosis [84].

1.4. Transforming growth factor – β1 (TGF-β1)

TGF-β1 at physiologically regulated levels are important for many roles like cell proliferation and growth, apoptosis, and maintaining immune homeostasis [85-87]. TGF-β1 is a pleotropic cytokine and its dysregulation plays a key role in the progression of pulmonary fibrosis [88].

TGF-β1 is synthesized as a precursor polypeptide consisting of latency-associated peptide (LAP) and the active TGF-β1 product [89]. The precursor polypeptide is processed in the endoplasmic reticulum (ER) within a cell and dimerizes to form a complex of two active TGF-β1 polypeptides enclosed in two LAPs [86]. For further processing, the nascent TGF-β1 is transferred from the ER to the Golgi, where it undergoes glycosylation/sialylation events on three asparagine residues, which are all present on LAP [86, 89, 90]. This processed complex is secreted from cells alone or in association with latent TGF-β-binding protein (LTBP) [86, 89]. Several mechanisms such as proteolysis, mechanical tension, or changes in pH cause LAP to release active TGF-β1 [89, 91]. In addition to above mechanisms, viral and bacterial sialidases can desialylate LAP causing LAP to change its conformation and thus releases active TGF-β1 [22, 92-96].

The released active TGF-β1 plays an important role in maintaining homeostasis within the lungs [88, 91, 97]. When homeostasis is disturbed and TGF-β1 is upregulated, it induces epithelial-to-mesenchymal transition (EMT) in the alveolar epithelial cells [98,

99], potentiates proliferation and differentiation of fibroblasts to myofibroblasts, and causes deposition of collagen in the surrounding tissue of the lungs [74, 84, 100, 101]. Since these are a few of many hallmarks of pulmonary fibrosis, targeting TGF-β1 can be a potential therapeutic strategy to control pulmonary fibrosis. This strategy has been previously tried, but the strategies that directly block TGF-β1 cause various side-effects, often interfering with the vital homeostatic functions of active TGF-β1 [102]. Thus, a better strategy needs to be devised to target the upregulation of TGF-β1 in a fibrotic lesion, rather than global TGF-β1.

A possible target to attenuate fibrosis is to inhibit the fibrosis-associated TGF-β1 activation step. Similar to viral and bacterial sialidases, we hypothesized that in a fibrotic lesion, mammalian sialidases can desialylate LAP, eventually releasing active TGF-β1 and thus, upregulating the levels of TGF-β1. If successful, inhibitors of sialidases can be used as potential therapeutics to control sialidase-induced TGF-β1 activation and inhibit progression of IPF, without negatively influencing the homeostatic role of active TGF-β1 in tissues where sialidases are not activating TGF-β1.

2. SIALIDASE INHIBITOR ATTENUATE PULMONARY FIBROSIS IN A MOUSE MODEL[*]

2.1. Summary

Fibrosis involves increasing amounts of scar tissue appearing in a tissue, but what drives this is unclear. In fibrotic lesions in human and mouse lungs, we found extensive desialylation of glycoconjugates, and upregulation of sialidases. The fibrosis-associated cytokine TGF-β1 upregulates sialidases in human airway epithelium cells, lung fibroblasts, and immune system cells. Conversely, addition of sialidases to human peripheral blood mononuclear cells induces accumulation of extracellular TGF-β1, forming what appears to be a sialidase - TGF-β1 - sialidase positive feedback loop. Monocyte-derived cells called fibrocytes also activate fibroblasts, and we found that sialidases potentiate fibrocyte differentiation. A sialylated glycoprotein called serum amyloid P (SAP) inhibits fibrocyte differentiation, and sialidases attenuate SAP function. Injections of the sialidase inhibitors DANA and oseltamivir (Tamiflu) starting either 1 day or 10 days after bleomycin strongly attenuate pulmonary fibrosis in the mouse bleomycin model, and by breaking the feedback loop, cause a downregulation of sialidase and TGF-β1 accumulation. Together, these results suggest that a positive

[*] Reprinted with permission from "Sialidase inhibitors attenuate pulmonary fibrosis in a mouse model" Karhadkar, T. R., Pilling, D., Cox, N., & Gomer, R. H., 2017. *Scientific Reports*, 7(1): p. 15069. Creative Commons Attribution 4.0 International License

feedback loop involving sialidases potentiates fibrosis, and suggest that sialidase inhibitors could be useful for the treatment of fibrosis.

2.2. Introduction

Fibrosing diseases such as severe asthma, ischemic heart disease, cirrhosis of the liver, end stage kidney disease, and idiopathic pulmonary fibrosis (IPF) involve the inappropriate formation of scar tissue in an internal organ, and are associated with an estimated 45% of all deaths in the US [1, 2, 103, 104]. In these diseases, insults to the tissue, such as particulate matter or toxins in the lungs, initiate an inappropriate and unnecessary wound healing response, leading to organ failure and death [1, 2, 9, 105]. What drives the fibrosis is poorly understood.

Many secreted and cell-surface mammalian proteins are glycosylated, and many of the glycosylation structures have sialic acids as the monosaccharide at the distal tip or tips of the polysaccharide on the protein [42-44]. Some viruses, bacteria, protozoa, and all mammals have sialidases (also known as neuraminidases) that remove the sialic acids from glycoconjugates [18, 19]. Viruses such as influenza require sialidase to release the virus from the sialic acids on the outside of a host cell, and the sialidase inhibitors oseltamivir (Tamiflu) and zanamivir (Relenza) are front-line therapeutics for influenza [20]. The bacterial respiratory pathogen *Pseudomonas aeruginosa* uses a sialidase to colonize the lungs [21]. Mammals have four sialidases, NEU1 – NEU4. NEU1, 2, and 4 prefer α-(2,3) linked sialic acids as a substrate, while NEU3 prefers α-(2,6) [18, 28, 32].

NEU1 is in the lysosome [23-25], NEU2 is a soluble, cytosolic enzyme, and NEU4 has 2 isoforms, one on mitochondria, and the other on intracellular membranes [26-28]. NEU3 is in endosomes and the extracellular side of the plasma membrane, and under some conditions can be released from the membrane to the extracellular environment [29].

The serum glycoprotein Serum Amyloid P (which has an α-(2,6)-linked terminal sialic acid) appears to have a calming effect on the innate immune system, and inhibits fibrosis in animal models and in early-stage clinical trials [14, 15, 106-111]. C-reactive protein (CRP) is closely related to SAP, but is not glycosylated [112]. Unlike SAP, CRP generally potentiates inflammation and fibrosis [113]. We mutated SAP protein surface amino acids that were different from CRP, and could not find a domain on the SAP protein surface that when mutated strongly altered SAP function [114, 115]. However, when SAP was desialylated with sialidase, the effects of SAP were largely abrogated [47]. When CRP was mutated to have a glycosylation similar to that of SAP (including a terminal sialic acid), the resulting CRP A32N was essentially indistinguishable from SAP in *in vitro* assays on neutrophils, monocytes, and macrophages [47]. Together, these results indicated that a terminal sialic acid on SAP plays a key role in its ability to regulate the innate immune system.

Intravenous immunoglobulin therapy is a treatment for some autoimmune diseases, where the intravenous immunoglobulin seems to act as an immunosuppressant [116]. Immunoglobulins are glycosylated, and there is a heterogeneity in the extent to

which the glycosylation have terminal sialic acids [117]. Fractionation of immunoglobulins, as well as treatment of immunoglobulins with sialidase, showed that only immunoglobulins with terminal sialic acids act as immunosuppressants [118, 119]. These results support the hypothesis that a lack of glycoconjugates with sialic acids permits inflammation. A variety of studies indicate that sialidases potentiate inflammation [30, 31, 33-36, 120, 121]. Conversely, other studies indicate that inflammation potentiates sialidase activity, with most of the reports showing that NEU1 is associated with inflammation [34, 53, 122-126].

In a study on patients with idiopathic pulmonary fibrosis (IPF), the bronchoalveolar lavage (BAL) fluid from 8 of 9 patients had a high sialidase activity, while the BAL fluid from 9 healthy controls showed no detectable sialidase activity [38]. In the 3 IPF patients where BAL was collected in subsequent years, the BAL fluid sialidase activity increased as the disease progressed. A recent report also found increased levels of NEU1 in lung fibroblasts of some but not all pulmonary fibrosis patients, and that adenoviral administration of NEU1 promoted bleomycin-induced lung inflammation and fibrosis [37]. In this report, we show that inhibiting sialidases can inhibit fibrosis in a mouse model.

2.3. Materials and methods

2.3.1. Cell isolation and culture

Human peripheral blood was collected from healthy volunteers who gave written consent and with specific approval from the Texas A&M University human subjects review board. Blood collection, isolation of PBMC, sources of culture media, supplements, and SAP, and PBMC culture and fibrocyte counts were done as described previously [127, 128]. using 96 well plates (#89626 ibidi, Madison WI). Adenocarcinomic human alveolar basal epithelial cells (A549) (PromoCell, Heidelberg, Germany) were cultured in RPMI-1640 supplemented with 10% bovine calf serum (BCS) (Seradigm, Randor, PA), 100U/ml penicillin, 100 µg/ml streptomycin, (Lonza, Walkersville, MD) and 2 mM glutamine (Invitrogen, Carlsbad, CA). Human small airway epithelial cells (Promocell) were cultured in small airway epithelial cell medium (PromoCell) following the manufacturer's protocol. Human pulmonary fibroblasts (PromoCell) were cultured in DMEM supplemented with 10% BCS, 100U/ml penicillin, 100 µg/ml streptomycin, and 2 mM glutamine. Where indicated, recombinant 10 ng/ml human TGF-β1 (Peprotech, Rocky Hill, NJ), 200 ng/ ml recombinant human NEU1, 2, 3, or 4 (Origene, Rockville, MD), or 2 µg/ ml human SAP (EMD Millipore, Billerica, MA; with the azide removed by centrifugal filters following [129]) were added to cells. Fibrocytes were counted as previously described [14, 127].

2.3.2. Mouse model of pulmonary fibrosis

All procedures were done with specific approval of the Texas A&M University institutional animal care and use committee. Mice were treated with an oropharyngeal aspiration of 3 U/kg bleomycin (Calbiochem, Billerica, MA) in 0.9% saline or saline alone as previously described [47, 111, 130, 131]. Starting either 10 days or 24 hours after bleomycin, when the bleomycin has been cleared from mice [132], mice were given daily intraperitoneal injections of 10 mg/kg DANA (N-Acetyl-2,3-dehydro-2-deoxyneuraminic acid; EMD, Millipore) or oseltamivir (Tamiflu; Sigma, St. Louis, MO), both formulated as 4 mg/ ml in PBS. Mice were euthanized 21 days after bleomycin aspiration, and bronchoalveolar lavage (BAL) cells collected, counted, and cytospins were prepared as described previously [47, 111, 130, 131]. After BAL, lungs were inflated with and embedded in OCT compound (VWR), frozen, and stored at -80 ˚C. 6 μm sections on glass slides were air dried for 48 hours before use. BAL cytospins were prepared and immunochemistry were performed as described previously [47, 111, 130] using anti- CD11b (clone M1/70 BioLegend, San Diego, CA) to detect blood and inflammatory macrophages or anti-CD11c (clone N418, BioLegend) to detect alveolar macrophages and dendritic cells with isotype-matched irrelevant antibodies (BioLegend) as controls. BAL fluid protein levels were measured as described previously [111].

2.3.3. Histology

HOPE-fixed chronic obstructive pulmonary disease (COPD) and idiopathic pulmonary fibrosis (IPF) patient lung sections were obtained from the Lung Tissue

Research Consortium (NIH, Bethesda, MD). Slides were prepared for staining as described previously [128] and incubated with 1 μg/ml biotinylated lectins SNA, PNA, and MAL II (Vector, Burlingame, CA) and then stained following the manufacturer's instructions. Sections were also stained with 1 μg/ml of sheep polyclonal anti-ST3GAL2 (AF7275-SP, R&D Systems, Minneapolis, MN), anti- ST6GAL2 (AF7747-SP, R&D Systems) or anti- ST8SIA1 (AF6716-SP, R&D Systems), 1μg/ml irrelevant sheep (#013-000-002, Jackson, West Grove, PA) or rabbit polyclonal antibody (#AB-105-C, R&D Systems, Minneapolis, MN), rabbit polyclonal anti-NEU1 (TA335236, Origene, Rockville, MD), anti-NEU2, (TA324482, Origene,) or anti-NEU4 (AP52856PU-N, Acris/Origene), in PBS/ 2% BSA (PBSB), or 0.5 μg/ml anti-NEU3 (TA590228, Origene) in PBSB/ 500 mM NaCl/ 0.1% NP-40 alternative (EMD Millipore, Billerica, MA) for 60 minutes. Washing 3 times with PBS for 10 minutes each and staining were then done as previously described [127, 128], except where required biotinylated donkey-anti-sheep (#713-066-147, Jackson) secondary antibody was used for staining. Where indicated, 1 mM DANA or 1 mM Tamiflu were added to the antibody incubation step and the subsequent wash steps. For PBMC, the medium was removed and the plate was air dried for 24 hours, treated with acetone for 20 minutes, dried for 10 minutes, hydrated with distilled water for 5 minutes, and then PBS for 5 minutes. For cells other than PBMC, the medium was removed and cells were fixed for 10 minutes with 2%(w/v) paraformaldehyde (EMS, Hatfield, PA) in PBS, blocked for 10 minutes in PBSB, and permeabilized for 8 minutes with PBS/ 0.1% (w/v) Triton X-100 (Alfa Aesar, Ward Hill, MA). Where indicated, PBMC, after five days incubation were

air dried, then incubated with 1 µg/ ml anti-active TGF-β1 antibodies (AB-100-NA, R&D Systems) in PBSB for 60 minutes. Staining of cells was then done as described above. After counter-staining, the plates were air-dried.

2.3.4. Lung tissue lysate preparation

Approximately half lobes of lungs frozen in OCT were cut off, thawed, washed once in PBS, weighed, and then frozen in liquid nitrogen. 300 µl of Pierce RIPA buffer (Thermo Scientific, Rockford, IL) with 1x proteases and phosphatases inhibitor cocktail (Cell Signaling Technology, Danvers, MA) was added per 5 mg of tissue and the tissue was crushed with a pestle. The mixture was then incubated on a rotator for 2 hours at 4°C. After centrifugation at 18000 x g for 10 minutes, the supernatant was collected as lung tissue lysate. Total protein was measured by OD 280/ 260 with a SynergyMX plate reader, (BioTek, Winooski, VT) using RIPA buffer with proteases/ phosphatases inhibitor as a blank.

2.3.5. Western blots

For Western blots, 20 µl of BAL fluid or lysate was mixed with 4 µl 5 x Laemmli sample buffer and heated to 95°C for 5 minutes. Western blots were done following [14] with the exceptions that 4 – 20% Tris/glycine gels were from Lonza (EMD, Gibbstown, NJ). For analysis of lectin staining, western blots were pre-incubated with Carbo-Free Blocking Solution (Vector), and then incubated with biotinylated lectins diluted in the same carbo-free solution at 2 µg/ml for 30 minutes at room temperature. Labelling was

detected with streptavidin-HRP (BioLegend), as described previously [111]. For other staining, blocking was in PBS/ 2% BSA/ 5% nonfat milk. Anti-NEU 1, 2, and 4 were incubated at 1:1000 in PBSB. For anti-NEU3, incubations were at 1:5000 in PBS/ 2% BSA/ 0.1% NP-40 alternative/ 0.01% SDS. All washes were in PBS/ 0.1% (v/v) Tween 20 (Fisher, Fair Lawn, NJ). SuperSignal West Pico Chemiluminescence Substrate (Thermo Scientific) was used following the manufacturer's protocol to visualize the peroxidase using a ChemiDoc XRS+ System (Bio-Rad, Hercules, CA).

2.3.6. Sialic acid quantitation

Approximately 1.2 x 1.2 x 1.2 mm pieces from lungs frozen in OCT were thawed and washed 3 times in PBS and the lung piece was weighed. Sample hydrolysis and sialic acid measurement was done following [133] using resorcinol (Alfa Aesar), with assays done in 900 µl final volumes. Sialic acid (Vector) was used for standards. Absorbances were measured with a SynergyMX plate reader. Values were then converted to mg sialic acid / g tissue.

2.3.7. TGF-β1 ELISA

PBMC were cultured in 96 well plates at 5 x 10^5 cells/ml and 200 µl/ well in Fibrolife serum-free medium as described above. When the cells were plated, recombinant human sialidases were added to final concentrations of 200 ng/ml, and DANA or Tamiflu were added to 3 µM. After 5 days, culture supernatants were analyzed

using a TGF-β1 ELISA kit, which detects total TGF-β1 (R&D Systems, Minneapolis, MN).

2.3.8. Sialidase ELISAs

Lung tissue lysates were diluted to 100 µg total protein/ ml in PBS. 55 µl of diluted lysate was added to a well of a 96-well Maxisorp immuno plate (#442404, Thermo Scientitic) and incubated at 4°C overnight. Serial dilutions of recombinant NEU 1, 2, 3 and 4 (Origene) in PBS were also incubated and used for standard curves. The solutions were removed and the wells were blocked with 200 µl PBSB for 2 hours at room temperature with shaking. Anti- NEU1, 2, 3 and 4 antibodies (Origene) were then added in PBSB for 1 hour at room temperature following the manufacturer's directions. After washing with PBSB, 1:1000 HRP-conjugated donkey-anti-rabbit IgG (Jackson) in PBSB was added for 1 hour. After washing, bound antibodies were detected using a TMB color development kit (Biolegend) and the reaction was stopped with 1 N HCl. Absorbances at 450nm and 550nm were measured using a SynergyMX plate reader.

2.3.9. Sialidase activity assays

Sialidase assays were done following [134, 135] with the following modifications. PBS was adjusted to pH 6.4 or 7.0 with 12N HCl, and BSA was added to a final concentration of 100 µg/ml. Recombinant human NEU 1, 2, 3, or 4 were added to the PBS/ BSA to 300 ng/ml. 2′-(4-methylumbelliferyl)-α-D-N-acetylneuraminic acid sodium salt hydrate (4MU-NANA) (Sigma) was dissolved in water to 50 mg/ ml. After

30 minutes at room temperature, 4MU-NANA was added to the enzymes to 200 µM final concentration. 100 µl of the reaction was placed in the well of a 96-well plate and fluorescence was measured every 20 minutes at 37°C for 15 hours in a prewarmed SynergyMX plate reader with excitation at 360 nm and emission at 460 nm. The fluorescence in the absence of sialidases was subtracted from all readings. The fluorescence of known concentrations of 4-methylumbelliferone (Alfa Aesar) was used to convert fluorescence to moles of product.

2.3.10. Flow cytometry

Human pulmonary fibroblasts were cultured in the presence or absence of 10 ng/ml TGF-β1. After 3 days, the cells were detached using Accutase cell detachment solution (VWR) and were fixed for 10 minutes with 2% (w/v) paraformaldehyde (EMS) in PBS, followed by permeabilization for 10 minutes with 0.1% (w/v) Triton X-100 (Alfa Aesar) in PBS. Cells were then blocked for 10 minutes in PBSB. Cells were incubated for 60 minutes with 0.5 µg/ml anti-NEU3 or irrelevant rabbit antibody, as described above, the cells were washed twice with ice cold PBS. The cells were then incubated with 1:1000 goat anti-rabbit Alexa Fluor 647 (#A21245, Life Technologies, Carlsbad, CA) in PBS/ BSA and washed twice with PBS. The cells were then analyzed on an Accuri C6 flow cytometer (BD Bioscience) as previously described [17]. The cells were kept on ice throughout the procedure.

2.3.11. Human PMN isolation and culture, and leukemia cell culture

Peripheral blood neutrophils (PMN) were isolated using Polymorphprep gradients (Axis-Shield, Oslo, Norway), as previously described [136]. K562, U937, THP-1, NALM-6, and CHO-K1 cells (all from ATCC, Manassas, VA) and Mono Mac 6 (DSMZ, Braunschweig, Germany) were cultured in RPMI 1640 with 10% bovine calf serum (BCS) (VWR-Seradigm, Radnor, PA) containing 2 mM glutamine, 100 U/ml penicillin, and 100 μg/ml streptomycin (all from Lonza, Walkersville, MD). A549 cells, pulmonary fibroblasts, and PBMC were isolated and cultured as described in the main methods section. K562 is a chronic myeloid leukemia cell line [137], U937 is a lymphoma cell line [138], and THP-1 [139] and Mono Mac 6 [140] are acute myeloid leukemia cell lines. NALM-6 is a leukemic pre-B cell line [141]. The CHO-K1 is an epithelial cell line derived from the ovary of the Chinese hamster [142]. 2 x 10^6 cells were lysed in RIPA buffer (#89900, Pierce, Rockford, IL) with 1X protease and phosphatase inhibitors (#5872S, Cell Signaling, Danvers, MA), on ice for 2 hours. The lysate was clarified by centrifugation at 18,000 x *g* for 10 minutes at 4˚C. The supernatant was collected and total protein concentration was estimated for each cell lysate. 10 μg of protein was loaded in each well. Western blotting with sialidase antibodies was as described in the main methods section. Coomassie staining was done as described previously [14].

2.3.12. Specificity of sialidase antibodies

800 ng of recombinant human NEU2 was added to 40 ng of anti-NEU2, or 800 ng of recombinant human NEU3 was added to 40 ng of anti-NEU3, in a total volume of 40 µl of PBSB. Protein: antibody mixtures were incubated at room temperature for 30 minutes, and then aggregates were removed by centrifugation at 18,000 x g for 5 minutes at 4 ^{o}C. Human lung sections were stained as described in the main methods section with anti-NEU2 or anti-NEU3 antibodies with or without pre-incubation with recombinant protein.

2.3.13. Image quantification

Images were converted to RGB stacks using Image J. The green channel (which shows the red staining) was used to adjust the intensity threshold level. The threshold level was kept the same for analyzing one set of images **[143, 144]**. The area stained as a percentage of the total area of the image was then determined using Image J.

2.3.14. Statistical analysis

Data were analyzed by ANOVA, with appropriate post-tests, or t-test when appropriate, using Prism software (Graphpad, La Jolla, CA).

2.4. Results

2.4.1. There is increased desialylation in fibrotic lungs

To determine if desialylation of proteins can be observed in pulmonary fibrosis, we stained tissue sections with *Sambucus nigra* lectin (SNA) or *Maackia amurensis* lectin II (Mal II), which detect sialic acids on glycoconjugates, or peanut agglutinin (PNA), which detects a variety of carbohydrates if they are not sialylated [36]. Compared to chronic obstructive pulmonary disease (COPD) patient lungs with relatively normal lung function (see Table 1 for patient details), or compared to control mouse lungs (intratracheal saline instead of intratracheal bleomycin), fibrotic human lungs and fibrotic mouse lungs showed less staining for sialylated glycoconjugates, and increased staining for desialylated glycoconjugates (Figure 1 a-d). In the bronchoalveolar lavage (BAL) fluid at day 21 from bleomycin-treated mice, we observed increased amounts of a desialylated protein and a decreased amount of a sialylated protein (Figure 1e).

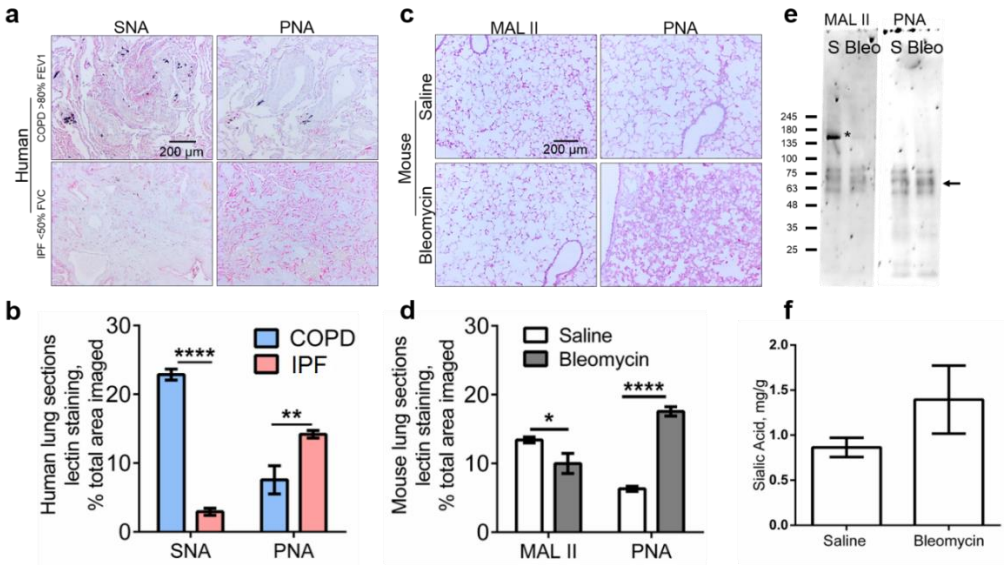

Figure 1. There is decreased sialylation in pulmonary fibrosis.
(a) Human lung sections were stained with SNA to detect sialic acids, or PNA to detect desialylated polysaccharides. IPF <50% FVC indicates a pulmonary fibrosis patient with poor lung function; COPD > 80% FEV1 indicates a chronic obstructive pulmonary disease patient with relatively normal lung function. Positive staining is red, with nuclei counterstained blue. Bar is 0.2 mm. **(b)** Quantification of lectin staining for human lung sections with ImageJ. **(c)** Mouse lungs at day 21 after saline or bleomycin treatment were stained with MAL II to detect sialic acid on glycoconjugates or with PNA to detect desialylated polysaccharides. Bar is 0.2 mm. **(d)** Quantification of lectin staining for mouse lung sections with ImageJ. For (b) and (d), values are mean ± SEM, n=3 or 4; ** indicates $p < 0.005$, ****$p < 0.0001$ (t-test). **(e)** BAL fluid from mice at day 21 after saline (S) or bleomycin were analyzed by western blotting, staining with MAL II or PNA. * indicates bleomycin causing decreased sialylation on a protein and arrow indicates bleomycin causing the gain of a desialylated protein. Molecular masses in kDa are at left. Images in a, c, and e are representative of 4 patients or 3 mice per group. **(f)** Total sialic acid from the day 21 lung tissue of saline- or bleomycin-treated mice. Values are mean ± SEM, n=3.

Table 1. Clinical details of human lung sections used in this study.
FVC indicates forced vital capacity; COPD indicates chronic obstructive pulmonary disease; ILD indicates interstitial lung disease; Fibrosis indicates uncharacterized ILD; UIP indicates usual interstitial pneumonia; IPF indicates idiopathic pulmonary fibrosis; NSIP indicates non-specific interstitial pneumonia. Because of a limited number of lung tissue sections obtained from the LTRC, each type of staining was performed on a randomly selected set of 4 of the 5 patients from each group.

Group	FVC (mean ± SEM)	Gender	Age in years (mean ± SEM)	Clinical Details
ILD <50%	35.00 ± 3.396	3 males; 3 females	46.00 ± 5.994	n = 3 IPF /UIP, n = 2 fibrosis, n = 1 NSIP
COPD >80%	83.80 ± 0.6633	3 males; 2 females	64.80 ± 5.417	n = 3 COPD, n = 2 emphysema
t-test	$p < 0.0001$	ns	$p = 0.0483$	

Sialyltransferases catalyze the sialylation of glycoconjugates. There are 20 identified mammalian sialyltransferases [145, 146]. Three representative sialyltransferases are ST3GAL2 and ST6GAL2, which sialylate oligosaccharides, and ST8SIA1, which sialylates gangliosides [145, 147]. In bleomycin-induced fibrotic lesions in mouse lungs, we observed increased levels of ST3GAL2 and ST6GAL2, and no change in levels of ST8SIA1 (Figure 2), suggesting that the reduced sialylation observed in Figure 1a-e is not due to reduced levels of these 3 sialyltransferases. Fibrotic mouse lungs showed normal levels of total (free + conjugated) sialic acid (Figure 1f), indicating that the reduced amount of sialic acid in glycoconjugates is not due to a reduced production of sialic acid.

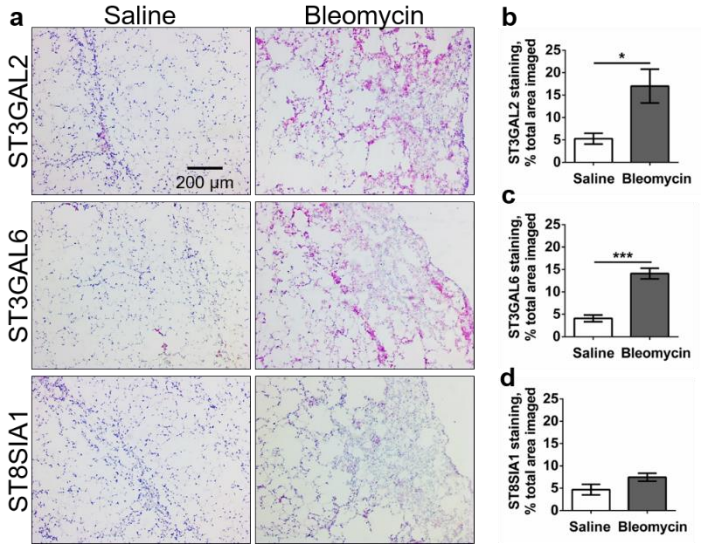

Figure 2. Sialyltrasferase expression in fibrotic mouse lungs.
(a) Sections of lungs from saline- or bleomycin- treated mice were stained with antibodies against sialyltransferase3 (ST3GAL2), sialyltransferase6 (ST3GAL6) and sialyltransferase8 (ST8SIA1). All images are representative of 3 mice per group. Bar is 0.2 mm. Quantification of staining for ST3GAL2 **(b)**, ST3GAL6 (c), and ST8SIA1 **(d)** with ImageJ. Values in b – d are mean ± SEM, n = 3 mice per group; * indicates $p < 0.05$, ***$p < 0.001$ (t-test).

2.4.2. Sialidases are upregulated in fibrotic lungs

In addition to the observation that there is sialidase activity in the BAL fluid from patients with IPF [38], the above results suggest the possibility that there may be increased sialidase protein in fibrotic lungs. To examine this, we stained lung sections from IPF patients and COPD patients with antibodies against the four human sialidases. The antibodies were made against domains of the sialidases that are different from each other, do not bind the other sialidases (Figure 3), and stain bands on western blots of whole cell lysates corresponding to bands observed by others (Figure 3) [33, 37, 148, 149].

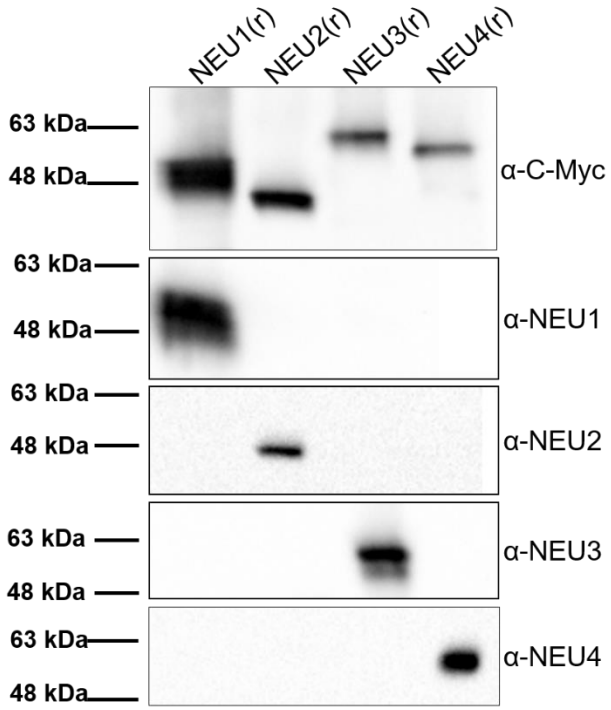

Figure 3. The specificity of anti-sialidase antibodies.
Western blots of recombinant (r) c-Myc tagged human sialidase proteins were stained with the indicated antibodies. Positions of molecular mass markers are at left. All four proteins were stained with anti-c-Myc antibodies (top panel). Each sialidase was detected by its corresponding antibody (bottom 4 panels). The antibody for a particular sialidase did not cross react with sialidases other than its target. All images are representative of three independent experiments.

The COPD lungs showed low levels of the four human sialidases (Figure 4a). Two of three IPF patient lungs showed no significant staining for sialidase 1 (NEU1) while one IPF patient did have increased levels of NEU1 staining. Compared to the COPD patients, the ILD patient lungs had increased levels of NEU2, NEU3, and NEU4 (Figure 4 a and c). To confirm the specificity of the sialidase antibodies,

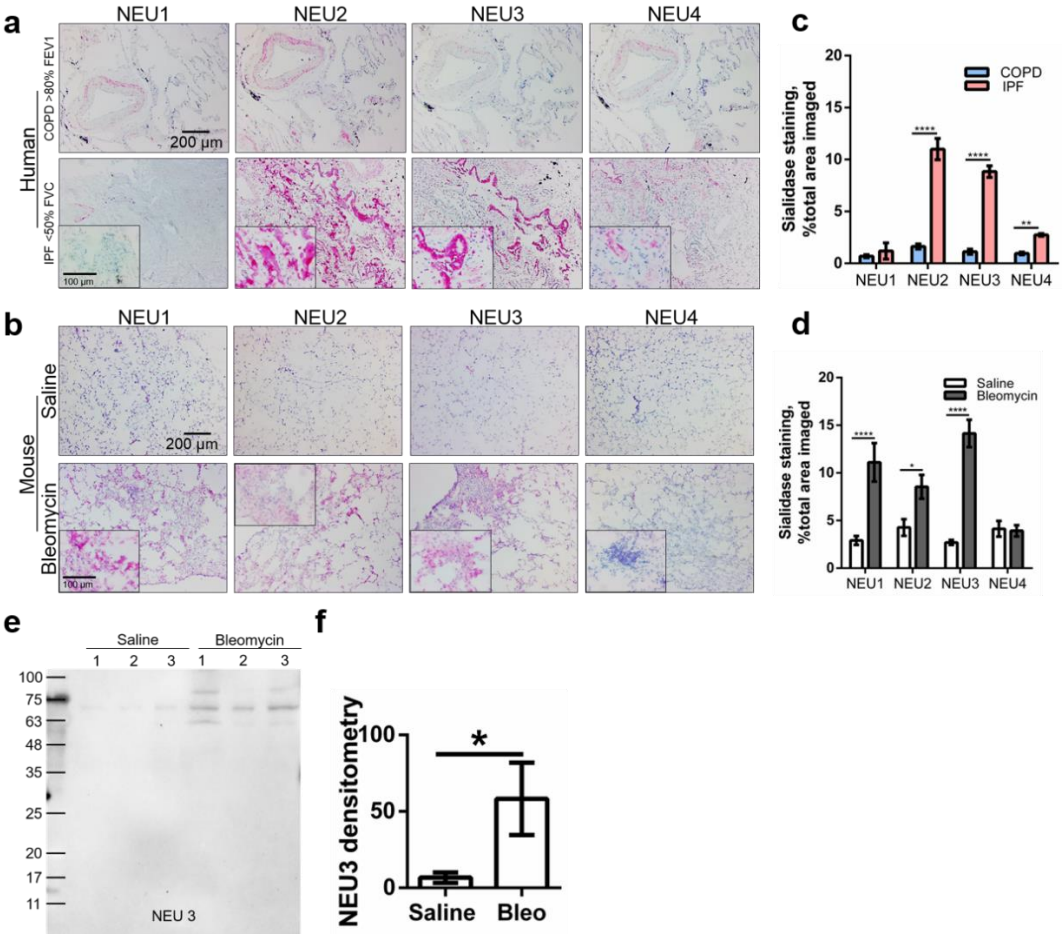

Figure 4. Some sialidases are upregulated in lung fibrosis.
Human **(a)** and mouse **(b)** lung sections as in Figure 1 were stained for the indicated sialidases. Outside image bars are at 0.2 mm. Inset in a and b are higher magnification images of the IPF (a) or bleomycin (b) lungs; bars are 0.1 mm. All images are representative of 4 patients or 3 mice per group. Quantification of sialidase staining for human **(c)** and mouse **(d)** lung sections with ImageJ. Values are mean ± SEM, n=3 or 4; * indicates $p < 0.05$, **** $p < 0.0001$ (t-test). **(e)** BAL fluid from mice at day 21 after saline or bleomycin were stained for sialidase3. 1, 2, and 3 refer to different individual mice. Positive staining appears black. Molecular masses in kDa are at left. **(f)** Quantification of NEU3 in (e) western blot, values expressed in percent relative density of black bands. Values are mean ± SEM, n=3 or 4; * indicates $p < 0.05$ (t-test).

we pre-incubated the NEU2 and NEU3 antibodies with recombinant NEU2 or NEU3

respectively, and found that this pre-treatment abrogated staining of fibrotic human lung

tissue (Figure 5). Mice treated with oropharyngeal bleomycin develop fibrotic lesions in the lungs at day 21 [150]. Mice treated with oropharyngeal saline as a control had low levels of all four mouse sialidases in their lungs (Figure 4b). Compared to the controls, bleomycin-treated mice had fibrotic lesions and increased levels of NEU1, NEU2, and NEU3, but no increase in NEU4 (Figure 4 b and d). Higher magnification images showed patchy distributions of the upregulated sialidases in fibrotic lesions (inset in Figure 4 a and b). In the BAL fluid from mice with bleomycin-induced lung fibrosis, NEU1, 2, and 4 were not detected, even on over-exposed western blots (Figure 6), while NEU3 was upregulated compared to the BAL fluid from control mice (Figure 4 e and f). For unknown reasons, one bleomycin-treated mouse also showed anti-NEU3 staining of a band with an apparent molecular mass higher than NEU3 (Figure 4 e) Together, these data indicate that the levels of some sialidases are increased in lung fibrosis in humans and mice.

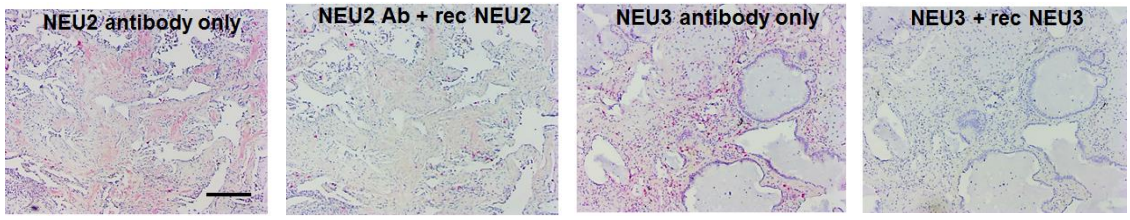

Figure 5. Specificity of sialidase antibodies.
To confirm the specificity of the NEU2 and NEU3antibodies, we pre-incubated the NEU2 and NEU3 antibodies with recombinant NEU2 or NEU3 respectively. Fibrotic human lung sections were then stained as described in Figure 2a. Bar is 0.2 mm. Pre-incubation of sialidase antibodies with recombinant protein abrogated staining, compared to sections incubated with sialidase antibodies alone.

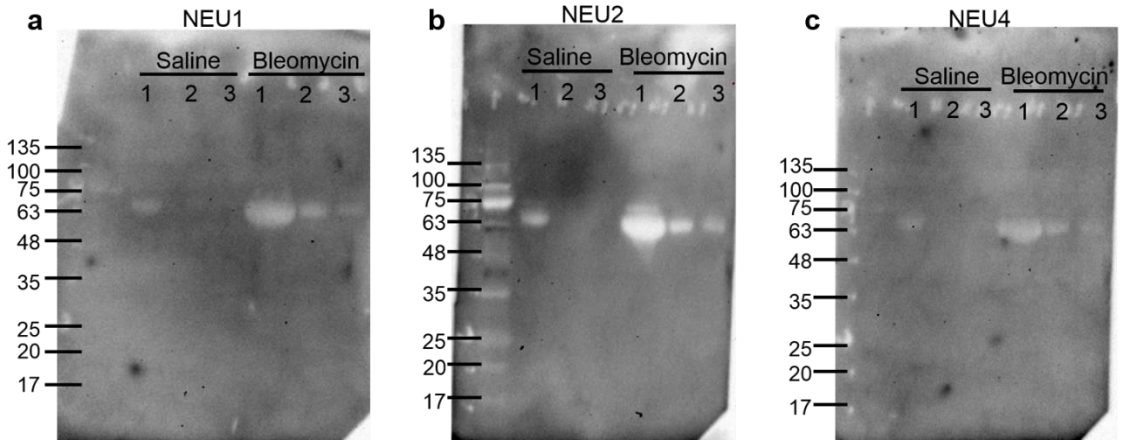

Figure 6. Sialidases 1, 2, and 4 are not detected in mouse BAL fluid.
BAL fluid from mice at day 21 after saline or bleomycin were stained for the indicated sialidases. 1, 2, and 3 refer to different individual mice. Positive staining would appear black. Molecular masses in kDa are at left. To determine if low levels of the sialidases were present, we over exposed the western blots. This reveal "negative" staining of albumin, especially in the BAL from bleomycin treated mice.

To further test the hypothesis that sialidases are upregulated in the fibrotic lungs, we prepared lung tissue lysates from saline and bleomycin treated mice. Total protein concentration and concentrations of the sialidases were measured in the lysates. Compared to saline controls, the bleomycin-treated mice had significantly higher levels of NEU1, NEU2 and NEU3, but not NEU4, in their lung lysates (Figure 7 a-d). In addition, on Western blots, compared to saline, bleomycin-treated mouse lung tissue lysates had significantly upregulated levels of NEU3 (Figure 7 e and f). Together, these results indicate that some sialidases are upregulated in pulmonary fibrosis in mice.

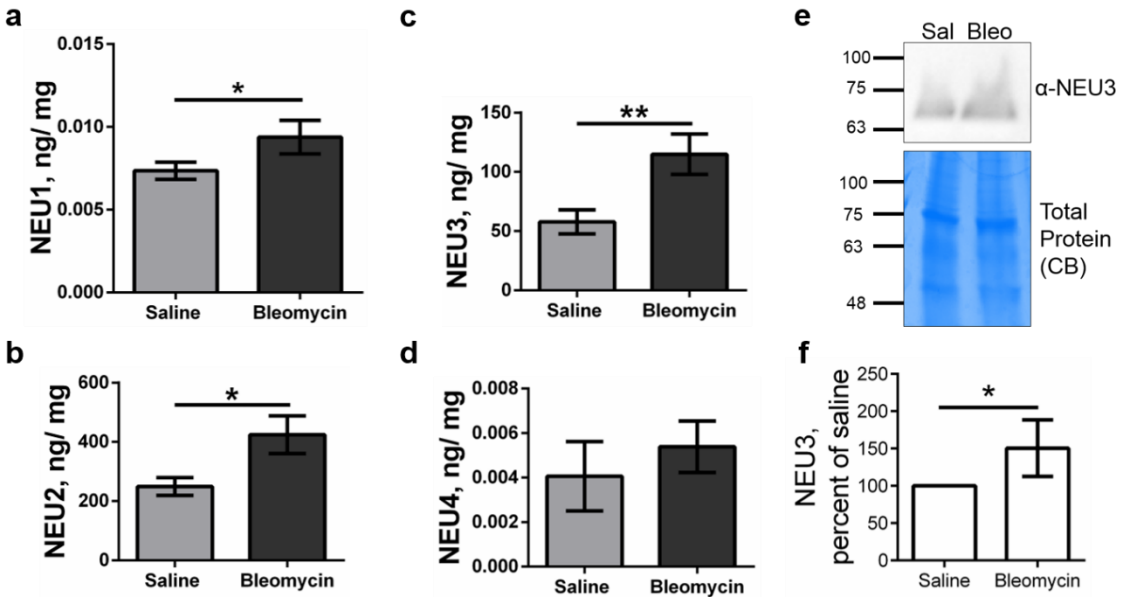

Figure 7. Detection of upregulated sialidases in bleomycin-treated mouse lung tissue lysates.
Lysates from the indicated treatment groups were assayed for total protein and assayed by ELISA for **(a)** NEU1**, (b)** NEU2**, (c)** NEU3**,** and **(d)** NEU4. **(e)** Western blot of lung tissue lysate from a saline (sal) and a bleomycin (bleo) treated mouse stained for NEU3 (upper panel); aliquots of the samples were run on an SDS-PAGE gel and stained with Coomassie brilliant blue (CB) (lower panel). The positions of molecular mass standards in kDa are at left. Images are representative of 3 pairs of mice. **(f)** Quantification of western blots. In (a-f) values are mean ± SEM, n=3; * indicates $p < 0.05$ (t-test).

2.4.3. The pro-fibrotic cytokine TGF-β1 upregulates sialidases in cells

TGF-β1 is strongly associated with fibrosis, and is the most potent, and well-characterized, inducer of fibrosis [101, 103]. As the main cell types involved in lung fibrosis are epithelial cells, fibroblasts, and immune cells, we cultured the human alveolar basal epithelial adenocarcinoma cell line A549, human small airway epithelial cells, human pulmonary fibroblasts, and human immune cells (PBMC) with or without 10 ng/ ml of recombinant active TGF-β1 (a standard concentration used in tissue culture

experiments [100, 105, 151, 152] for five days. After five days, the cells were stained with antibodies against

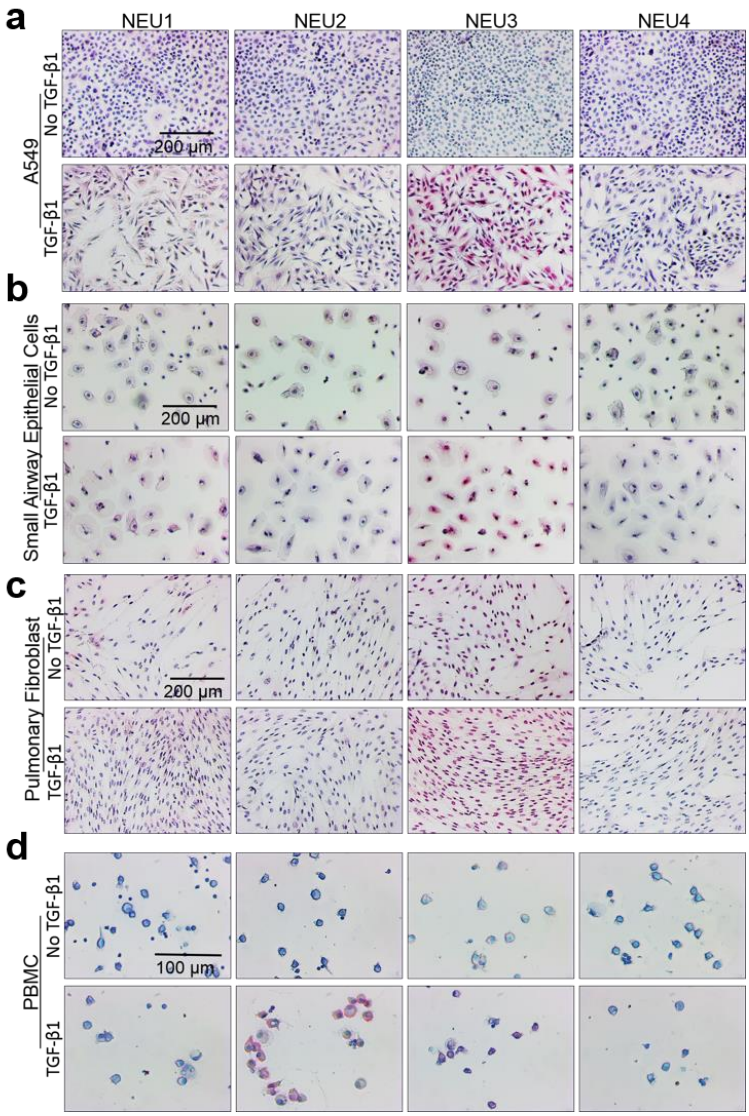

Figure 8. TGF-β1 increases sialidase expression in cultured cells.
(a-d) The indicated human cell types were cultured in the presence or absence of 10 ng/ml TGF-β1 for 3 days and then stained for the indicated sialidases. All images are representative of 3 independent experiments. Bars are 0.2 mm in (a-c) and 0.1 mm in (d).

sialidases. TGF-β1 caused A549 cells to undergo a characteristic change in morphology [153] and to increase levels of NEU3 and the percent of cells positive for Neu3 (Figure 8 a and Figure 9 a). TGF-β1 also caused human small airway epithelial cells to increase

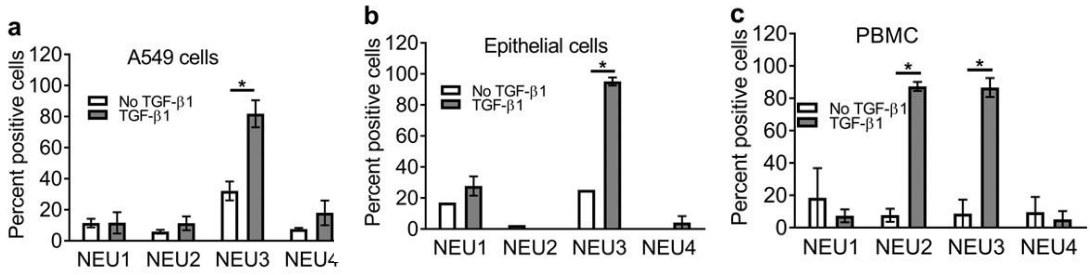

Figure 9. Quantification of TGF-β1 increased sialidase expression.
(a) A549 cells, **(b)** lung epithelial cells, and **(c)** PBMC were incubated with and without TGF-β1 as in Figure 4c, and analyzed for sialidase expression. Values are mean ± SEM of the percent positive cells, n = 3. The absence of an error bar indicates that the error was smaller than the plot symbol. * $p < 0.05$ (t-test).

levels of NEU3, the percent of cells positive for Neu3 and slightly increased levels of NEU1 (Figure 8b and Figure 9 b). As previously observed, TGF-β1 increased the proliferation of human pulmonary fibroblasts [154], and caused these cells to increase levels of NEU3 (Figure 8c and Figure 10). TGF-β1 increased levels of NEU2 and NEU3 in some cells in cultures of human PBMC (Figure 8 d and Figure 9 c).

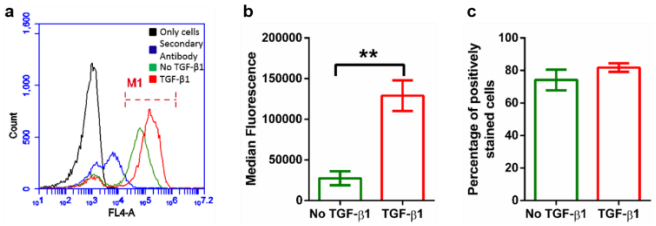

Figure 10. TGF-β1 increases NEU3 expression in human pulmonary fibroblasts.
Human pulmonary fibroblasts were incubated with and without TGF-β1 as in Figure 8c, and analyzed for anti- NEU3 staining by flow cytometry. **(a)** Flow cytometry plot representative of 3 separate experiments. M1 indicates gate of positively stained cells used for panel c. **(b)** Median fluorescence intensity in arbitrary units. **(c)** Percentage of positively stained cells. Values in b and c are mean ± SEM, n = 3. ** $p < 0.01$ (t-test).

2.4.4. Sialidases show some activity at neutral pH

The enzymatic activity of the four human sialidases has been characterized [155, 156], with >50% activity between pH of 3.5 to 5.5, although NEU4 is still ~50% active at pH 7.4 [155, 157]. To determine if sialidases might have enzymatic activity at the pH of the extracellular environment, we assayed recombinant human sialidases at pH 6.4, approximately corresponding to the extracellular pH that might occur in a fibrotic tissue [158], and at pH 7.0, approximately corresponding to a normal extracellular pH [158]. All four recombinant sialidases showed activity at pH 6.4 and pH 7.0 (Table 2), indicating that sialidases could be active in an extracellular environment.

Table 2. Sialidases have activity at neutral pH.
Recombinant human sialidases were assayed for activity at pH 6.4 and pH 7.0. Values are mean ± SEM, n=3.

Activity, μmole / min / mg protein		
Sialidase	pH 6.4	pH 7.0
NEU1	12.8 ± 1.3	7.2 ± 0.9
NEU2	16.4 ± 1.2	8.9 ± 1.2
NEU3	15.2 ± 1.0	8.3 ± 1.2
NEU4	3.8 ± 0.8	2.6 ± 0.9

2.4.5. NEU2 and NEU3 upregulate the intracellular and extracellular accumulation of TGF-β1 by PBMC

To determine if sialidases might cause cells to accumulate intracellular and extracellular TGF-β1, cells were cultured with sialidases. The levels of active TGF-β1 in or on the cells was detected by staining with an antibody against active TGF-β1 (Figure 11 a-c) and an ELISA was performed on the media supernatant to measure the

extracellular accumulation of total TGF-β1 (Figure 11 d). When added to human PBMC, human NEU1 and NEU4 had no significant effect on the accumulation of TGF-β1, while NEU2 and NEU3 increased both cell-associated and extracellular TGF-β1 (Figure 11 a-d). The addition of the sialidase inhibitors DANA or Tamiflu blocked the effects of NEU2 and NEU3 on extracellular TGF-β1 (Figure 11 d), indicating that the effects of NEU2 and NEU3 are due to their sialidase activities. These data suggest that sialidases might be able to potentiate fibrosis by increasing levels of extracellular TGF-β1.

2.4.6. NEU2, NEU3, and NEU4 counteract the ability of SAP to inhibit fibrocyte differentiation

In support of the hypothesis that sialidases potentiate fibrosis, we observed that recombinant human NEU2, 3 and 4, when added to human PBMC, potentiate fibrocyte differentiation and counteract the ability of human SAP to inhibit fibrocyte differentiation (Figure 11 e). NEU1 however did not potentiate fibrocyte differentiation or counteract SAP.

2.4.7. Sialidase inhibitors decrease fibrosis

The sialidase inhibitor DANA inhibits all mammalian sialidases [159]. Although Tamiflu is a poor inhibitor of human sialidases, it is a potent inhibitor of murine sialidases, and inhibits LPS-induced mouse macrophage sialidase activity with an IC50 of 1 μm [31]. To test the hypothesis that blocking sialidase might decrease fibrosis, mice

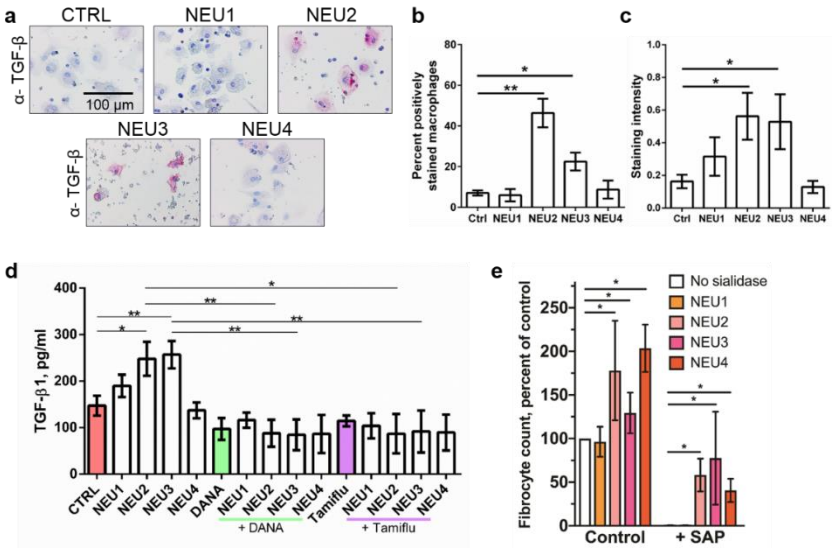

Figure 11. Some sialidases upregulate TGF-β1 and counteract the ability of SAP to inhibit fibrocyte differentiation.
(a) Human PBMC were incubated with or without recombinant human sialidases for five days, then air dried and stained for TGF-β1. All images are representative of 3 independent experiments. Positive staining appears pink and counter staining is blue. Bar is 0.1 mm. **(b)** After staining, positively stained macrophages were counted and expressed as a percent of total cells. Values are mean ± SEM, n=3. * $p < 0.05$, ** $p < 0.005$ (t-test). **(c)** Quantification of staining intensity by ImageJ. Values are mean ± SEM, n=3. * $p < 0.05$ (t-test). **(d)** Human PBMC were incubated with or without recombinant human sialidases, DANA, or Tamiflu for 5 days in serum-free medium. The conditioned media were analyzed by ELISA for total TGF-β1. Values are mean ± SEM, n=7. * $p < 0.05$, ** $p < 0.01$ (t tests). **(e)** Human PBMC were incubated in serum-free medium in the presence or absence of recombinant human sialidase or 2 µg/ ml human SAP. After 5 days, fibrocytes were counted. Values are mean ± SEM, n=3. * $p < 0.05$ (1-way ANOVA, Dunnett's test). No fibrocytes were detected in the cultures with SAP and no sialidase or SAP and NEU1.

were treated with oropharyngeal bleomycin to induce symptoms of pulmonary fibrosis [150] and then starting 10 days after bleomycin (when fibrosis has begun in this model [150]), mice were given daily intraperitoneal injections of 10 mg/kg DANA or 10 mg/kg Tamiflu. Both inhibitors are quite polar, and thus probably remain in the extracellular space. Assuming 2 ml of extracellular space in a 20 g mouse, these doses

would then be ~3 μM. The DANA and Tamiflu treatments did not significantly affect mouse weights (Figure 12). At day 21, the DANA and Tamiflu treatments decreased the bleomycin-induced fibrosis, (Figure 13 a-c) and also counteracted the bleomycin-increased number of inflammatory CD11b cells in the BAL (Figure 13 d).

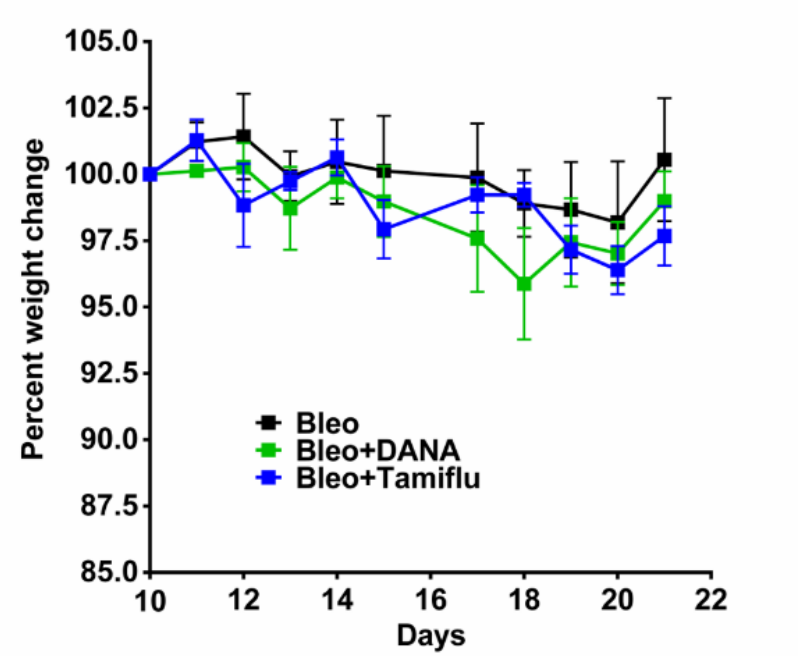

Figure 12. DANA and Tamiflu have no significant effect on the weight of bleomycin-treated mice.
Weights of mice used for the data in Figure 6 were recorded daily starting on day 10 (when mice were randomly assigned to the treatment groups). Values are mean ± SEM, n = 3 mice per group.

Unlike SAP treatment [111], Tamiflu treatment resulted in less protein in the BAL (Figure 13 e), suggesting that Tamiflu may inhibit edema or epithelial barrier destruction following bleomycin instillation. The DANA and Tamiflu treatments also reduced staining for TGF-β1 (Figure 14). Similar results were observed with DANA and Tamiflu injections starting 24 hours after bleomycin, with the exception that DANA also

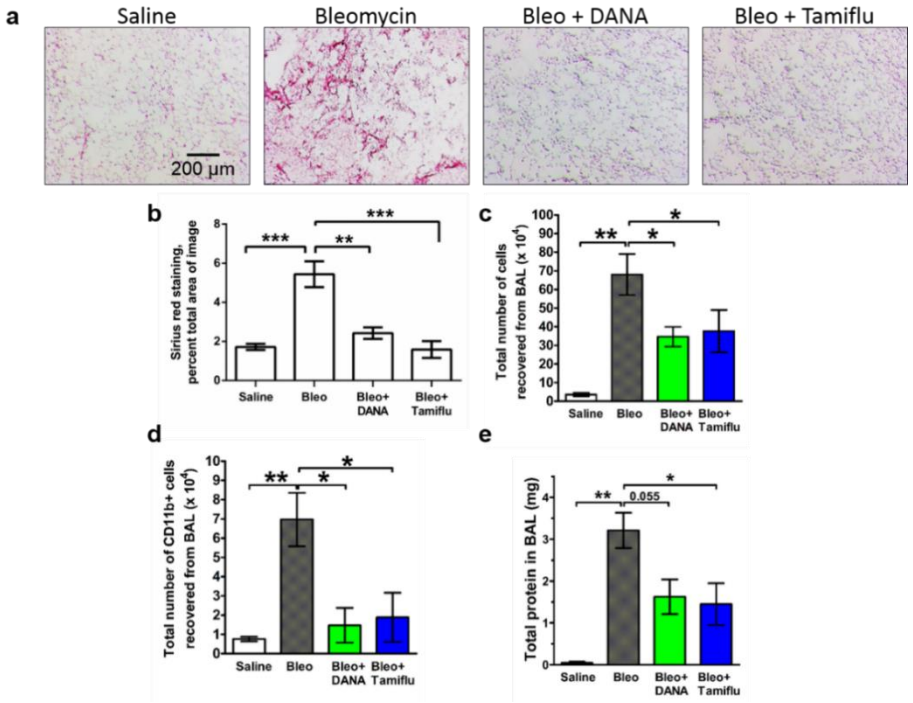

Figure 13. Inhibition of sialidases starting at day 10 after bleomycin attenuates fibrosis.
(a) Sections of lung tissue from mice treated with bleomycin or saline, and then injected daily with saline, DANA, or Tamiflu starting at day 10 after bleomycin, and then euthanized at day 21, were stained for collagen with Sirus Red. Bar is 0.2 mm. All images are representative of 3 mice per group. **(b)** Quantification of staining with ImageJ. The percentage of area stained was quantified as a percentage of the total area of the lung. **(c,d)** The total number of cells and number of CD11b+ cells in the BAL. **(e)** Total protein in the BAL. For B-E, values are mean ± SEM, n = 3 mice per group. * indicates $p < 0.05$, **$p < 0.01$ (1-way ANOVA, Tukey's test). In B and D, the differences between Saline, Bleo+DANA, and Bleo+Tamiflu were not significant.

significantly reduced BAL protein content [160]. Together, these results suggest that sialidase inhibitors can decrease fibrosis.

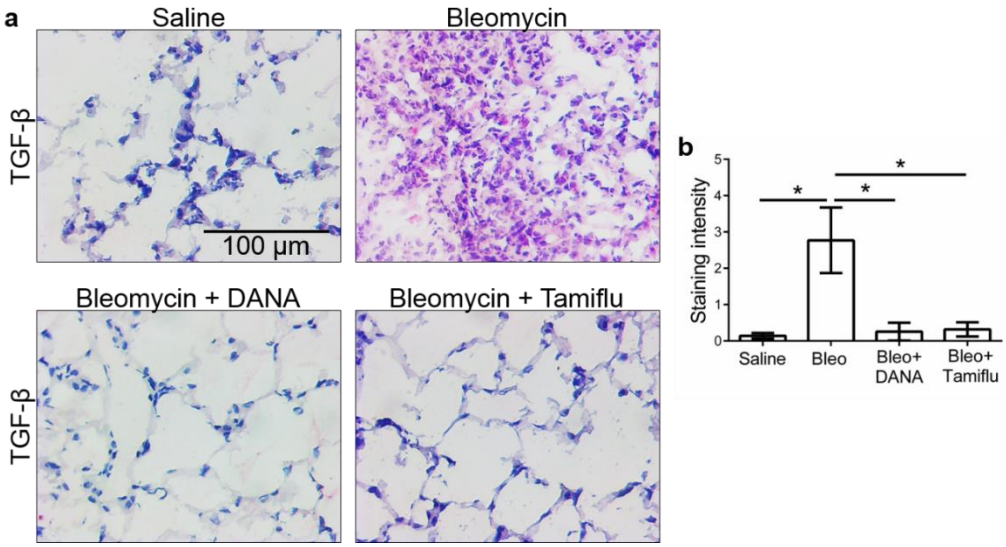

Figure 14. Sialidase inhibitors reduces TGF-β1 staining.
(a) Sections of lung tissue from mice treated with bleomycin or saline, and then injected daily with saline, DANA, or Tamiflu starting at day 10 after bleomycin, and then euthanized at day 21, were stained for TGF-β1. All images are representative of 3 mice per group. **(b)** Quantification of staining intensity with ImageJ. Values are mean ± SEM, n = 3 mice per group. * indicates $p < 0.05$ (t-test).

In further support of the hypothesis that inhibiting sialidases can break a sialidase → fibrosis → sialidase positive feedback loop, we observed that DANA treatment starting 10 days after bleomycin decreased NEU1, NEU2 and NEU3 staining at 21 days [160]. When staining of serial sections of fibrotic lesions with anti-NEU2 was done with DANA or Tamiflu present in the antibody and wash solutions, staining was still observed [160], indicating that residual DANA or Tamiflu that might have been present in the DANA or Tamiflu-treated lungs was not blocking the anti-NEU2 staining. Similar results were observed for DANA and Tamiflu not inhibiting NEU3 staining [160]. Together, these results indicate that DANA and Tamiflu treatments reduce fibrosis, and appear to break the sialidase → fibrosis → sialidase positive feedback loop as evidenced by a reduction in sialidase levels.

2.5. Discussion

In this report, we observe desialylation of glycoconjugates in human and mouse pulmonary fibrosis, which is likely due to the observed elevated levels of sialidases. We found what may be a positive feedback loop, with high levels of sialidases increasing extracellular TGF-β1 accumulation by human PBMC, and TGF-β1 increasing sialidases in human lung epithelial cells, fibroblasts, and PBMC. In support of the hypothesis that sialidases play a role in fibrosis, two different sialidase inhibitors strongly decreased fibrosis in the mouse bleomycin model of pulmonary fibrosis.

A recent report found increased levels of NEU1 in lung fibroblasts of some but not all pulmonary fibrosis patients [37]. We also observed increased NEU1 in mouse pulmonary fibrosis, and in one of three ILD patients. We also observed increased levels of NEU2 and NEU3 in mouse and pulmonary fibrosis, and observed that TGF-β1 can increase NEU2 and NEU3 in PBMC, and NEU3 in epithelial cells and fibroblasts. Other workers found elevated levels of sialidase activity in the BAL fluid from IPF patients [38], and we detected upregulated levels of NEU3 in the BAL fluids from mice with bleomycin-induced pulmonary fibrosis. Compared to healthy individuals, in IPF patients there are no significant increases in the mRNAs encoding NEU1 – 4 [161]. This suggests that, like many other proteins that are upregulated post-transcriptionally by TGF-β1 [162], sialidases may be upregulated post-transcriptionally by TGF-β1. In addition, sialidase protein production, secretion, and activity, can also be regulated by proteins that bind to sialidases, especially protective protein/cathepsin A (PPCA) binding to

NEU1 [23, 26, 163]. Together, these results suggest that post-transcriptional upregulation of multiple sialidases may contribute to fibrosis.

Desialylation of SAP blocks all of its known activities on cells [47], and NEU2, 3 and 4 counteract SAP. These results suggest the possibility that in addition to sialidase upregulating TGF-β1 accumulation by immune cells, sialidase may potentiate fibrosis by desialylating SAP and inhibiting its activity, and that SAP is a key sentinel monitoring extracellular sialidase activity. The only known variation in serum SAP from healthy humans, other than concentration, is a small percentage of desialylated SAP [164-166]. Desialylated SAP is rapidly cleared from the circulation [165], and an intriguing possibility is that the low serum SAP levels observed in patients with IPF [108, 167], myelofibrosis [168], and non-alcoholic fatty liver disease [109] may be due to increased sialidase activity associated with fibrosis. Some tumors have elevated levels of NEU3 [156]. The high levels of NEU3 inhibit apoptosis, and intriguingly decreased apoptosis is a hallmark of fibrotic fibroblasts [169]. In tumors, high levels of NEU3 increase extracellular interleukin-6 (IL-6) [156], and IL-6 is also associated with fibrosis [170]. Sialidases may thus potentiate fibrosis by a combination of increasing TGF-β1, causing clearance of SAP, inhibiting apoptosis, and increasing IL-6.

Since fibrosis has very close similarities to the formation of scar tissue in a wound, a possible explanation for the fibrosis → sialidase → fibrosis positive feedback loop is that it may have originally evolved to accelerate wound healing. In electrical and

control systems engineering, a small amount of positive feedback, as long as the gain of the system is less than 1 (i.e. a small amount of noise does not cause the system to oscillate or swing to one extreme or another), can dramatically increase both the sensitivity and the response time of a system [171]. If this feedback loop has a gain of less than 1, it would allow a faster response to wounds and faster wound healing. We think that in some individuals, or in some perturbed situations, the fibrosis → sialidase → fibrosis feedback loop develops a gain greater than 1, significantly contributing to fibrosis.

3. ATTENUATED PULMONARY FIBROSIS IN SIALIDASE-3 KNOCKOUT *(NEU3$^{-/-}$)* MOUSE[†]

3.1. Summary

Pulmonary fibrosis involves the formation of inappropriate scar tissue in the lungs, but what drives fibrosis is unclear. Sialidases (also called neuraminidases) cleave terminal sialic acids from glycoconjugates. In humans and mice, pulmonary fibrosis is associated with desialylation of glycoconjugates and upregulation of sialidases. Of the four mammalian sialidases, we previously detected only NEU3 in the bronchoalveolar lavage fluid from mice with bleomycin-induced pulmonary fibrosis. In this report, we show that NEU3 upregulates extracellular accumulation of the pro-fibrotic cytokines IL-6 and IL-1β, and IL-6 upregulates NEU3, in human peripheral blood mononuclear cells, suggesting that NEU3 may be part of a positive feedback loop potentiating fibrosis. To further elucidate the role of NEU3 in fibrosis, we used bleomycin to induce lung fibrosis in wild-type C57BL/6 and *Neu3$^{-/-}$* mice. At 21 days after bleomycin, compared to male and female C57BL/6 mice, male and female *Neu3$^{-/-}$* mice had significantly less inflammation, less upregulation of other sialidases and the profibrotic cytokine active TGF-β1, and less fibrosis in the lungs. Our results suggest that NEU3 participates in fibrosis, and that NEU3 could be a target to develop treatments for fibrosis.

[†] Reprinted with permission from "Attenuated pulmonary fibrosis in sialidase-3 knockout *(Neu3$^{-/-}$)*mice." Karhadkar, T. R., Chen, W., & Gomer, R. H., 2020. *American Journal of Physiology-Lung Cellular and Molecular Physiology*, 318(1): p. L165-L179.

3.2. Introduction

Fibrosis involve the inappropriate formation of scar tissue in an internal organ, and 45% of deaths in the US are associated with fibrosis [2, 9, 10]. Pulmonary fibrosis is the generic term for a broad category of lung diseases that includes idiopathic pulmonary fibrosis (IPF). IPF is a chronic and fatal disease characterized by fibrosis of lungs with a median survival of 3-5 years after initial diagnosis [10, 12]. IPF affects ~3 million people worldwide, with an incidence of 1 in 400 in the elderly [10, 12].

Sialic acid is a monosaccharide frequently located at the terminal positions of glycoconjugates [42, 44]. Sialidases, which are also called neuraminidases, remove the terminal sialic acid from these glycoconjugates [18, 19]. There are four known mammalian sialidases, NEU1, NEU2, NEU3, and NEU4, and these have different subcellular localizations and substrate specificities [52]. Sialidase activity was detected in the bronchoalveolar lavage (BAL) fluid from 8 of 9 pulmonary fibrosis patients, but no sialidase activity was detected in the BAL fluid from healthy controls [38]. There is upregulation of the sialidase NEU1 in pulmonary fibrosis [37], and in addition to upregulation of NEU1, we detected desialylation of glycoconjugates and upregulation of NEU2 and NEU3 in fibrotic lesions in human and mouse lungs [160]. NEU3, but not NEU1, NEU2, or NEU4 was detected in the BAL fluid from mice with bleomycin induced pulmonary fibrosis.; no detectable sialidases were in the BAL fluid from control mice [160]. When added to human immune cells, NEU2 and NEU3 upregulated the fibrosis-associated cytokine transforming growth factor-β1 (TGF-β1), and conversely,

TGF-β1 added to human lung fibroblasts, lung epithelial cells, and peripheral blood mononuclear cells (PBMC) upregulated NEU3 expression [160]. Serum amyloid P (SAP) is a serum protein that inhibits fibrosis in humans, mice, and rats [172], while fibrocytes are monocyte derived cells that participate in fibrosis [64, 173, 174]. NEU2, 3, and 4 counteract SAP function and potentiate fibrocyte differentiation in the presence or absence of SAP [160]. The small molecules DANA and Oseltamivir are sialidase inhibitors. We found that DANA and Oseltamivir reduce bleomycin-induced pulmonary fibrosis in mice, even when treatment was initiated at day 10 after bleomycin [160]. These results suggested that sialidases are involved in pulmonary fibrosis.

Many of the effects of sialidases in fibrosis, such as the sialidase activity in pulmonary fibrosis patient BAL fluid [38], appear to be in the extracellular environment. NEU1, NEU2, and NEU4 are localized inside cells [52], while NEU3 is localized on the extracellular side of the plasma membrane [52, 175, 176]. NEU3 may thus be a key sialidase involved in fibrosis. NEU3 is upregulated in colon [55], renal [56], ovarian [57], and prostate cancers [58]. Overexpression of NEU3 in human colon cancer cells promotes cell proliferation and adhesion, suggesting that the high levels of NEU3 observed in some tumors may potentiate the tumor [177]. To elucidate the function of NEU3, NEU3 deficient (*Neu3*$^{-/-}$) mice were generated in a C57BL/6 background by disrupting exon 3 of *Neu3* [178]. Compared to control C57Bl/6 mice, *Neu3*$^{-/-}$ mice have normal lifespans, appearance, fertility, ganglioside composition of tissues, and histology of a variety of tissues, and *Neu3*$^{-/-}$ mice generated in a Balb/c background are also

similar to parental mice [178]. In support of the role of NEU3 in cancer, *Neu3*$^{-/-}$ mice have a reduced incidence of colitis-associated colon cancer [178].

To elucidate the role of NEU3 in pulmonary fibrosis, in this report we used bleomycin to induce pulmonary fibrosis in wildtype and *Neu3*$^{-/-}$ mice, and find that *Neu3*$^{-/-}$ mice have strongly attenuated inflammation and fibrosis in response to bleomycin, suggesting that NEU3 plays a major role in bleomycin-induced pulmonary fibrosis in mice.

3.3. Materials and methods

3.3.1. Mouse strains

A breeding colony of C57BL/6 background *Neu3*$^{-/-}$ mice strain B6.129-Neu3^{tm1Yamk} [178], originally from Kazunori Yamaguchi from Miyagi Cancer Center Research Institute, Natori, Japan, was established by Dr. Jamey Marth at UC Santa Barbara, and some of the mice from this colony were sent to Texas A&M. Sex- and age-matched C57BL/6 wild type mice were from Jackson Laboratories (Bar Harbor, ME). Tailsnip DNA was collected as described previously [179], and PCR was used to check the *Neu3* gene disruption and the presence of the *Neu1, Neu2,* and *Neu4* genes using the primers [180]. As a control, the presence of the β-actin gene in the tailsnip DNA samples was checked by PCR using the primers [180]. Wild-type C57BL/6 mice showed a *Neu3* PCR product that was absent in *Neu3*$^{-/-}$ mice, and actin controls showed that template DNA was present in all samples tested (Figure 15 a – b). All experiments with the

animals were carried out in accordance with National Institutes of Health guidelines. All experimental protocols were approved by the Texas A&M University Institutional Animal Care and Use Committee.

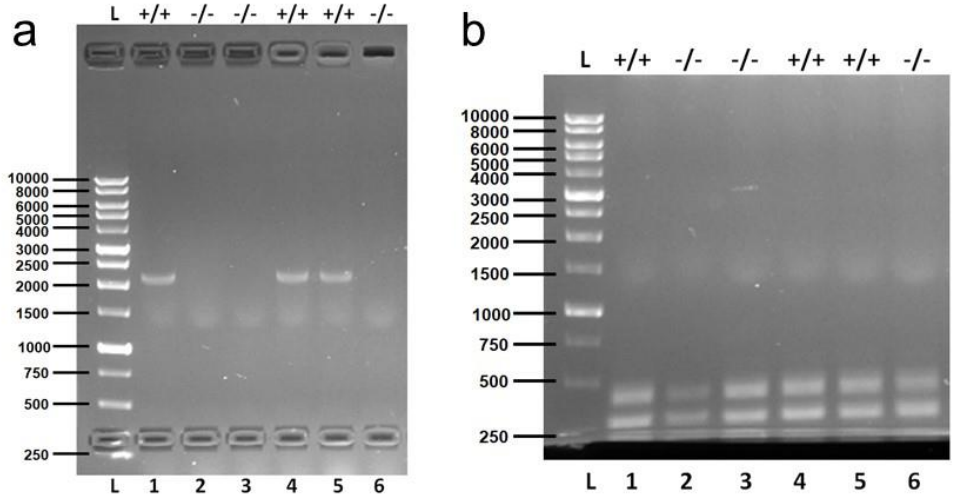

Figure 15. *Neu3*$^{-/-}$ mice genotyping.
(a) Tailsnip DNA was prepared from wildtype C57BL/6 (+/+) and *Neu3*$^{-/-}$ (-/-) mice, and PCR was used to check for the presence of a 2.1 kBP piece of the *Neu3* gene. Molecular mass markers in BP are at left. **(b)** PCR was used to check for the presence of a 310 BP fragment of the β-actin gene in the DNA samples.

3.3.2. Mouse model of pulmonary fibrosis

Mice were used in three separate groups to achieve 3 male and 3 female *Neu3*$^{-/-}$ mice treated with saline, 3 male and 3 female *Neu3*$^{-/-}$ mice treated with bleomycin, 3 male and 3 females C57BL/6 mice treated with saline, and 5 male and 4 female C57BL/6 mice treated with bleomycin. An additional female C57BL/6 mouse treated with bleomycin developed signs of distress on day 10 and was immediately sacrificed and not included in the study; an autopsy showed that this mouse had a blocked intestine. All of the mice were 7 – 9 weeks old except for two 18-week old females in

the *Neu3*$^{-/-}$ bleomycin group and one 18-week old female in the *Neu3*$^{-/-}$ saline group. In all of the assays, the 18-week old females did not show any obvious differences compared to the other *Neu3*$^{-/-}$ females. All other mice survived until sacrifice at day 21, and were used in the study. The mice were sedated for 60 seconds with 4% isoflurane in oxygen and then treated with an oropharyngeal aspiration of 50 µl of 3 U/kg bleomycin (Calbiochem, Billerica, MA) in 0.9% saline or saline alone as previously described [47, 111, 130, 131]. Mice were sacrificed 21 days after bleomycin aspiration, and bronchoalveolar lavage fluid (BAL) and blood were collected. The liver, heart, kidneys, and spleen were removed and weighed. After BAL collection, lungs were inflated at equal pressures with, and embedded in, OCT compound (VWR, Radnor, PA), frozen, and stored at -80˚C. The cells collected from BAL were counted, and cytospins were prepared as previously described [47, 111, 130, 131]. Blood was clarified by centrifugation at 10,000 x g for 5 minutes to obtain serum, which was stored at -80 ˚C.

3.3.3. Histology

10 µm lung cryosections on glass slides and BAL cytospins were air dried for 48 hours before use. Lung cryosections or BAL cytospins were fixed in fresh acetone for 20 minutes at room temperature and then rehydrated in water for 5 minutes and then PBS for 5 minutes. Slides were blocked with PBS containing 2% BSA (PBSB) for 30 minutes and further processed as described previously [47, 160]. Slides with cryosections or BAL cytospins were incubated with 5 µg/ml anti- CD11b (clone M1/70 BioLegend, San Diego, CA) to detect blood and inflammatory macrophages, anti-CD11c (clone N418,

BioLegend) to detect resident alveolar macrophages and dendritic cells, anti-CD45 (clone 30-F11, BioLegend) to detect all leukocytes, and anti-Ly6G (1A8, BioLegend) or anti-Ly6C (HK1.4, BioLegend) to detect macrophage subsets and neutrophils which have been reported to be upregulated in the bleomycin induced pulmonary fibrosis mouse model [47, 111, 127, 128, 160]. Slides with BAL cytospins were also incubated with 5 ug/ml anti-CD3 (clone 17A2, #100202, Biolegend) to detect T cells or 5 ug/ml anti-CD19 (90176T, Cell Signaling Technology, Danvers, MA) to detect B cells. Some lung section slides were stained with 1 μg/ml rabbit polyclonal anti-NEU1 (TA335236, Origene, Rockville, MD), anti-NEU2, (TA324482, Origene,), anti-NEU4 (AP52856PU-N, Acris/Origene), or anti-TGF-β1 (AB-100-NA, R&D systems, Minneapolis, MN) in PBSB, or 0.5 μg/ml anti-NEU3 (TA590228, Origene) in PBSB/ 500 mM NaCl/ 0.1% NP-40 alternative (EMD Millipore, Billerica, MA) for 60 minutes. Isotype-matched mouse irrelevant antibodies (BioLegend) were used as controls. After washing 3 times with PBS for 10 minutes each, the slides were incubated with 1:500 biotinylated donkey-anti-rabbit (#711-066-152, Jackson ImmunoResearch Laboratories, West Grove, PA) or biotinylated donkey-anti-goat (#713-066-147, Jackson) secondary antibodies and staining was then done as previously described [127, 128]. Lung sections were stained with hematoxylin and eosin or Sirius red to detect collagen as previously described [15]. Light microscopy images were taken using a 4x lens on a Microphot-FX microscope (Nikon, Melville, NY) or 10x and 40x lenses on a DM6B microscope (Leica, Buffalo Grove, IL). Polarized light images were also taken on the DM6B microscope. Images of a 1 mm calibration slide (#MA663, Swift Microscope World, Carlsbad, CA) were used

for size bars. Fields were chosen randomly and counted blindly. Image quantification was done as previously described [160]. Images were converted to RGB stacks using Image J. The green channel (which shows the red staining) was used to adjust the intensity threshold level. The threshold level was kept the same for analyzing a set of images. The total area of the image, and the area stained as a percentage of the total area of the image, were then determined using Image J.

3.3.4. Immunofluorescence staining

Glass slides with 10 μm lung cryosections were fixed in acetone for 20 minutes at room temperature and then rehydrated in water for 5 minutes and then PBS for 5 minutes. Slides were blocked with PBSB for 30 minutes. After blocking, the slides were incubated with 1 μg/ml rabbit anti-NEU3 (21630002, Novus Biologicals LLC, Centennial, CO), 5 μg/ml rat anti- mouse CD11b (BioLegend), rat anti-mouse CD11c (BioLegend), rat anti- mouse CD31 (BioLegend), rat anti-mouse Ly6c (BioLegend), rat anti-αSMA (NB300-978, Novus Biologicals LLC) or rat anti-EpCAM (BioLegend) in PBSB containing 500 mM NaCl at 4°C overnight. After washing 3 times with PBS for 10 minutes, slides were incubated with 2 μg/ml donkey-anti-rat Rhodamine-Red-X (#712-296-153, Jackson) or donkey-anti-rabbit Alexa Fluor 488 (#711-546-152, Jackson) in PBSB for 30 minutes at room temperature. After washing 3 times with PBS, slides were mounted with DAPI containing mounting media (H-1500, Vector Laboratories, Burlingame, CA). The slides were kept in the dark at 4°C for 1 hour to harden the mounting media. Images were captured with a 20x lens on a Nikon ECLIPSE

Ti2 microscope. The number of cells stained for NEU3 (green) but not the other cell marker (red), the number stained for both NEU3 and the other cell marker, and the number stained for the other cell marker but not NEU3 were counted in 3 randomly chosen fields of view. The percentage of cells of a specific type (stained red) which co-stained for NEU3 was calculated.

3.3.5. Differential cell staining

BAL cytospins were fixed and treated with Wright-Giemsa stain (#08711, Polysciences, Inc. Warrington, PA) following the manufacturer's instructions. 200 cells per mouse were examined and scored for cell type following the manufacturer's instructions.

3.3.6. Alveolar wall area fraction

Because alveolar wall thickness increases due to fibrosis or interstitial oedema [181], the alveolar wall area fraction was determined from the hematoxylin and eosin stained lung slides. The quantification of alveolar wall area fraction was performed as described previously [181, 182], where 5 randomly selected 1.19 x 0.92 mm fields without blood vessels or airways were imaged using a 4× objective on a Microphot-FX microscope. ImageJ was used to measure the area of all stained tissue as a percentage of the total image area. The alveolar wall area fraction value for 5 fields was averaged for each mouse in the indicated groups.

3.3.7. 13-plex mouse inflammation panel analysis

BAL, and serum samples collected at day 21 post bleomycin aspiration were processed following the manufacturer's protocol (#740150, LEGENDplex™ Mouse Inflammation Panel (13-plex), Biolegend) for simultaneous quantification of 13 mouse cytokines using an Accuri C6 (BD Bioscience, Franklin Lakes, NJ) flow cytometer.

3.3.8. Western blots

For Western blots, 20 µl of BAL fluid was mixed with 4 µl 5x Laemmli sample buffer and heated to 95°C for 5 minutes. Western blots were done following [14, 160] with the exceptions that 4 - 20% Tris/glycine Mini-Protean TGX gels were used (#456-1096, Bio-Rad, Hercules, CA). Equal volumes (1 µl) of BAL fluid were loaded on gels. 50 – 140 ng of recombinant human NEU1 (TP300386, Origene), NEU2 (TP319858, Origene), NEU3 (TP316537, Origene), NEU4 (TP303948, Origene), or active-TGF-β1 (100-21-10UG, PeproTech, Rocky Hill, NJ) were loaded on gels as positive controls. 0.1 – 1.0 µg of human serum albumin (A1653-1G, Sigma-Aldrich) was loaded on other gels as a positive control. For western blot staining, blocking was in PBS/ 2% BSA/ 5% nonfat milk. Blots were incubated with anti-NEU 1, 2, and 4 antibodies (Origene) at 1:1000 in PBSB for 60 minutes at room temperature as described previously [160]. For anti-NEU3, incubations were at 1:5000 in PBS/ 2% BSA/ 0.1% NP-40 alternative/ 0.01% SDS for 60 minutes at room temperature as described previously [160]. 1:5000 peroxidase-conjugated donkey-anti-rabbit (#711-036-152, Jackson) was used as secondary antibody. All washes were in PBS/ 0.1% (v/v) Tween 20 (PBST) (Fisher, Fair

Lawn, NJ). For western blot detection of active TGF-β1, non-reducing/ no SDS conditions to prepare samples and electrophoresis were used [183]. For western blot staining of albumin, blocking was in 5% nonfat milk in immunoblot buffer (25mM Tris, 0.15M NaCl, and 0.1% Triton X-100). 1:50,000 anti-albumin antibody (AF3329, R&D systems) incubations were in immunoblot buffer. Western blots stained for albumin were washed in Tris-buffered Saline (TBS)/ 0.1% (v/v) Tween 20 (TBST). Peroxidase-conjugated donkey anti-rabbit (Jackson), and biotin-conjugated donkey anti-goat (Jackson) were used as secondary antibodies. SuperSignal West Pico Chemiluminescence Substrate (Thermo Scientific, Rockford, IL) was used following the manufacturer's protocol to visualize the peroxidase using a ChemiDoc XRS+ System (Bio-Rad). Some blots were incubated with 0.1% Ponceau stain (Matheson, Norwood, OH) in 5% acetic acid for 30 minutes and washed 2 times with PBST for 10 minutes each.

3.3.9. Cell isolation and culture

Human peripheral blood was collected from healthy volunteers who gave written consent and with specific approval from the Texas A&M University human subjects review board. All the methods were performed in accordance with the relevant guidelines and regulations. Peripheral blood mononuclear cells (PBMC) were isolated and collected from blood using Ficoll-Paque density gradient centrifugation (GE Healthcare, Cincinnati, OH) following the manufacturer's protocol. PBMCs were cultured at 10^4 cells/ well in a total volume of 200 µl/ well in 96-well flat bottom tissue

culture plates (VWR) with RS (RPMI-1640 (VWR) supplemented with 10 mM HEPES (VWR), 1X non-essential amino acids (VWR), 1 mM sodium pyruvate (VWR), 2 mM glutamine (VWR), 100 U/ml penicillin, 100 μg/ml streptomycin (VWR), and 1X ITS-3 (Sigma-Aldrich, St. Louis, MO)). When the cells were plated, recombinant human NEU3 (TP316537, Origene), was added to a final concentration of 0 – 500 ng/ml. The NEU3 was diluted in RS and added to cells to make the total volume of 200 μl in a well. The cells were then incubated at 37 ˚C with 5% CO_2. The culture media supernatants were collected after 48 hours and assayed using interleukin-1β (IL-1β), IL-4, IL-6, IL-10, IL-12, IL-13, or IFN-γ ELISA kits (Biolegend) following the manufacturer's protocols, reading absorbance with a SynergyMX plate reader (BioTek, Winooski, VT).

3.3.10. Flow cytometry analysis of sialidase expression in human PBMCs

Human PBMC were cultured as above with 8.3 x 10^5 cells/ well with 2 ml/ well in 6-well tissue culture plates (VWR) in the presence or absence of recombinant human IL-6 (Biolegend) and IL-1β. After 72 hours, the medium was carefully removed and the cells were washed with 1 ml of sterile phosphate buffered saline (PBS) at room temperature. The cells were detached with 500 μl of Accutase cell detachment solution (VWR) per well for 6 minutes at 37 °C. 1 ml of RS was added per well. After pipetting the cell solutions 4 times, the cells were placed in sterile 1.7 ml microtube tubes (Genesee Scientific, San Diego, CA) and cells were collected by centrifugation at 500 x g for 10 minutes at 4 °C. The pelleted cells were washed twice by resuspension with 1 ml of ice-cold PBS and centrifugation. The cells were resuspended in 200 μl of ice-cold

2%(w/v) paraformaldehyde (EMS, Hatfield, PA), in PBS for 10 minutes on ice for fixation. 1 ml of ice-cold PBS was added and cells were collected by centrifugation. The cells were resuspended in 200 µl of ice-cold PBSB, for 10 minutes on ice for blocking. 1 ml of ice-cold PBS was added and cells were collected by centrifugation. The pellet was resuspended in 200 µl of ice-cold 0.1% (w/v) Triton X-100 (Alfa Aesar, Ward Hill, MA) in PBS and cell membranes were lysed for 10 minutes on ice. 1 ml of ice-cold PBS was added and cells were collected by centrifugation. Cells were resuspended in 500 µl of PBSB, and 125 µl was then collected by centrifugation for a staining reaction.

The pelleted cells for a staining reaction were resuspended in 100 µl of 1 µg/ml rabbit polyclonal anti-NEU1 (Origene), anti-NEU2, (Origene,) anti-NEU4 (Acris/Origene), irrelevant rabbit polyclonal antibody (AB-105-C, R&D Systems, Minneapolis, MN), or no antibody in 2% (w/v) PBSB, or 1 µg/ml anti-NEU3 (Origene) in 2% (w/v) PBSA with 0.1% (v/v) NP-40 alternative (EMD Millipore, Billerica, MA). Cells were incubated with antibodies for 60 minutes on ice. 500 µl of ice-cold PBS was added and cells were collected by centrifugation. Cells were washed twice by resuspension in 1 ml of ice-cold PBS followed by centrifugation. The cells were then incubated with 100 µl of 1:1000 goat anti-rabbit Alexa Fluor 647 (Life Technologies, Carlsbad, CA), in PBSB for 30 minutes on ice. The cells were then washed twice as described above. The cells were then resuspended in 100 µl of PBSB, kept on ice, and the fluorescence of cells was analyzed on an Accuri C6 flow cytometer (BD Bioscience),

using forward- and side-scatter to identify monocytes and lymphocytes as described previously [47].

3.3.11. Lung tissue lysate preparation

Approximately 10 – 12 mg of mouse lung tissue frozen in OCT was cut off, thawed, washed twice in 0.5 ml PBS by centrifugation at 2,000 x g for 5 minutes in a preweighed Eppendorf tube and resuspension. After the last centrifugation, the supernatant was carefully removed, and the tissue was weighed and the tube with tissue was frozen in liquid nitrogen. 500 µl of Pierce RIPA buffer (Thermo Scientific, Rockford, IL) with 1x proteases and phosphatases inhibitor cocktail (Cell Signaling Technology, Danvers, MA) was added per 5 mg of tissue and tissue was crushed with a pestle. The mixture was then incubated on a rotator for 2 hours at 4 °C. After centrifugation at 18,000 × g for 20 minutes at 4 °C, the supernatant was collected as lung tissue lysate. Total protein was measured by OD 280/260 with a SynergyMX plate reader, (BioTek, Winooski, VT) using RIPA buffer with protease and phosphatase inhibitor as a blank.

3.3.12. NEU3 ELISA

ELISA assays for NEU3 from BAL fluid were performed as described previously [160], with the exception that BAL fluid was diluted to 10 µg of protein in 100 µl of PBS. Serial dilutions of human recombinant NEU3 (Origene) in PBS were also incubated and used as standard curves.

3.3.13. Hydroxyproline assay

Approximately half lobes of lungs frozen in OCT were cut off, thawed, and washed 3 times with PBS to remove OCT in preweighed Eppendorf tubes as described above. After the last centrifugation, the tubes were kept inverted for 5 minutes to allow PBS to blot onto blotting paper, and the tissue was then weighed. Tissues were then processed using a hydroxyproline quantification kit (MAK008-1KT, Sigma Aldrich, St. Louis, MO), following the manufacturer's directions.

3.3.14. Statistical analysis

Data were analyzed by t-test or ANOVA using Prism 7 (Graphpad, La Jolla, CA). Significance was defined as $p < 0.05$.

3.4. Results

3.4.1. *Neu3*$^{-/-}$ mice do not lose weight after bleomycin treatment

We previously observed that fibrotic lesions from human and mouse lungs have elevated levels of NEU3, and that in the bleomycin mouse model of pulmonary fibrosis, sialidase inhibitors attenuate fibrosis [160]. To determine if loss of NEU3 affects bleomycin-induced pulmonary inflammation and fibrosis, wild-type C57BL/6 and *Neu3*$^{-/-}$ mice [178] were treated with an oropharyngeal aspiration of saline or bleomycin. The *Neu3*$^{-/-}$ mice had a disruption of the *Neu3*$^{-/-}$ gene (Figure 15 a – b), and undisrupted fragments of the *Neu1*, *Neu2*, and *Neu4* genes (Figure 16 a – c). All of the mice survived the saline or bleomycin treatment and were included in the study, except for one female

C57BL/6 mice which developed a blocked intestine on day 10 after bleomycin aspiration and was sacrificed on day 10; this mouse was not included in the study. As previously observed [184, 185], compared to saline treated C57BL/6 mice (control), bleomycin treated C57BL/6 mice had lower body weights from days 6 to 12 after bleomycin (Figure 16 d). The weight gain of saline or bleomycin treated *Neu3*$^{-/-}$ mice was not significantly different from controls (Figure 16 c). Although there are differential effects of bleomycin in male and female mice [186, 187], similar trends were observed for male and female mice (Figure 16 e – f). Bleomycin treatment and/ or loss of NEU3 did not significantly affect liver, heart, kidneys or spleen weights (as a percent of total body weight) for combined male and female mice, (Figure 16 g), although *Neu3*$^{-/-}$ female mice had slightly increased liver weights after bleomycin (Figure 16 i). These data suggest that loss of NEU3 attenuates bleomycin-induced total body weight loss in mice.

3.4.2. *Neu3*$^{-/-}$ mice have an attenuated protein increase in the BAL at day 21 after bleomycin treatment

Bleomycin treatment of mouse lungs causes protein levels in the BAL fluid to increase [111, 188, 189]. To determine if loss of NEU3 affects this, we measured protein in the BAL. As previously observed [111, 160], at day 21, bleomycin caused an upregulation of protein levels in BAL fluid in C57BL/6 mice as determined by scanning protein gels or by nanodrop assays (Figure 17 a, b, d, and f). Saline treated *Neu3*$^{-/-}$ mice had comparable levels of protein in BAL to those of C57BL/6 mice, and bleomycin did not significantly affect the protein levels in in *Neu3*$^{-/-}$ mouse BAL (Figure 17 a – b). As

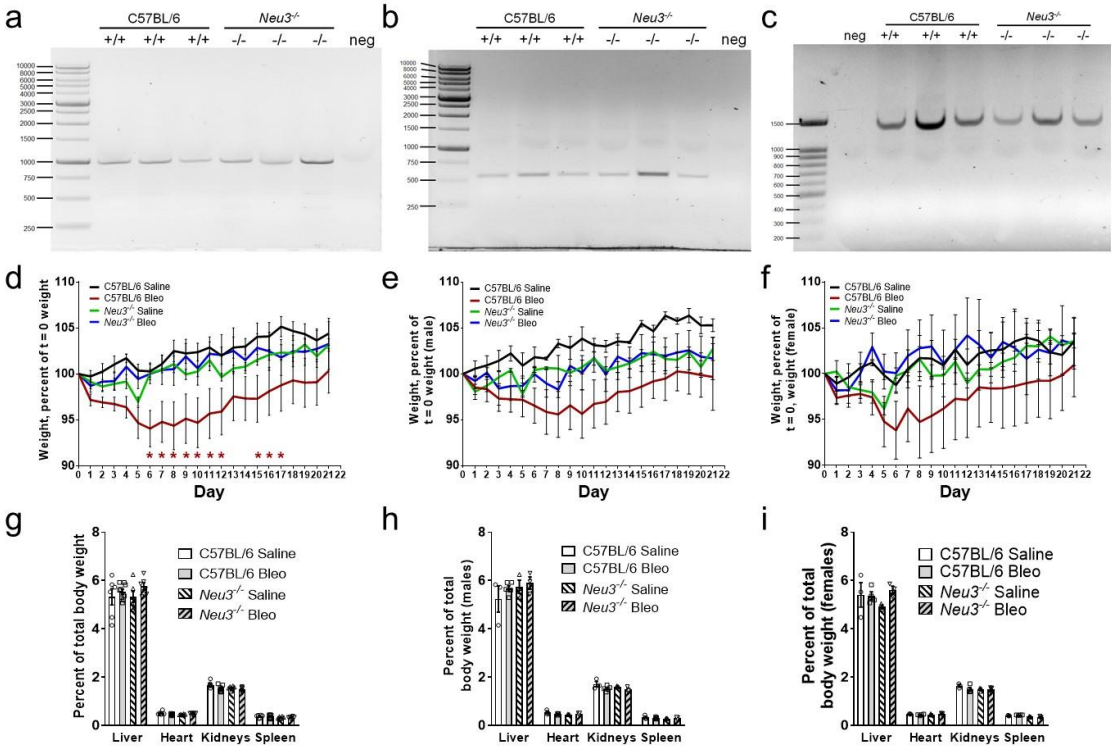

Figure 16. Sialidase genes, body weights, and organ weights.
Tailsnip DNA was prepared from 3 randomly chosen wildtype C57BL/6 (+/+) and 3 randomly chosen *Neu3*$^{-/-}$ (-/-) mice, and PCR was used to check for the presence of **(a)** a 1041 basepairs (bp) fragment of the *Neu1* gene, **(b)** a 572 bp fragment of the *Neu2* gene, and **(c)** a 1482 bp fragment of the *Neu4* gene. Molecular mass markers in basepairs are at left. neg indicates no-DNA control. **(d)** Percent change in body weight after saline or bleomycin treatment at day 0. Values are mean ± SEM, n = 6 except for bleomycin-treated C57BL/6, where n=9. * indicates $p < 0.05$ comparing bleomycin treated *Neu3*$^{-/-}$ mice to bleomycin treated C57BL/6 mice (2way ANOVA, Bonferroni's test). Percent change in body weight after saline or bleomycin treatment at day 0 for **(e)** male mice and **(f)** female mice. Values are mean ± SEM, n = 3 except for bleomycin-treated C57BL/6 mice, where n=5 for males and 4 for females. **(g)** Organ weights as percent of total body weight at day 21 of male and female mice together. Percent change in organ weights after saline or bleomycin treatment at day 0 for **(h)** male mice and **(i)** female mice. Values are mean ± SEM, n = 6 except for bleomycin-treated C57BL/6 mice, where n=9. The presence or absence of NEU3, and treatment with or without bleomycin, had no significant effect on organ weights (1way ANOVA, Bonferroni's test).

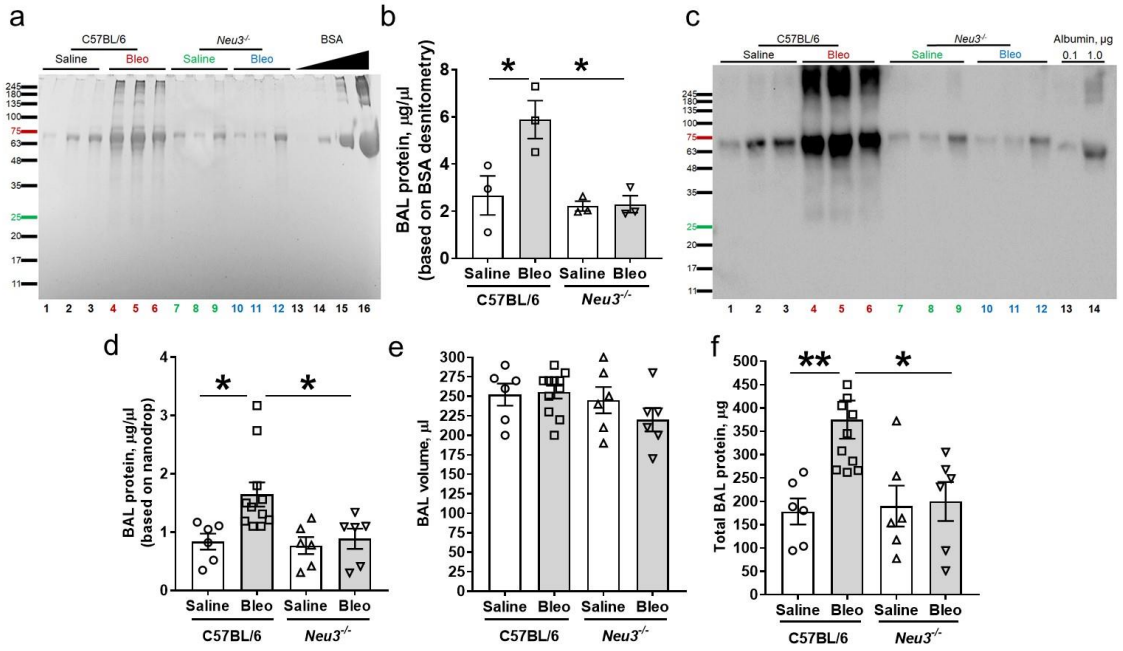

Figure 17. *Neu3*$^{-/-}$ mice do not have elevated BAL protein following bleomycin aspiration.

BAL was collected at day 21 following saline or bleomycin treatment. **(a)** BAL from 3 randomly selected mice per group were analyzed by PAGE on a 4-12 % reducing gel, and stained with Coomassie. Molecular mass markers in kDa are at left. Bovine serum albumin (BSA) at 0.01, 0.1, 1.0, and 10.0 µg was loaded at right. From left, lane # 1 - 12, the sex of mice is M, F, F, M, M, F, M, F, M, M, M, F, with M - Male and F - Female. **(b)** Quantification of protein in lanes # 1 – 12, using the BSA band densities as standards. Values are mean ± SEM, n=3. * $p < 0.05$, (1way ANOVA, Bonferroni's test). **(c)** BAL from the same mice were analyzed by PAGE on a reducing gel, and stained with anti- albumin antibodies. Molecular mass markers in kD are at left. Human albumin at 0.1 and 1.0 µg are in lanes 13 and 14. **(d)** BAL protein was measured using nanodrop (spectrophotometry). Values are mean ± SEM, n = 6 except for bleomycin-treated C57BL/6, where n=9. * $p < 0.05$ (t-test). **(e)** BAL volumes. Values are mean ± SEM, n = 6 except for bleomycin-treated C57BL/6, where n=9. **(f)** Total BAL protein. BAL protein concentration was assessed by nanodrop spectrophotometry for each mouse, and multiplied by the BAL volume from that mouse to obtain total BAL protein. Values are mean ± SEM, n = 6 except for bleomycin-treated C57BL/6, where n=9. * $p < 0.05$, ** $p < 0.01$ (1way ANOVA, Bonferroni's test).

previously observed [188], the bleomycin-induced protein in BAL appeared to be mainly albumin, which was confirmed by an immunoblot with anti-albumin antibodies

(Figure 17 c). Similar results were observed for female and male mice (Figure 18), although as previously observed [186], C57BL/6 female mice had an attenuated response to bleomycin, compared to C57BL/6 male mice. Although bleomycin seemed to increase BAL protein levels in female *Neu3*$^{-/-}$ mice, the effect was not statistically significant. Together these data suggest that loss of NEU3 attenuates bleomycin-induced upregulation of protein in BAL.

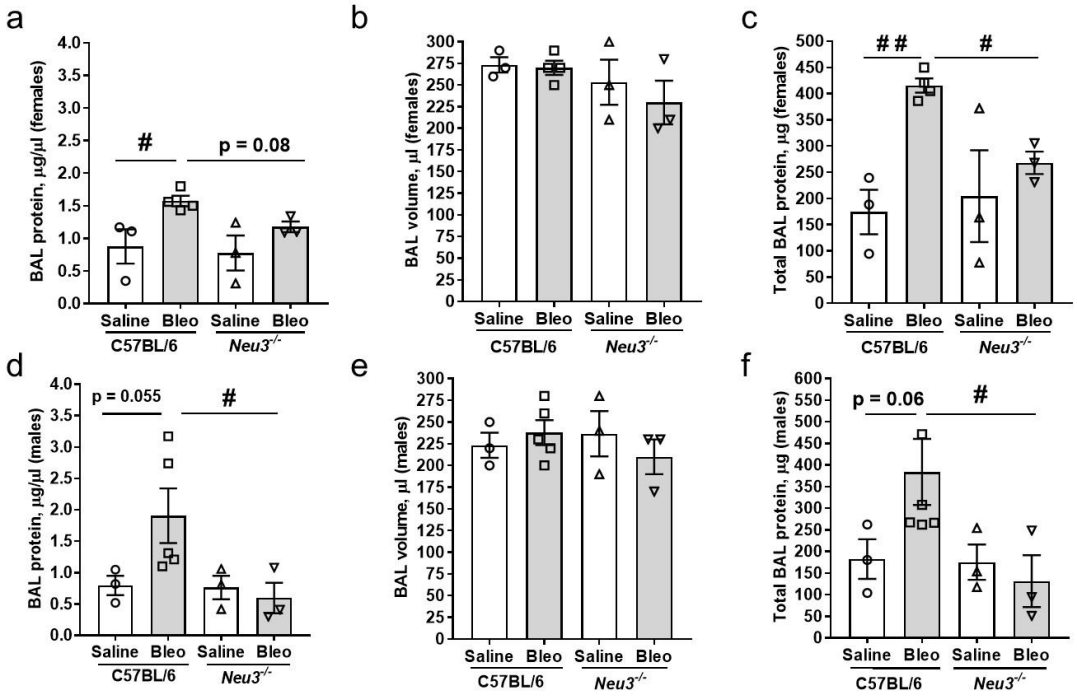

Figure 18. BAL protein for male and female mice.
The data from Figure 17 d, e, and f were separated for female **(a – c)** and male **(d – f)** mice. All values are mean ± SEM, n = 3 except for bleomycin-treated C57BL/6 mice, where n=5 for males and 4 for females. # $p < 0.05$, ## $p < 0.01$ (t-test).

3.4.3. *Neu3*$^{-/-}$ mice have an attenuated inflammatory cell increase at day 21 after bleomycin treatment

Bleomycin upregulates inflammatory cell counts in mouse lung BAL [47, 107, 111, 130]. Compared to saline treated C57BL/6 mice, saline treated *Neu3*$^{-/-}$ mice had similar BAL cell numbers (Figure 19 a). Compared to saline treated *Neu3*$^{-/-}$ mice, bleomycin treated *Neu3*$^{-/-}$ mice had upregulated BAL cell counts, but these were significantly less compared to bleomycin treated C57BL/6 mice (Figure 19 a). Similar effects were seen with male and female mice (Figure 20 a and b). Wright-Giemsa staining indicated that bleomycin treatment increased the lymphocyte percentage in both C57BL/6 and *Neu3*$^{-/-}$ BALs (Figure 19 b), but did not significantly affect monocyte/ macrophage percentages, compared to saline treatment (Figure 19 c). In C57BL/6 BAL, as previously observed [47, 111, 130], bleomycin increased the numbers of CD3 positive lymphocytes (Figure 19 d), CD11b positive inflammatory macrophages (Figure 19 e), CD11c positive resident alveolar macrophages (Figure 19 f), CD45 positive leukocytes (Figure 19 g), and Ly6G positive cells in the BAL (Figure 19 i). Significant differences were not observed for CD19 positive lymphocytes (Figure 19 h) and Ly6C positive cells in the BAL (Figure 19 j). Compared to saline treated C57BL/6 mice, saline treated *Neu3*$^{-/-}$ mice had similar BAL cell numbers for the above cell types, and in *Neu3*$^{-/-}$ mice, bleomycin upregulated CD11c positive cells in the BAL (Figure 19 f). Similar effects were seen in male and female mice with the exception that bleomycin caused an increase in CD45 positive cells in the BAL in *Neu3*$^{-/-}$ female, but not *Neu3*$^{-/-}$ male mice (Figure 20 c – d). Bleomycin treated C57BL/6 mice had increased numbers of NEU1 and NEU3

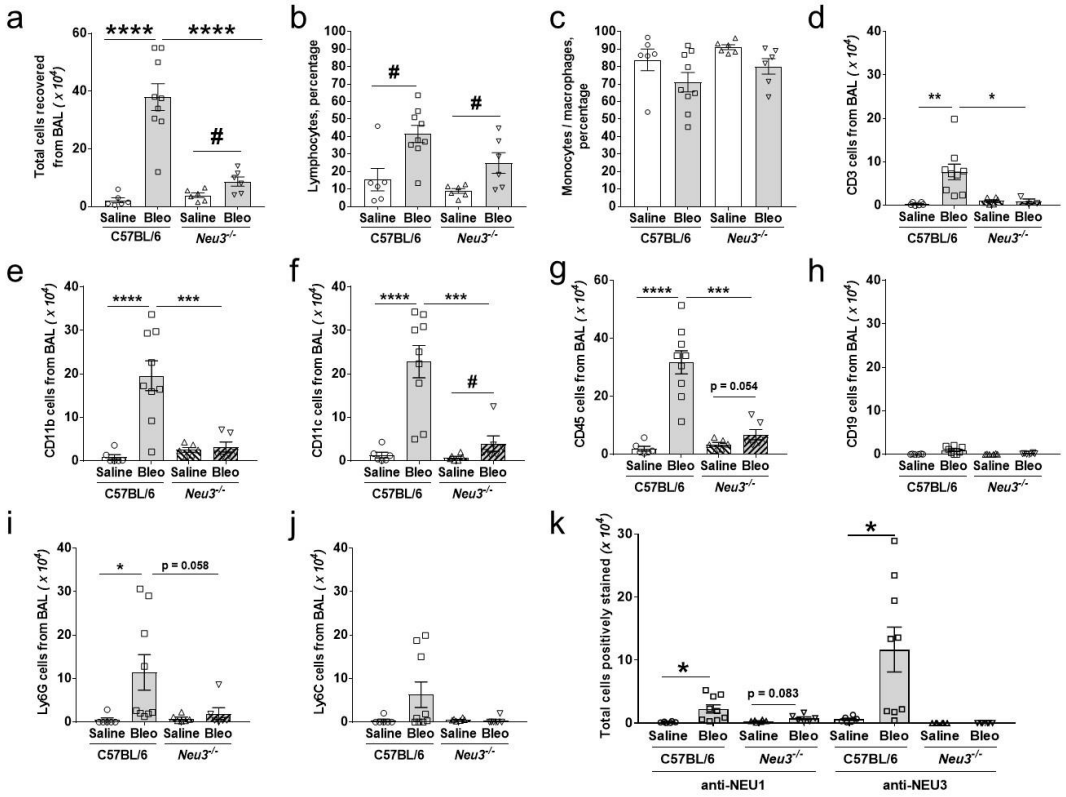

Figure 19. *Neu3*$^{-/-}$ mice have fewer BAL cells after bleomycin treatment.
(a) The total number of cells collected from the BAL at day 21. Values are mean ± SEM, n = 6 mice per group except for bleomycin-treated C57BL/6, where n=9 mice per group. **** $p < 0.0001$ (1way ANOVA, Bonferroni's test), # $p < 0.05$ (t-test). Cytospins of BAL at day 21 were stained with Wright-Giemsa stain, the percent of **(b)** lymphocytes and **(c)** monocytes / macrophages was determined by examining 200 cells per mouse BAL sample. Values are mean ± SEM, n = 6 except for bleomycin-treated C57BL/6, where n=9. # $p < 0.05$ (t-test). Cytospins of BAL at day 21 were stained for the markers **(d)** CD3, **(e)** CD11b **(f)** CD11c, **(g)** CD45, **(h)** CD19, **(i)** Ly6G, **(j)** Ly6C, and **(k)** NEU1 and NEU3. The percent of cells stained was determined in 5 randomly chosen fields of 100-150 cells, and the percentage was multiplied by the total number of BAL cells for that mouse to obtain the total number of BAL cells staining for the marker. Values are mean ± SEM, n = 6 except for bleomycin-treated C57BL/6, where n=9. * $p < 0.05$, *** $p < 0.001$, **** $p < 0.0001$ (1-way ANOVA, Bonferroni's test), # $p < 0.05$ (t-test).

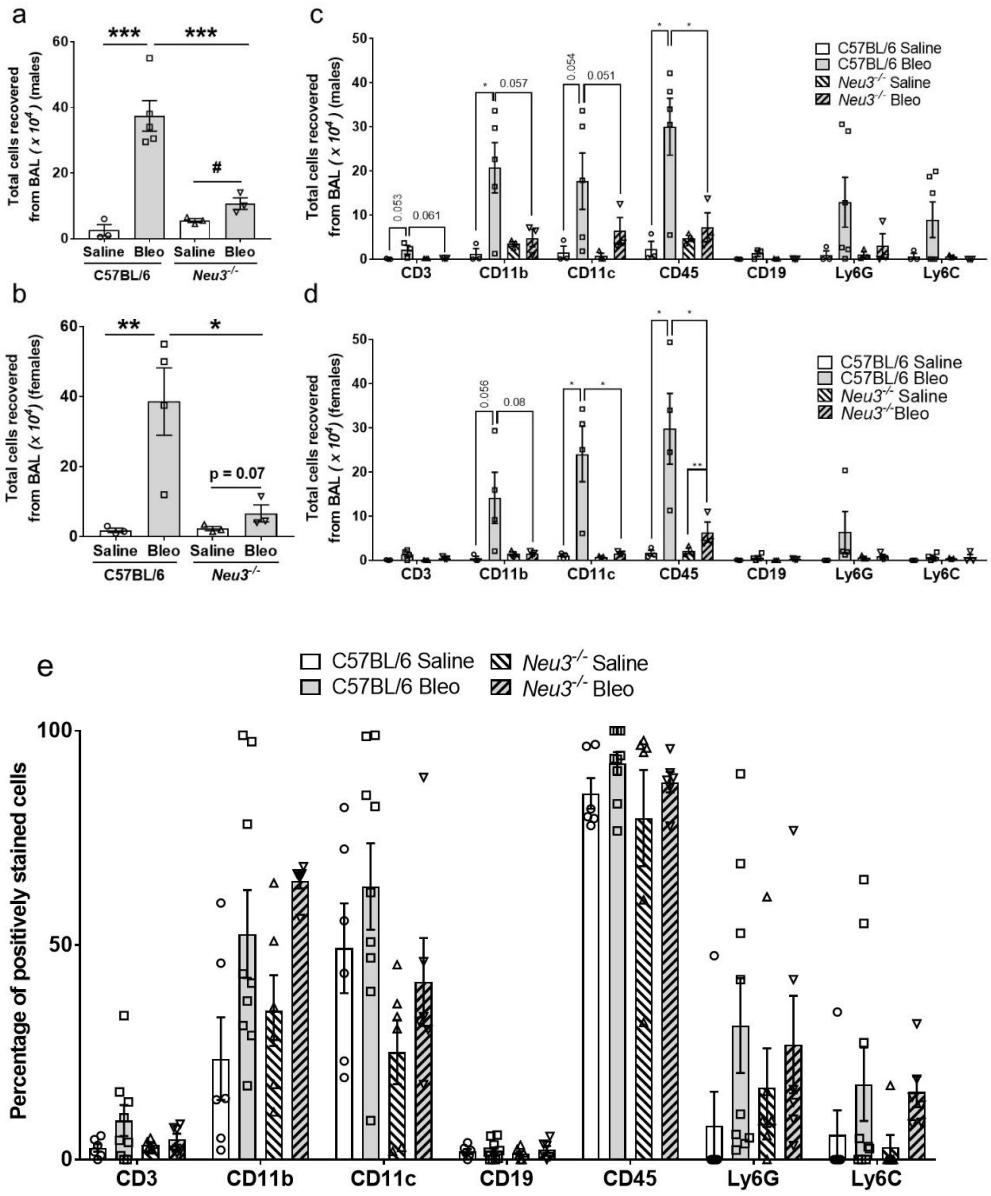

Figure 20. BAL cells for male and female mice.
The data from Figure 19 a and d – j were separated for male **(a and c)** and female **(b and d)** mice. All values are mean ± SEM, n = 3 except for bleomycin-treated C57BL/6 mice, where n=5 for males and 4 for females. * $p < 0.05$ ** $p < 0.01$, *** $p < 0.001$ (1way ANOVA, Bonferroni's test), # $p < 0.05$ (t-test). **(e)** Percentage of positively stained cells for the indicated cell markers, from BAL cytospins of the indicated groups.

expressing cells in BAL, compared to saline treated C57BL/6 mice (Figure 19 k). We did not observe any significant difference due to loss of NEU3 or presence of bleomycin in the percent of the above cell types in the BAL (Figure 20 e). Together, these data suggest that loss of NEU3 attenuates the bleomycin-induced increase of inflammatory cell counts in the BAL of *Neu3*$^{-/-}$ mice.

Following BAL, lungs were sectioned and stained to detect cells that were not removed by BAL. As previously observed [47, 111, 130], in C57BL/6 mice bleomycin increased the numbers of Cd11b+, CD11c+, and CD45+ cells remaining in the lungs after BAL (Figure 21 a and b, Figure 22 a – c). Compared to saline treated C57BL/6 mice, saline treated *Neu3*$^{-/-}$ mice had similar numbers for the above cell types, and in *Neu3*$^{-/-}$ mice, bleomycin did not significantly affect counts for the above cell types (Figure 21 a and b). As previously observed [190, 191], bleomycin did not affect counts of Ly6G+ or Ly6C+ cells in C57BL/6 lungs after BAL at day 21, and loss of NEU3 did not affect Ly6G+ or Ly6C+ counts (Figure 21 b, Figure 22 a – c). Female mice tended to have lower densities of the above cell types in the lungs (Figure 22 a and b). The positively stained cells were primarily clustered in the fibrotic regions of bleomycin-treated C57BL/6 lungs (Figure 22 d). Together, these data indicate that *Neu3*$^{-/-}$ mice show an attenuated inflammatory response at day 21 after bleomycin aspiration.

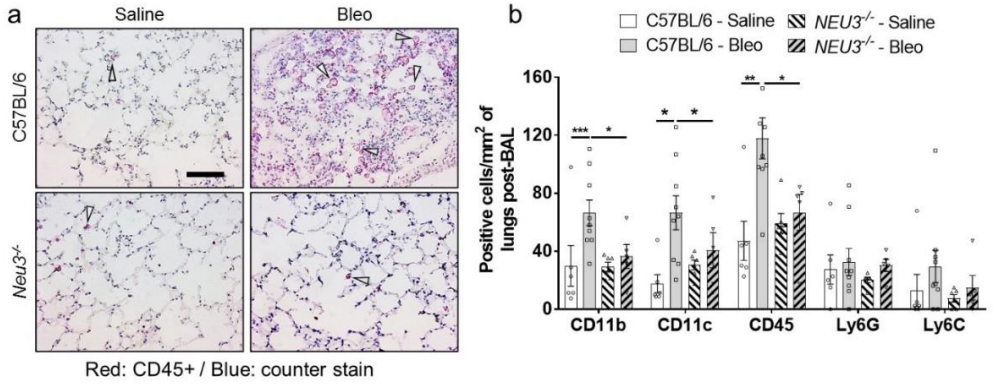

Figure 21. Immune cells remaining in the lungs after BAL.
(a) Cryosections of day 21 lungs were stained with antibodies against CD45. Red is positive staining; blue is counter stain. Bar is 100 μm. **(b)** Cryosections of mouse lungs were stained for the indicated markers, and cells in 5 randomly chosen fields of view of 45 μm diameter were counted, and the number was then calculated to number per mm^2. Vales are mean ± SEM, $n \geq 6$. * $p < 0.05$, ** $p < 0.01$, and *** $p < 0.001$ (1-way ANOVA, Bonferroni's test).

3.4.4. NEU3 upregulates the pro-fibrotic cytokines IL-6 and IL-1β and IL-6 upregulates NEU3 expression in human PBMCs

We previously observed significant upregulation of extracellular and intracellular active TGF-β1 from human peripheral blood mononuclear cells (PBMCs) when cultured with human recombinant NEU3 [160]. To further investigate the role of NEU3 in upregulation of fibrotic cytokines, we cultured human PBMC with recombinant human NEU3 for 48 hours and then assayed the media supernatant by ELISA for the cytokines IL-1β, IL-4, IL-6, IL-10, IL-12, IL-13, and IFN-γ. We observed significant upregulation of extracellular accumulation of IL-6 and IL-1β with increasing concentrations of recombinant human NEU3 (Figure 23 a and b). We did not observe any significant effect of NEU3 on extracellular accumulation of IL-10, IL-13, and IFN-γ (Figure 24 a – c). The levels of extracellular IL-4 and IL-12 were below the level of detection.

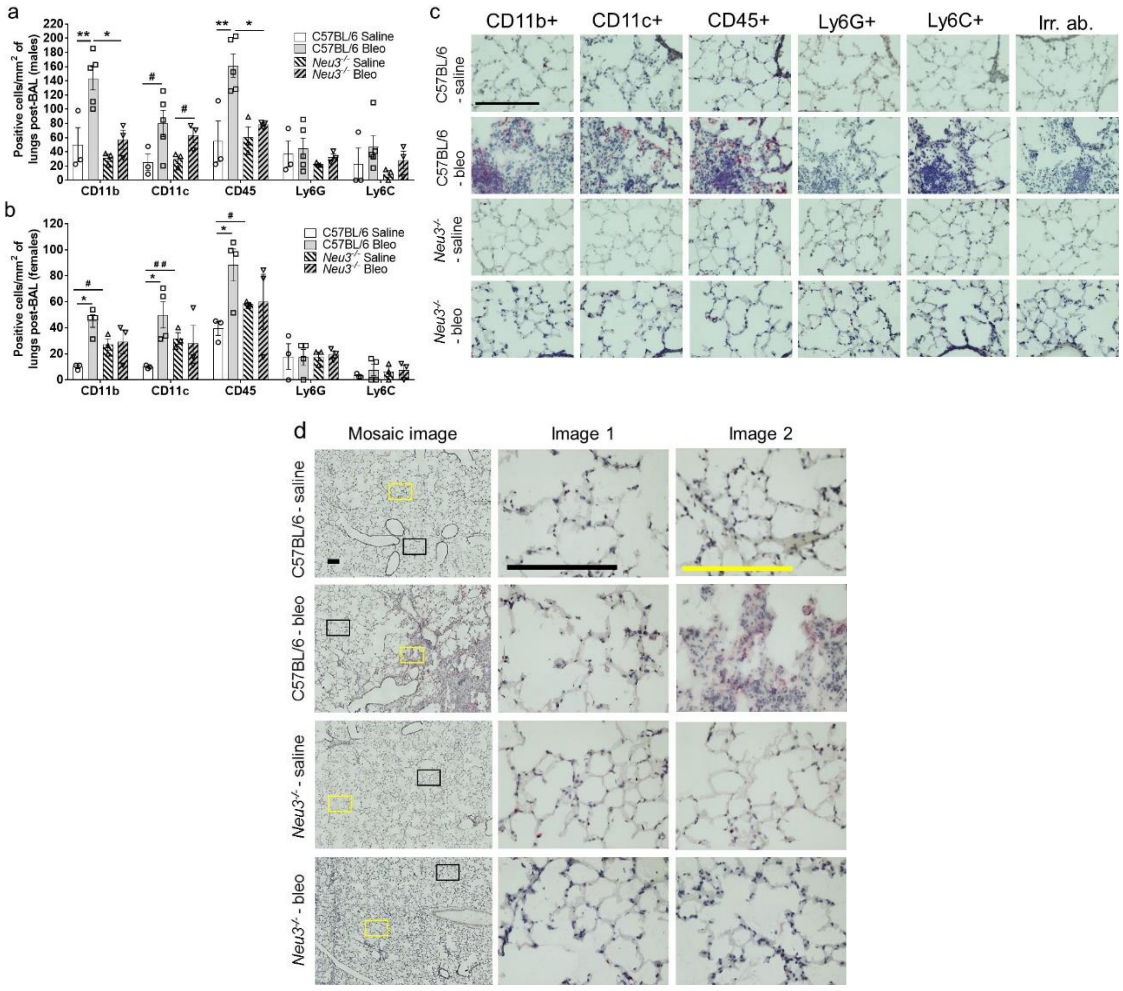

Figure 22. Immune cells remaining in the lungs after BAL for male and female mice.

The data from Fig. 21 b were separated for male **(a)** and female **(b)** mice. All values are mean ± SEM, n = 3 except for bleomycin-treated C57BL/6 mice, where n=5 for males and 4 for females. * $p < 0.05$, ** $p < 0.01$ (1-way ANOVA, Bonferroni's test), # $p < 0.05$, ## $p < 0.01$ (t-test). **(c)** Serial cryosections of mouse lungs post BAL at day 21 were stained for the indicated markers (top) for the indicated groups (left). Red is staining, blue is counter stain. Bar is 200 μm. Images are representative of n = 6 mice per group except for bleomycin-treated C57BL/6 mice, where n=9. **(d)** Representative mosaic images of mouse lung cryosections stained with antibodies against CD45. Two individual images from the mosaic (black and yellow boxes) are shown at center and right. Red is staining, blue is counter stain. Bars are 200 μm. Images are representative of n = 6 mice per group except for bleomycin-treated C57BL/6 mice, where n=9.

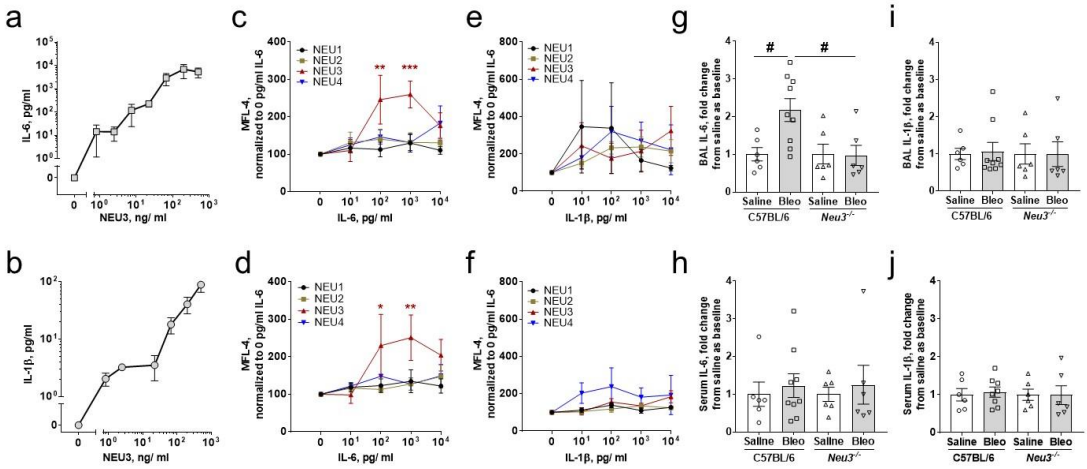

Figure 23. NEU3 upregulates IL-6 and IL-1β, IL-6 upregulates NEU3, and *Neu3*$^{-/-}$ mice have less BAL IL-6 after bleomycin treatment.
Human PBMC were cultured with recombinant human NEU3 and culture supernatants were assayed by ELISA for **(a)** IL-6 and **(b)** IL-1β. Values are mean ± SEM, n = 3. **(c)** Human monocytes and **(d)** human lymphocytes were cultured in human recombinant IL-6 and cells were assayed for NEU 1 – 4 expression by flow cytometry. Values are mean ± SEM, n = 3. * $p < 0.05$, ** $p < 0.01$, and *** $p < 0.001$ (2-way ANOVA, Bonferroni's test). **(e)** Human monocytes and **(f)** human lymphocytes were cultured in human recombinant IL-1β and cells were assayed for NEU 1 – 4 expression by flow cytometry. Values are mean ± SEM, n = 3. **(g)** BAL and **(h)** serum from the indicated mouse groups were collected at day 21 and assayed by ELISA for IL-6. Values are mean ± SEM, n = 6 except for bleomycin-treated C57BL/6, where n=9. # $p < 0.05$ (t-test). **(i)** BAL **(j)** serum from the indicated mouse groups were collected at day 21 and assayed by ELISA for IL-1β. Values are mean ± SEM, n = 6 except for bleomycin-treated C57BL/6, where n=9. For (G) and (I), IL-6 and IL-1β were measured as μg per mg of total BAL protein, and values were normalized to the C57BL/6 saline mean values (4.6 ± 0.8 μg IL-6 / mg BAL protein and 1.8 ± 0.3 μg IL-1β/ mg BAL protein). For H and J, values were measured as pg/ ml of serum, and similarly normalized to the C57BL/6 saline mean values (8.1 ± 2.5 pg IL-6/ ml serum and 2.8 ± 0.5 pg IL-1β / ml serum).

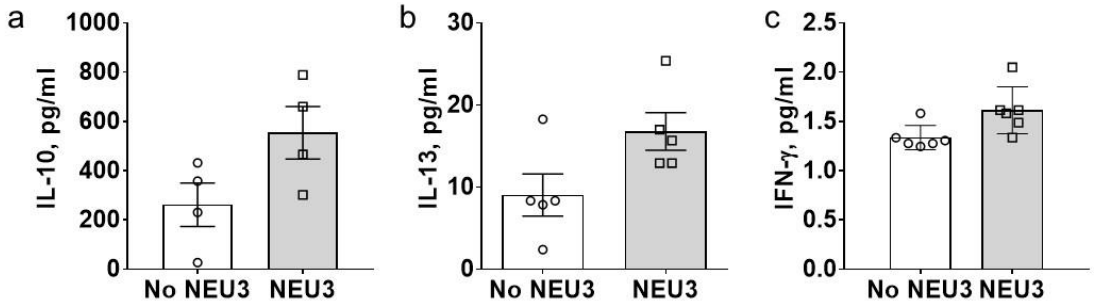

Figure 24. Cytokine levels from human PBMCs.
Human PBMCs were cultured with or without recombinant human NEU3 for 48 hours and culture supernatants were assayed by ELISA for **(a)** IL-10, **(b)** IL-13, and **(c)** IFN-γ. Values are mean ± SEM, n = 4 different donors for IL-10 and 5 different donors for IL-13 and IFN-γ. No significant differences were observed (t-test).

IL-6 upregulates NEU3 expression in carcinomas [192, 193]. To determine the effects of IL-6 and IL-1β on NEU3 expression by human PBMC, PBMC were cultured in the presence or absence of recombinant human IL-6 and IL-1β. 100 and 1000 pg/ml of IL-6 significantly increased NEU3 expression in monocytes (Figure 23 c) and lymphocytes (Figure 23 d). IL-1β did not significantly affect expression of NEU 1 – 4 in monocytes (Figure 23 e) or lymphocytes (Figure 23 f). Together, these results suggest that NEU3 can upregulate pro-fibrotic cytokines such as TGF-β1 [160], IL-6, and IL-1β. Conversely, the ability of TGF-β1 [160], and IL-6 to upregulate NEU3 suggests that under some conditions, a positive feedback loop involving NEU3 and pro-fibrotic cytokines might form.

3.4.5. *Neu3*$^{-/-}$ mice have an attenuated IL-6 increase in the BAL at day 21 after bleomycin treatment

To further investigate the role of NEU3 in bleomycin-induced pulmonary fibrosis, we tested if *Neu3*$^{-/-}$ mice have altered levels of fibrosis-associated cytokines in the BAL and serum. In C57BL/6 mice, bleomycin increased levels of the cytokine IL-6 in the BAL but not the serum (Figure 23 g and h). Saline treated C57BL/6 and *Neu3*$^{-/-}$ mice had comparable levels of IL-6 in the BAL and serum, but bleomycin did not increase IL-6 in *Neu3*$^{-/-}$ BAL (Figure 23 g and h). No significant changes were observed in the levels of BAL and serum IL-1β in saline and bleomycin treated C57BL/6 and *Neu3*$^{-/-}$ mice (Figure 23 i – j). As observed previously [194-196], for C57BL/6 at day 21, bleomycin did not significantly affect levels of IL-1α, IL-10, IL-12p70, IL-17A, IL-23, IL-27, MCP-1, TNF-α, GM-CSF, IFN-β, and IFN-γ in BAL or serum (Figure 25 a and b). With or without bleomycin, the loss of NEU3 did not affect the levels of these cytokines in BAL or serum (Figure 25 a and b). These data suggest that NEU3 is required for a bleomycin-induced increase in BAL IL-6 at day 21 in mice.

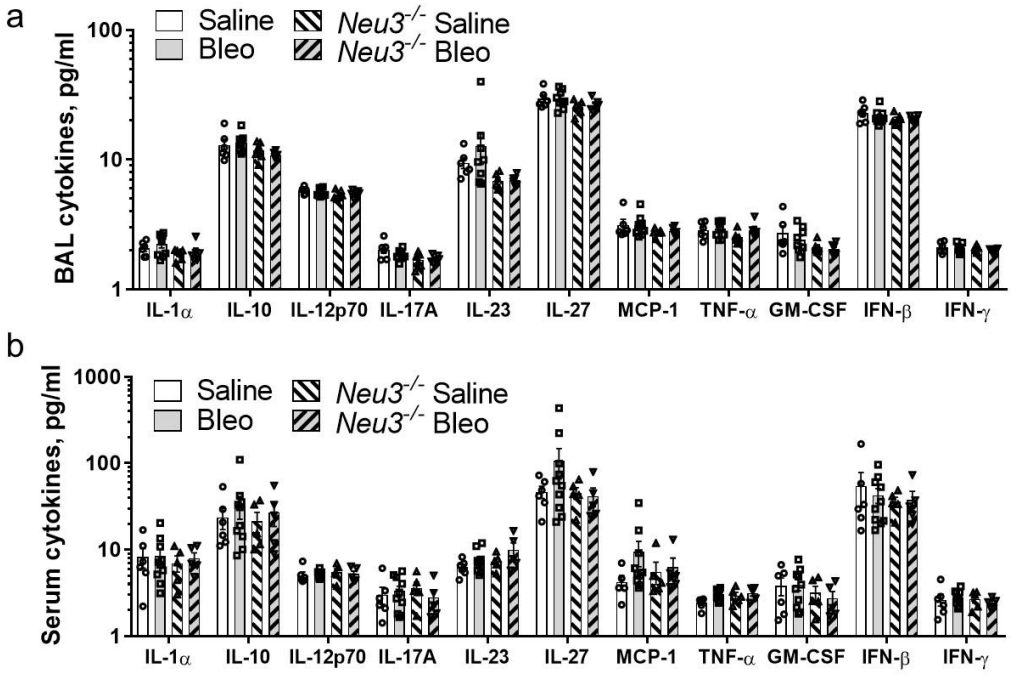

Figure 25. Cytokine levels from mouse BAL and serum.
(a) BAL and **(b)** sera were collected at day 21 and assayed by ELISA for the indicated cytokines. Values are mean ± SEM, n = 6 except for bleomycin-treated C57BL/6 mice, where n=9. Comparing the values in each group of four (C57BL/6 saline, C57BL/6 bleo, *Neu3*$^{-/-}$ saline, and *Neu3*$^{-/-}$ bleo), there were no significant differences (1-way ANOVA, Bonferroni's test).

3.4.6. *Neu3*$^{-/-}$ mice show an attenuated upregulation of other sialidases at day 21 after bleomycin treatment

As observed previously [160], compared to the BAL from saline treated C57BL/6 mice, upregulated levels of NEU3 were detected in the BAL from bleomycin treated C57BL/6 mice (Figure 26 a – c). No NEU3 was detected in saline or bleomycin treated *Neu3*$^{-/-}$ mouse BAL, when analyzed by western blot staining or ELISA for NEU3 (Figure 26 a – c). Mice and humans have 3 other sialidases (NEU1, 2, and 4) in addition to NEU3

[52]. We previously observed that anti NEU1, NEU2, NEU3, and NEU4 antibodies are specific for the different sialidases [160]. As observed previously [160], the sialidases NEU1, NEU2, and NEU4 were not detected in the BAL from saline or bleomycin treated C57BL/6 mice, and these sialidases were also not detected in the BAL from saline or bleomycin treated *Neu3*$^{-/-}$ mice, even though some protein was present in these samples as determined by Ponceau-stained blots [180].

Following BAL, lungs were sectioned and stained. As previously observed for C57BL/6 mice [37, 101, 103, 160], bleomycin increased staining for NEU1, NEU2, NEU3, and TGF-β1 in the lungs (Figure 26 d and e). As we observed for fibrotic human lungs, we also observed that bleomycin increased staining for NEU4 in the C57BL/6 lungs (Figure 26 d and e); this was due to bleomycin increasing staining for NEU4 in female but not male lungs [180]. Further, as previously observed for C57BL/6 mice [197], females have smaller alveoli than males, and this appears to also be the case for *Neu3*$^{-/-}$ mice. (Figure 26 d).

Compared to saline treated C57BL/6 mice, saline treated *Neu3*$^{-/-}$ mice had similar amounts of staining for NEU1, NEU2, NEU3, NEU4 and TGF-β1 in the lungs, and in *Neu3*$^{-/-}$ mice, bleomycin did not significantly affect staining for the above markers (Figure 26 d and e). The positive staining for NEU3 was primarily observed in the fibrotic

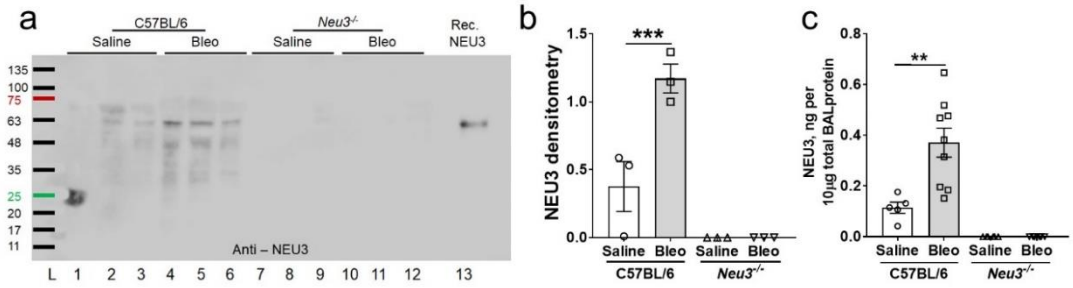

Figure 26. *Neu3*$^{-/-}$ mice have less sialidases and TGF-β1 in the lungs after bleomycin treatment.
(a) BAL was collected at day 21 and BAL from 3 randomly chosen mice per group was analyzed by staining a western blot with anti-NEU3 antibodies. From left, in lane # 1 – 12, the sex of mice is M, F, F, M, M, F, M, F, M, M, M, F, with M - Male and F - female. 50 ng recombinant human NEU3 was loaded in lane # 13. Molecular mass markers in kDa are at left. **(b)** Densitometry of ~51 kDa NEU3 band, arbitrary units. *** $p < 0.001$ (1way ANOVA, Bonferroni's test). **(c)** BAL from the indicated groups were assayed by direct ELISA for NEU3 protein. Values are mean ± SEM, n = 6 except for bleomycin-treated C57BL/6, where n=9.

regions of bleomycin-treated C57BL/6 lungs (Figure 27 a). The lung sections from bleomycin treated C57BL/6 mice were co-stained with antibodies against different cellular markers and antibodies against NEU3. In agreement with previous reports [149, 160], where NEU3 is primarily expressed by epithelial cells, we observed NEU3 expressed in CD11b positive monocyte derived macrophages, CD11c positive alveolar macrophages, CD31 positive cells, EpCAM positive epithelial cells, and αSMA positive fibroblasts, with a high percentage of EpCAM positive epithelial cells expressing NEU3 (Figure 26 f and Figure 27 b).

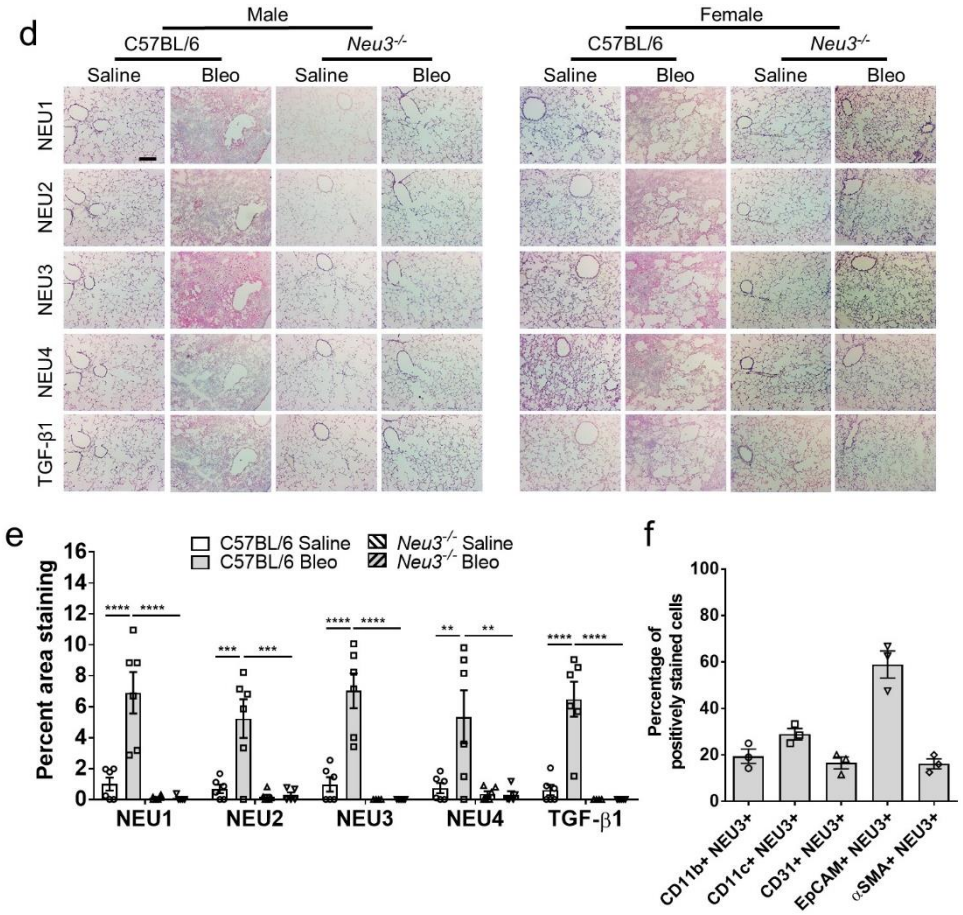

Figure 26. Continued.

(d) Cryosections of male and female mouse lungs at day 21 were stained with antibodies against NEU1, NEU2, NEU3, NEU4, and active TGF-β1. Bar is 200 μm. Images are representative of 6 mice per group. **(e)** For each mouse, for each stain, three randomly chosen fields of view of the size shown in D were imaged, and the percent area of the field of view showing staining was measured, and the average was calculated. Values are mean ± SEM, n = 6 averages. ** $p < 0.01$, *** $p < 0.001$, and **** $p < 0.0001$ (1-way ANOVA, Bonferroni's test). **(f)** Cryosections of bleomycin treated C57BL/6 mice were co-stained with antibodies against the indicated cell markers and NEU3. The percentage of cells stained for the indicated marker that also stained for NEU3 was calculated. Values are mean ± SEM, n=3.

Western blots of lung tissue lysates were stained for NEU1, NEU2, NEU3, NEU4, and TGF-β1 (Figure 28 a – e). The relative protein levels were normalized to total protein from Coomassie gels (Figure 28 f). Compared to saline treated C57BL/6 lysates, bleomycin treated C57BL/6 lysates had upregulated levels of NEU1 (Figure 28 a and g), NEU2 (Figure 28 b and h), NEU3 (Figure 28 c and i), NEU4 (Figure 28 d and j), and

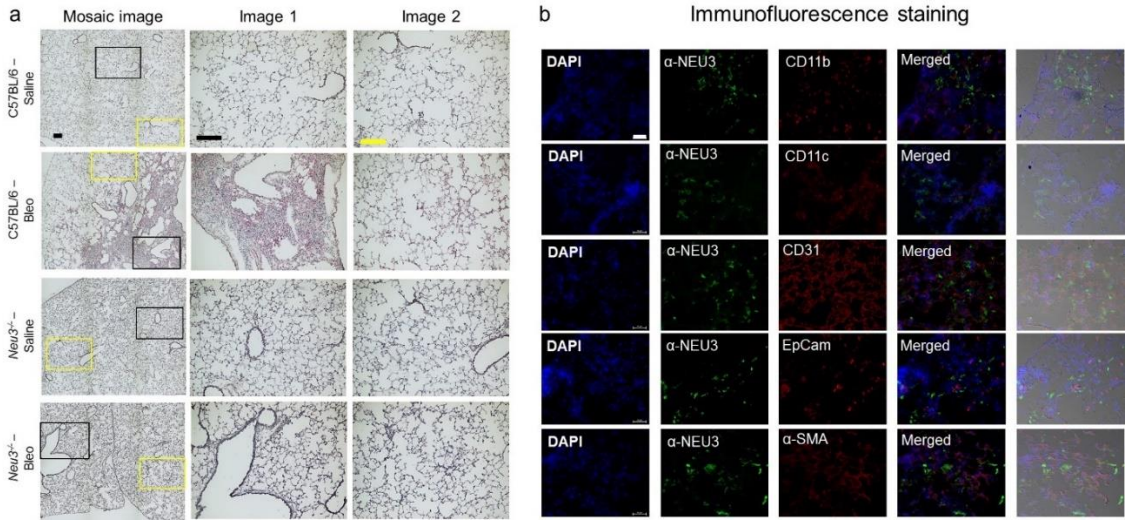

Figure 27. Representative images for NEU3 staining and cellular localization of NEU3 in fibrotic lesion.
(a) Representative mosaic images of lung cryosections stained with anti-NEU3 antibodies. Two fields of views (black and yellow box) are shown at center and right. Red is staining, blue is counter stain. Bars are 200 μm. Images are representative of n = 6 mice per group except for bleomycin-treated C57BL/6 mice, where n=9. **(b)** Serial cryosections of bleomycin treated C57BL/6 mouse lungs post BAL at day 21 were stained with anti-NEU3 antibodies (green), the indicated cell markers (red), and DAPI (blue). Bar is 50 μm. Images are representative of 3 randomly selected bleomycin treated C57BL/6 mouse lungs.

active TGF-β1 (Figure 28 e and k). Compared to saline treated C57BL/6 mice, saline treated *Neu3*$^{-/-}$ mice had normal levels of NEU2 and active TGF-β1, and less NEU1,

NEU3, and NEU4 in lung lysates (Figure 28 a – k). Bleomycin did not upregulate NEU2, NEU3, or active TGF-β1 but did upregulate NEU1 and NEU4 in *Neu3*$^{-/-}$ lysates, albeit to a lesser level than in C57BL/6 lysates (Figure 28 a – k). Together, these results suggest that NEU3 protein is not detected in *Neu3*$^{-/-}$ mouse lungs, and that loss of NEU3 reduces bleomycin induced increases in the levels of NEU1, NEU2, NEU4, and active TGF-β1 in the lungs.

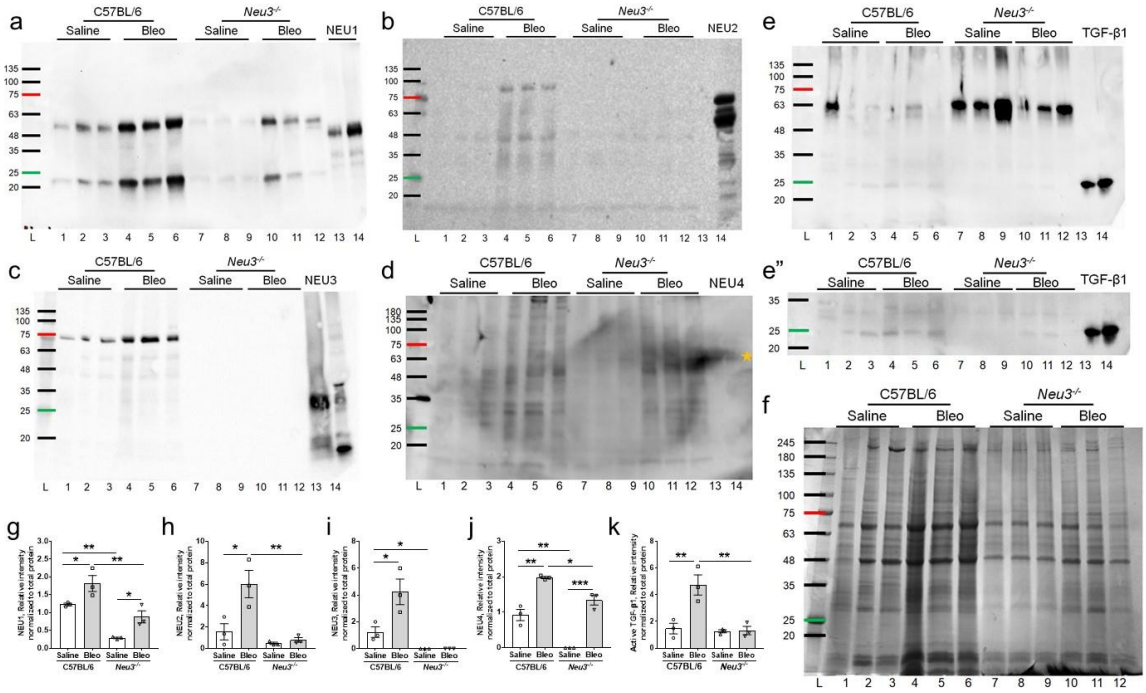

Figure 28. Sialidases and TGF-β1 in lungs lysates at day 21.
Lysates of lung tissue from 3 randomly chosen mice per group were analyzed by western blots stained with **(a)** anti-NEU1 antibodies, **(b)** anti-NEU2 antibodies, **(c)** anti-NEU3 antibodies, **(d)** anti-NEU4 antibodies, and **(e)** anti-TGF-β1 antibodies. **(e")** A long exposure of 'e' was used to detect active TGF-β1 at ~ 25 kDa. **(f)** A gel of the samples was stained with Coomassie blue to detect total protein. Molecular mass markers in kDa are at left. 100 – 140 ng of human recombinant NEU1, NEU2, NEU3, NEU4, and active TGF-β1 was added in lane #13-14 of gels (a), (b), (c), (d), and (e – e"). Quantification of relative intensity normalized with total protein for **(g)** NEU1, **(h)** NEU2, **(i)** NEU3, **(j)** NEU4, and **(k)** active TGF-β1 from the e" image. Values are mean ± SEM, n = 3. * $p < 0.05$, ** $p < 0.01$, and *** $p < 0.001$ (1-way ANOVA, Bonferroni's test).

3.4.7. *Neu3*$^{-/-}$ mice have decreased fibrosis at day 21 after bleomycin treatment

To determine if loss of NEU3 affects the fibrotic response to bleomycin, lung sections were stained with hematoxylin and eosin to detect tissue, antibodies to detect collagen-I, picrosirius red to detect total collagen (which was also imaged using polarized light microscopy for qualitative analysis), and hydroxyproline levels were

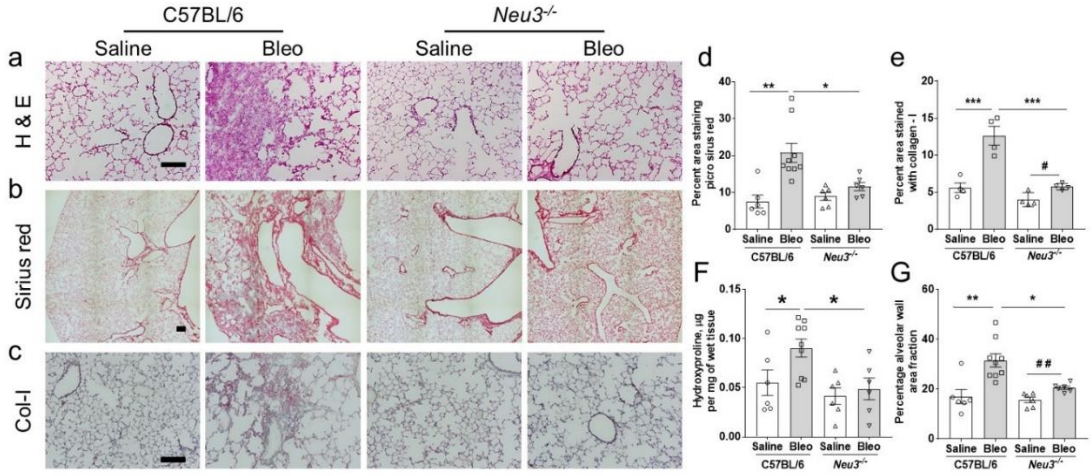

Figure 29. ***Neu3***$^{-/-}$ **mice have less fibrosis in the lungs after bleomycin treatment.** Day 21 lung cryosections were stained with **(a)** H&E, **(b)** picrosirius red to show collagen content, and **(c)** antibodies against collagen-I. Bars are 200 µm. For A and B, images are representative of n = 6 mice per group except for bleomycin-treated C57BL/6, where n=9. For C, images are representative of 4 randomly chosen (2 male and 2 female) mice per group. For **(d)** picrosirius red quantification and **(e)** collagen-I quantification, 5 randomly chosen fields of view of the sizes shown in B and C were imaged for each mouse, and the average percent area of the field of view showing staining for each mouse was measured. **(f)** Estimation of hydroxyproline from saline or bleomycin treated C57BL/6 wildtype and *Neu3*$^{-/-}$ mice lungs. **(g)** Percent of alveolar wall area fraction was determined by the ratio of area of alveolar walls to the total image area. For d, f, and g, values are mean ± SEM, n = 6 except for bleomycin-treated C57BL/6, where n=9, and for E values are mean ± SEM, n = 4. * $p < 0.05$, ** $p < 0.01$, *** $p < 0.001$ (1-way ANOVA, Bonferroni's test), # $p < 0.05$ (t-test).

measured in tissue hydrolysates. As previously observed for C57BL/6 mice [182, 198-200], bleomycin caused fibrosis in the mouse lungs (Figure 29 a – f). Bleomycin did not significantly affect sirius red staining for collagen or hydroxyproline levels, but

increased collagen-I staining and increased alveolar wall area fraction in *Neu3*$^{-/-}$ mouse lungs, but the increase was less than in bleomycin treated C57BL/6 mice (Figure 29 d – f; Figure 30 a). Similar results were observed for male and female mice (Figure 30 b – g) with the exception that bleomycin treated *Neu3*$^{-/-}$ female mice had significantly upregulated sirius red staining compared to saline treated *Neu3*$^{-/-}$ female mice, whereas this was not observed for male mice (Figure 30 b and c). Conversely, bleomycin treated *Neu3*$^{-/-}$ male mice had significantly upregulated alveolar wall area fraction, compared to saline treated *Neu3*$^{-/-}$ male mice, whereas this effect did not reach significance for female mice (Figure 30 f and g). Polarized light microscopy of lung sections stained with sirius red showed qualitative upregulation of collagen in bleomycin treated C57BL/6 mice, compared to saline treated C57BL/6 mice or saline and bleomycin treated *Neu3*$^{-/-}$ mice (Figure 30 h). These results suggest that loss of NEU3 significantly decreases the fibrotic response to bleomycin in mouse lungs.

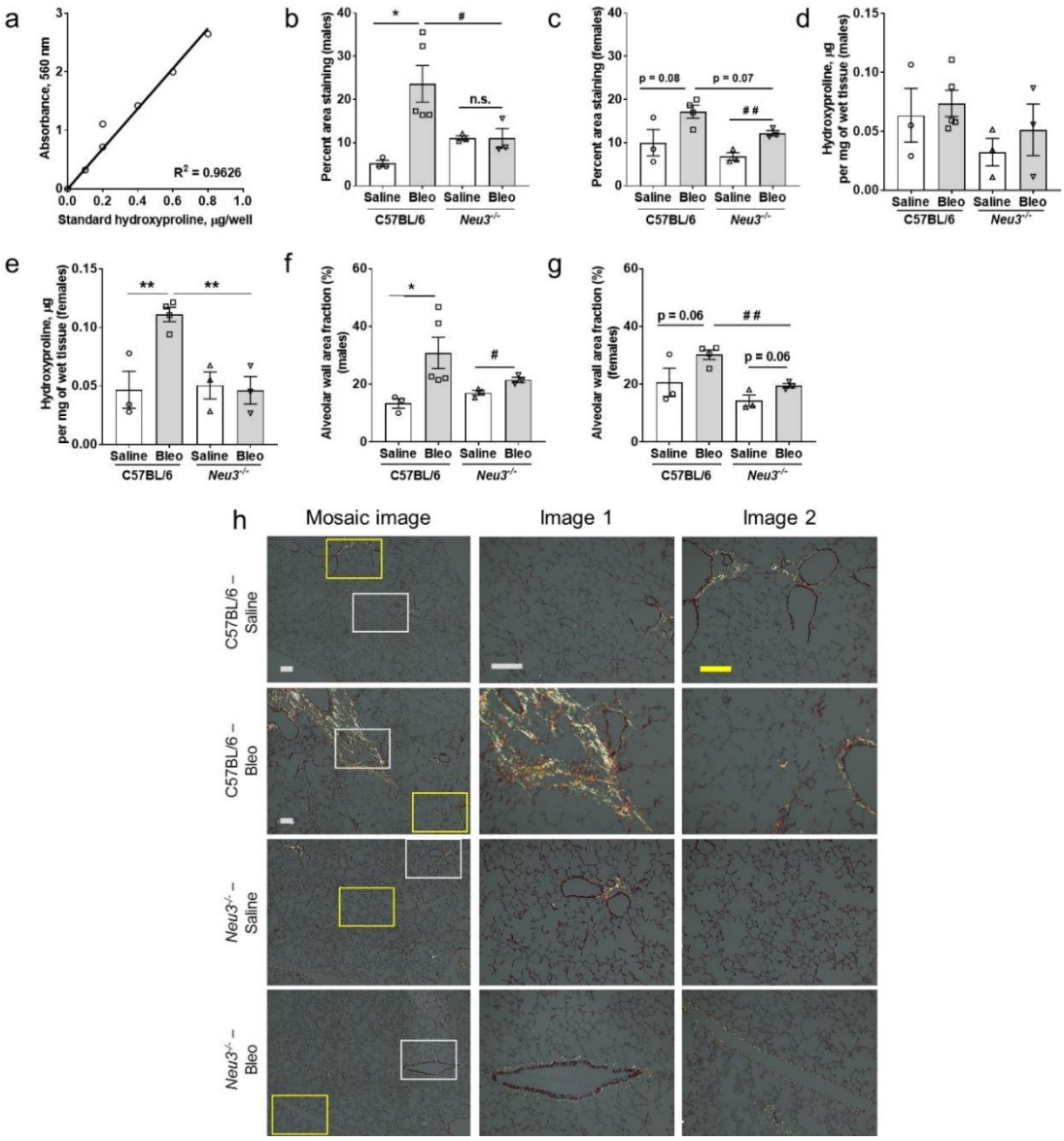

Figure 30. Fibrosis in male and female mice.
(a) Hydroxyproline standard curve. The data from Fig. 29 d, f and g were separated for male **(b, d and f)** and female **(c, e and g)** mice. All values are mean ± SEM, n = 3 except for bleomycin-treated C57BL/6 mice, where n=5 for males and 4 for females. * $p < 0.05$, ** $p < 0.01$ (1way ANOVA, Bonferroni's test), # $p < 0.05$, ## $p < 0.01$ (t-test). **(h)** Representative mosaic images of cryosections stained with Sirius red and imaged with polarized light. Two individual images from the mosaic (black and yellow boxes) are shown at center and right. Bars are 200 µm. Images are representative of n = 6 mice per group except for bleomycin-treated C57BL/6 mice, where n=9.

3.5. Discussion

In this report, we observed that loss of the sialidase NEU3 in male and female mice attenuated bleomycin-induced weight loss, upregulation of protein levels in the BAL, inflammation, TGF-β1 upregulation, and fibrosis, and that the loss of NEU3 did not appear to be compensated by the upregulation of other sialidases. These results suggest that NEU3 may have a major role in bleomycin-induced pulmonary fibrosis in mice.

We observed attenuated total inflammatory cell counts, but no significant differences in the percentages of the different cell types, in the BAL of bleomycin treated *Neu3*$^{-/-}$ compared to bleomycin treated C57BL/6 mice, suggest that attenuation of bleomycin-induced pulmonary fibrosis in the *Neu3*$^{-/-}$ mice is not dependent on the ratios of the different cell types in the BAL.

Changes in cytokine levels are associated with, and appear to drive, fibrosis [83]. We observed that NEU3 upregulates extracellular accumulation of IL-6 by human PBMCs, which is in agreement with previous reports where addition of NEU3 to cells upregulates IL-6 [192, 193]. IL-6 potentiates fibrosis [170], and is actively involved in epithelial-to-mesenchymal transition (EMT) which is associated with fibrosis [201, 202]. We observed bleomycin-induced upregulation of IL-6 in the BAL fluid of C57BL/6 mice but not *Neu3*$^{-/-}$ mice, suggesting that NEU3 may be an important driver of the upregulation of IL-6 levels in fibrosis. Conversely, we observed upregulation of NEU3

in human PBMCs by IL-6, which is in agreement with a previous report where IL-6 increases NEU3 expression in renal cell carcinoma cells [56]. Together, these results suggest that NEU3 mediated upregulation of IL-6, and IL-6 mediated upregulation of NEU3, might form a NEU3 – IL-6 – NEU3 positive feedback loop that potentiates fibrosis.

IL-1β is also associated with inflammatory and fibrotic responses [203]. In the presence of serum, IL-1β upregulates NEU1 but not NEU3 in human neutrophils [34] and in monocytes/macrophages in a positive feedback loop [54]. In the absence of serum, we observed that NEU3 upregulates IL-1β, but IL-1β does not upregulate NEU3 in human PBMC. Together, these results suggest that as with IL6, NEU3 may form a positive feedback loop with IL-1β and that something is serum is necessary for IL-1β upregulation of NEU3.

We previously reported upregulation of NEU1, NEU2, and NEU3, but not NEU4, in fibrotic lesions of lung tissue from male mice at day 21 after bleomycin aspiration [160]. A recent report found that NEU1 is down regulated in IPF, that *Neu1*$^{-/-}$ fibroblasts have characteristics of myofibroblasts, and that *Neu1*$^{-/-}$ fibroblasts release the pro-fibrotic cytokine TGF-β1, suggesting that NEU1 does not potentiate fibrosis [204]. Here we observed upregulation of NEU4 in lung tissue from C57BL/6 female mice but not male mice at day 21 after bleomycin. Bleomycin has different effects on male versus female mice [186, 187], and the upregulation of NEU4 appears to be an additional sex-

linked differential effect of bleomycin in mice. The lack of NEU4 upregulation in fibrosis in male mice suggests that NEU4 upregulation is not a key driver of fibrosis. The observation that mice lacking NEU3 do not upregulate NEU2, and the above observations about NEU1 and NEU4, suggest that NEU2 and/or NEU3 may be responsible for the extensive desialylation that occurs in the lungs in response to bleomycin [160].

The Ensembl database ENSG00000162139 for human [205] shows that for *NEU3* there are 7 different protein coding splice variants. Similarly, for mouse, the NCBI gene ID: 50877 shows at least three NEU3 protein coding transcripts. In agreement with the concept of different *NEU3* splice variant transcripts, at least 5 variants of *NEU3* transcripts have been observed in zebrafish [206]. Transcriptomic data shows that there are at least 9 different splice variants for *NEU3* from human IPF patient lungs [161]. There are multiple NEU3 proteins in human cell lines [207]. Other workers also found multiple NEU3 variant proteins in human cells [37, 149, 208], and looking at 10 different human cell lines, we also observed multiple variants, with different variants expressed by different cell types [160]. In the same publication, we observed that TGF-β1 causes upregulation of NEU3 in PBMC, airway epithelial cells, A549 cells, and lung fibroblasts. We observed NEU3 expressed in multiple cell types in fibrotic mouse lungs. Together, this suggests the possibility that in bleomycin-induced fibrosis, multiple cell types express multiple NEU3 variants, leading to the multiple NEU3 bands we observed in Figure 26 a and Figure 28 c. In Figure 26 a and Figure 28 c, we observed that several

of these bands were upregulated by bleomycin treatment. None of these bands were observed in the BAL or lung tissue from saline- or bleomycin-treated NEU3 knockout mice, indicating that the multiple NEU3 bands observed in the WT mice are bona fide NEU3 proteins.

There are upregulated levels of the mRNA encoding NEU1 in the lung fibroblasts from some pulmonary fibrosis patients [37]. Single-cell transcriptomic analysis also showed upregulated levels of NEU1 transcripts in lung cells from pulmonary fibrosis patients [209]. A different study however found no significant increases in the mRNAs encoding NEU1 – 4 in IPF patients compared to healthy individuals [161]. However, we consistently found elevated levels of NEU3 protein in the fibrotic lesions in human and mouse lungs [160]. We also found that the profibrotic cytokine TGF- β1 [101, 103] causes a variety of cell types to upregulate NEU3 [160]. Since TGF-β1 regulates the levels of some proteins by a post-transcriptional mechanism [162], we previously hypothesized that the increased levels of NEU3 observed in pulmonary fibrosis may be due to a post-transcriptional mechanism [160]. The observation that the antibody we used for the previous work does not detect proteins in mice lacking NEU3 reinforces the validity of this assay, and in combination with the *NEU3* transcriptomic analysis suggests that in fibrosis there may be post-transcriptional regulation of NEU3 levels.

Active TGF-β1 is a key driver of fibrosis [101, 103]. We previously discussed a possible positive feedback loop involving NEU3 – TGF-β1 – NEU3 in the progression of pulmonary fibrosis [160]. In this report we observed upregulated levels of active TGF-β1 in lung tissues of bleomycin treated C57BL/6 mice, but not in the lung tissues of bleomycin treated *Neu3*$^{-/-}$ mice. TGF-β1 is sequestered in an inactive state by latency-associated peptide (LAP) in a complex called latent TGF-β1 protein (LTGF-β1) [89]. LTGF-β1 has three glycosylated asparagine residues at position 82, 136, and 176, all in the LAP sequence [89, 91]. Bacterial and viral sialidases can desialylate LAP, causing a conformational change that releases active TGF-β1, and this is thought to explain the elevated TGF-β1 levels observed during some infections [92, 93, 96, 210, 211]. In bleomycin treated *Neu3*$^{-/-}$ mice, we did not observe upregulated levels of active TGF-β1 (~25 kDa). On Western blots of saline or bleomycin treated *Neu3*$^{-/-}$ mouse lung tissue electrophoresed on non-reducing/ no SDS gels (which preserve the LAP/ TGF-β1 complex [96, 212]), we observed anti- TGF-β1 antibodies staining a ~60kDa band, which is the previously reported size of the LAP/ TGF-β1 complex (Figure 28 e). These results suggest that NEU3 may be involved in releasing active TGF-β1 from LTGF-β1 in bleomycin induced pulmonary fibrosis.

The loss of NEU3 attenuates bleomycin-induced increases in protein and albumin in BAL fluid, which may well be due to vascular leakage. IL-6 causes vascular leakage [213-215] . The loss of NEU3 also attenuates bleomycin-induced inflammation, and IL-6 can cause inflammation [216-218] . NEU3 upregulates IL-6, and loss of NEU3

inhibits bleomycin-induced IL6 upregulation in the BAL. Thus, one possible explanation for the reduced inflammation in, and reduced levels of protein and albumin in the BAL of, bleomycin treated *Neu3*$^{-/-}$ cells is that in a wild-type lung, the damage caused by bleomycin causes an upregulation of NEU3, the upregulated NEU3 upregulates IL-6, and the IL-6 induces inflammation and vascular leakage. In the absence of NEU3, the upregulation of IL-6, inflammation, and leakage then do not occur.

We previously observed that TGF-β1 upregulates NEU3, and that NEU3 upregulates TGF-β1, which suggested that a NEU3 - TGF-β1 – NEU3 positive feedback loop potentiates fibrosis. [160]. In this report we observed that IL-6 upregulates NEU3, and that NEU3 upregulates IL-6 and IL-1β. These results suggest that NEU3 participates in at least 2 positive feedback loops, one with TGF-β1 driving fibrosis, and the other with IL-6 driving vascular leakage, inflammation, and fibrosis. Thus, the extent to which NEU3 - dependent bleomycin-induced vascular leakage and inflammation contribute to NEU3 – dependent bleomycin-induced fibrosis is unclear.

Given that we previously observed increased levels of NEU3 in the fibrotic lesions in the lungs of IPF patients, and that the sialidase inhibitors DANA and Oseltamivir attenuate bleomycin induced pulmonary fibrosis in mice, our results suggest that NEU3 may be a potential target for the development of therapeutics for pulmonary fibrosis.

4. INHIBITING SIALIDASE-INDUCED TGF-B1 ACTIVATION ATTENUATES PULMONARY FIBROSIS IN MICE [‡]

4.1. Summary

Pulmonary fibrosis involves the formation of inappropriate scar tissue in the lungs, but what drives fibrosis is unclear. The active form of transforming growth factor-β1 (TGF-β1) plays a key role in potentiating fibrosis. TGF-β1 is sequestered in an inactive state by a latency associated glycopeptide (LAP). Sialidases (also called neuraminidases) cleave terminal sialic acids from glycoconjugates. The sialidase NEU3 is upregulated in fibrosis, and mice lacking Neu3 show attenuated bleomycin-induced increases in active TGF-β1 in the lungs, and attenuated pulmonary fibrosis. Here we observe that recombinant human NEU3 upregulates active human TGF-β1 by releasing active TGF-β1 from its latent inactive form by desialylating LAP. Based on the proposed mechanism of action of NEU3, we hypothesized that compounds with a ring structure resembling picolinic acid might be transition state analogues and thus possible NEU3 inhibitors. Some compounds in this class showed nanomolar IC_{50}s for recombinant human NEU3 releasing active TGF-β1 from recombinant human latent inactive form. The compounds given as daily 0.1 mg/kg – 1 mg/kg injections starting at day 10 strongly attenuated lung inflammation, lung TGF-β1 upregulation, and pulmonary fibrosis at day

---

[‡] Reprinted with permission from "Inhibiting Sialidase-induced TGF-β1 Activation Attenuates Pulmonary Fibrosis in Mice." TR Karhadkar, TD Meek, and RH Gomer (2020).
DOI: https://doi.org/10.1124/jpet.120.000258

21 in the mouse bleomycin model. These results suggest that NEU3 participates in in fibrosis by desialylating LAP and releasing TGF-β1, and that the new class of NEU3 inhibitors are potential therapeutics for fibrosis.

4.2. Introduction

Fibrosis involves scar-like tissue forming in an internal organ leading to organ failure [10]. Pulmonary fibrosis has an incidence of 1 in 400 in the elderly, and there are no FDA-approved therapeutics that stop the progression of this disease [2, 12, 13]. Transforming growth factor-β1 (TGF-β1) in its active mature form is a key factor which potentiates fibrosis [101, 103]. TGF-β1 is synthesized as a precursor protein made of latency-associated peptide (LAP) and the active TGF-β1 in a complex called latent-TGF-β1 (LTGF-β1) [86, 89]. Two dimerized TGF-β1 precursor proteins are processed to cleave active TGF-β1 from the LAP, with the LAP remaining essentially wrapped around, and sequestering, the TGF-β1 [86]. There are also additional processes that takes place on the dimerized precursor protein as it passes through the endoplasmic reticulum (ER) to the Golgi complex which includes glycosylation and sialylation of the LAP sequence before the complex is secreted [86, 89-91, 219] .

Several things can release active TGF-β1 from sequestration by the LAP. Both the integrin αvβ6, which generates mechanical traction on the LAP, and thrombospondin-1 can release active TGF-β1 [220, 221]. Proteases such as plasmin, thrombin, MMP-2, and MMP-9, and reactive oxygen species- mediated conformational

changes in LAP, can also release TGF-β1 from the LAP [222-225] However, it is unclear if these are the only mechanisms that cause upregulation of active TGF-β1 in fibrotic lesions.

Neuraminic acid (also known as sialic acid) is a nine-carbon monosaccharide sugar found at the terminal ends of some glycoproteins [39, 42, 44]. The presence or absence of sialic acid on terminal ends of the these glycoconjugates have a central role in various cellular regulatory mechanisms [45, 226]. For instance, adding sialic acids to the glycan residues on immunoglobulin G (IgG) confers anti-inflammatory functions to IgG [227]. Conversely, the loss of sialic acid from the plasma protein Serum amyloid P (SAP) attenuates the potency of SAP to inhibit the differentiation of some human peripheral blood mononuclear cells (PBMC) to fibrosis-associated fibroblast-like cells called fibrocytes [47].

Neuraminidases (also known as sialidases) are enzymes that catalyze a hydrolysis reaction which removes terminal sialic acids from glycoconjugates [18, 19, 28]. There are four known mammalian sialidases [19, 28]. Of the four, the sialidase NEU3 is localized in endosomal structures and on the extracellular side of the plasma membrane, and under some conditions can also be released by cells, and thus can desialylate glycoproteins and glycolipids present outside the cell [29, 52, 207, 228, 229]. Sialidases, especially NEU3, are upregulated in pulmonary fibrosis [38, 160, 230]. TGF-β1 upregulates NEU3 in human lung epithelial cells, pulmonary fibroblasts, small airway

epithelial cells, and PBMC [160]. In the epithelial cells, TGF-β1 increases levels of NEU3 by decreasing the NEU3 degradation rate and increasing *NEU3* mRNA translation [231]. Conversely, NEU3 upregulates TGF-β1 in human PBMCs and human pulmonary fibroblasts [160]. Intratracheal delivery of bleomycin upregulates TGF-β1 in the lungs [84, 232], and is a standard model of pulmonary fibrosis in mice [151, 198]. Mice lacking NEU3, or wild-type mice treated with sialidase inhibitors, do not upregulate TGF-β1 in the lungs after bleomycin treatment, and show attenuated bleomycin-induced pulmonary fibrosis [160, 180]. Together, these observations suggested that a positive feedback loop where TGF-β1 upregulates NEU3, and NEU3 upregulates TGF-β1, may potentiate fibrosis [160, 180]. How NEU3 upregulates TGF-β1 is unknown.

In vitro, bacterial and viral sialidases can desialylate LTGF-β1, leading to the release of active mature TGF-β1, possibly explaining why there are elevated levels of active TGF-β1 levels during infection with sialidase-expressing pathogens [92, 93, 96, 210, 212]. There have been many previous attempts to develop inhibitors for viral [233] or human [155] sialidases. Examples of viral sialidase inhibitors include Tamiflu (oseltamivir) and Relenza (zanamivir), which can attenuate the progression of influenza in a patient [234-237]. Potent inhibitors for viral neuraminidases exert poor inhibition for human neuraminidases [238, 239]. There are a variety of inhibitors for human sialidases, but all have published IC_{50}s of ~10 μM for NEU3, making them relatively weak inhibitors for NEU3 [134, 155, 240-243].

In this report, we find that NEU3 desialylates LAP to release active TGF-β1. We then identified a new class of potent NEU3 inhibitors, some with IC_{50}s in the nM range. These compounds inhibit bleomycin induced pulmonary fibrosis in mice, further supporting the idea that NEU3 inhibitors may be potential therapeutics for fibrosis.

4.3. Materials and methods

4.3.1. Cell isolation and culture

Human peripheral blood was collected from healthy volunteers who gave written consent and with specific approval from the Texas A&M University human subjects review board. All methods were performed in accordance with the relevant guidelines and regulations. Blood collection, isolation of PBMC, and cell culture were done as described previously [127, 128].

4.3.2. Mouse NEU3 expression in HEK 293-f cells

HEK 293 freestyle cells (Life Technologies, Grand Island, NY) were cultured in FreeStyle 293 media (12338-018, Life Technologies). 1 x 10^5 cells were mixed with 2 μg of 100 μg/ml of murine Neu3 expression clone (MR223297, Origene, Rockville, MD) in 100 μl PBS (GE Lifesciences, Marlborough, MA), and were transfected by electroporation using a 4D-Nucleofector System (Lonza, Walkersville, MD) following the manufacturer's protocol. The transfected cells were kept at room temperature for 15 minutes for recovery, after which the cells were cultured in 25 ml Freestyle 293 media in a humidified incubator at 37 °C with 5% CO_2. After 24 hours, 400 μg/ml of G418

(345812, Calbiochem EMD, San Diego, CA) was added to select for transfected cells. After 10 days, the cells were isolated, lysed, and c-Myc tagged recombinant mouse NEU3 was purified using a Myc-Trap_A kit (ytak-20, Chromotek, Hauppauge, NY) following the manufacturer's protocol. The eluted protein was stored in 50 µl of 10% glycerol, 100 mM glycine, 25 mM Tris-HCl pH 7.3, at 4 °C.

4.3.3. Human NEU3 expression in E. coli

The human NEU3 cDNA sequence was amplified from a human NEU3 ORF clone (RC216537, Origene). The amplified NEU3 sequence was inserted between the *Nde*I and *EcoR*I sites of the pMAL-c5X vector (N8108S, NEB, Ipswich, MA). The resulting construct encoding a fusion of maltose-binding protein (MBP) and NEU3 was transformed into chemically competent *E. cloni* cells (Lucigen, Middleton, WI) mixed in 37 °C pre-warmed Luria-Bertani (LB) broth (#240230, BD, Franklin Lakes, NJ), grown with shaking at 37 °C, 240 rpm for 1 hour and plated on LB agar with ampicillin (100 µg/ml). Clones were selected and grown in 100 µg/ml ampicillin LB broth medium, and the plasmids were isolated using a GeneJET Plasmid Miniprep Kit (#K0502, Thermo Scientific, Waltham, MA). Clones were verified by sequencing (Eton Bioscience, San Diego, CA). The sequence verified clones were transformed into chemically competent BL21(DE3) *E. coli* cells (Lucigen), grown with shaking at 37 °C, 240 rpm, for 1 hour in pre-warmed LB broth, and plated on LB agar with 100 µg/ml ampicillin. Individual colonies were selected and added to 10 ml pre-warmed LB broth with 100 µg/ml ampicillin and grown at 37 °C, 240 rpm, for no longer than 16 hours. The culture was

added to 1 L of LB broth and incubated at 37 °C, 240 rpm until OD_{600} ~0.6. To induce protein expression, isopropyl β- d-1-thiogalactopyranoside (IPTG, Goldbio, St. Louis, MO) solution was added to 0.5 mM, and incubated at 20 °C at 240 rpm overnight. Protein purification was done as described previously [241] with the following modifications. Bacterial cells were harvested after 16 – 18 hours of induction by centrifugation at 4000 × g at 4 °C. The pellet was resuspended in resuspension buffer (20 mM Tris, pH 7.2, 300 mM NaCl, 1 mM EDTA and 0.1% Triton X-100) supplemented with 1x protease inhibitor (PIA32965, VWR, Radnor, PA). The lysate was sonicated three times for three minutes with the tube submerged in ice at setting 16 of a Microson ultrasonic cell disruptor (Misonix Incorporated, Farmingdale, NY), and then clarified by centrifugation at 10,000 × g for 20 minutes at 4 °C. The supernatant was loaded onto an amylose column (New England Biolabs) equilibrated with 20 mM Tris/ 300 mM NaCl, pH 7.2. MBP-NEU3 was eluted with running buffer containing 10% glycerol (v/v) and 20 mM maltose.

4.3.4. Sialidase effects on LAP assay

To determine the effect of sialidases on latency associated peptide (LAP), 400 ng/ml human recombinant latency-associated peptide (LAP), (246-LP/CF, R&D Systems, Minneapolis, MN) was incubated with and without 200 ng/ml of human recombinant sialidases NEU1 (TP300386, Origene), NEU2 (TP319858, Origene), NEU3 (TP316537, Origene), or NEU4 (TP303948, Origene), or *C. perfringens* neuraminidase (N2876-2.5UN, Sigma-Aldrich, St. Louis, MO) in a total volume of 20 µl of 1x

phosphate buffered saline (PBS; #SH30256.01, GE Lifesciences) pH 6.9. The PBS was adjusted to pH 6.9 with 12N HCl (H613-05, Avantor Performance Materials, Radnor Township, PA). The reaction mixtures were incubated at 37 °C for 2 hours. Following incubation, 5 µl of 4x Laemmli's buffer (GTX16355, GeneTex, Irvine, CA) containing 20 mM dithiothreitol was added to the reaction mixtures, and these were heated at 100 °C for 5 minutes. 15 µl of the heated reaction mixture was electrophorized on a 4-20% Tris/glycine polyacrylamide pre-cast gel (12001-058, VWR, Radnor, PA) in Tris/glycine/SDS running buffer (13.5 g Tris base, 7.2 g glycine, 5 g SDS / liter) at room temperature for 90–120 minutes.

Western blots, and staining the blots with lectin, was done as previously described [47], and immunostaining western blots for NEU3 was done as previously described [160, 180]. Silver staining of gels was done following [244]. Staining intensity was quantified by Image Lab software (Bio Rad, Hercules, CA).

4.3.5. NEU3 induced L-TGF-β1 activation assay

To determine if NEU3 can cause latent transforming growth factor-β1 (L-TGF-β1) to release active TGF-β1, 200 ng/ml recombinant human latent transforming growth factor-β1 (L-TGF-β1) (299-LT/CF, R&D Systems) was incubated with varying concentrations of recombinant human NEU3 (TP316537, Origene) or bacterially expressed recombinant human NEU3, in a total volume of 100 µl of PBS pH 6.9 in a 96-well microplate. The microplates were covered with aluminum foil and incubated at 37

°C for 2 hours. Following incubation, the reaction mixtures were assayed using an active TGF-β1 ELISA kit (DY240, R&D Systems) following the manufacturer's protocol with the exception that the reaction mixtures were not processed for acid treatment, so as to measure only active TGF-β1 and not total TGF-β1. The absorbance was read with a SynergyMX plate reader (BioTek, Winooski, VT). To determine the enzyme kinetics of NEU3 with L-TGF-β1 as a substrate, varying concentrations of L-TGF-β1 were incubated with 100 ng/ml of recombinant human NEU3 (Origene), in a total volume of 100 µl, and the samples were processed as described above.

4.3.6. Sialidase activity assay with 2′-(4-methylumbelliferyl)-α-D-N-acetylneuraminic acid sodium salt hydrate (4MU-NANA)

Sialidase assays were done following [134, 135] with the following modifications. PBS was adjusted to pH 6.9 with 12N HCl and bovine serum albumin (BSA, VWR) was added to a final concentration of 100 µg/ml (PBS-BSA). Varying concentrations of bacteriailly expressed recombinant human NEU3 were prepared in PBS-BSA. A final concentration of 200 µM 4MU-NANA (M8639, Sigma-Aldrich) was added to the NEU3 in a total volume of 100 µl in a 96-well plate. Where indicated, inhibitors were added for 30 minutes before adding the 4MU-NANA. The reactions were incubated at 37 °C for 30 minutes, and the fluorescence was measured at 37 °C in a prewarmed SynergyMX plate reader with excitation at 360 nm and emission at 440 nm. The fluorescence in the absence of sialidases was subtracted from all readings.

4.3.7. Inhibition of NEU3 induced L-TGF-β1 activation

2,3-didehydro-2-deoxy-N-acetyl-neuraminic acid (DANA) was purchased from EMD-Millipore (Burlington, MA), Oseltamivir phosphate (Tamiflu) was purchased from Sigma, 2-acetyl pyridine (sc-254121) and methyl picolinate (sc-228575) were from Santa Cruz Biotechnology (Dallas, TX), and 2-piperidinecarboxylic acid, 4-amino-1-methyl (A00285-13785-026) was from Sundia (Shanghai, China). These compounds were dissolved in water to 20 mM. All stocks were stored at 4 °C and used within 2 weeks of preparation. Dilution series of the compounds were made in PBS pH 6.9. 100 µl of diluted compound was added to the well of a 96 well plate and then 50 µl of 400 ng/ml recombinant human sialidase NEU3 (TP316537,Origene) in PBS pH 6.9 was added to each well (50 µl PBS pH 6.9 for the control), and the plate was incubated for 30 minutes at 37 °C. 50 µl of 800 ng/ml L-TGF-β1 (299-LT/CF, R&D Systems) in PBS pH 6.9 was then added to the well. The plate was covered with aluminum foil and incubated for 2 hours at 37 °C, and released active TGF-β1 was assayed as described above.

4.3.8. Inhibition of NEU3 induced IL-6 accumulation

Dilutions of the above compounds were made in serum-free medium prepared as previously described [127, 180], and 50 µl of diluted compound was added to the well of a 96 well plate and then 50 µl of 400 ng/ml recombinant human sialidase NEU3 (TP316537, Origene) in serum-free medium was added to each well (50 µl serum-free medium for control), and the plate was incubated for 30 minutes at 37 °C in a humidified incubator with 5% CO_2. 100 µl of PBMC at 1 x 10^5 cells/ml was then added to the well

to make the total volume in a well 200 µl with 1 x 10^4 cells/well, and this was incubated at 37 °C in a humidified incubator with 5% CO_2 for 48 hours. IL-6 in the culture supernatant was then assayed with an IL-6 ELISA kit (430501, BioLegend, San Diego, CA) following the manufacturer's protocol, reading absorbance with a SynergyMX plate reader (BioTek). At least three different donors were used for each assay.

4.3.9. Mouse model of pulmonary fibrosis

To determine if the NEU3 inhibitors affect pulmonary fibrosis in mice, 8-10 week old 26–30 g male C57BL/6 mice (Jackson Laboratories, Bar Harbor, ME) were given an oropharyngeal aspiration of 3 units/kg bleomycin (2246-10, BioVision Incorporated, Milpitas, CA) in 50 µl of 0.9% saline to induce symptoms of pulmonary fibrosis or oropharyngeal saline alone as a control as previously described [47, 111, 130]. Starting 10 days after bleomycin had been administered, some of the bleomycin-treated mice were given daily intraperitoneal injections of 100 µl of PBS or 1 mg/kg 2-acetyl pyridine, 1 mg/kg methyl picolinate, or 0.1 mg/kg of 2-piperidinecarboxylic acid, 4-amino-1-methyl in 100 µl PBS. All mice were weighed daily for 21 days after bleomycin was adminstered. At day 21, mice were euthanized by CO_2 inhalation, and bronchoalveolar lavage (BAL) fluid and cell-spots of BAL cells were obtained as previously described [47, 111, 130, 131]. The liver, heart, kidneys, spleen, white fat tissue, and brown fat tissue were removed and weighed. The total cells from BAL cell-spots were quantified as described previously [111, 131]. The lungs were removed and inflated with Surgipath frozen section compound (3801480, Leica, Buffalo Grove, IL)

and preserved at -80 °C. 6–10 μm cryosections of lungs were placed on glass slides (48311-703, VWR) and were air dried for 48 hours before use. The mouse experiments were performed in accordance with the recommendations in the Guide for the Care and Use of Laboratory Animals of the National Institutes of Health. The Texas A&M University Animal Use and Care Committee approved the protocol (IACUC 2017-0414).

4.3.10. Histology, immunohistochemistry, and BAL analysis

Air dried cryosections were stained with hematoxylin and eosin or with Sirus red to detect collagen, or with 1 μg/ml anti-active TGF-β1 antibodies (AB-100-NA, R&D Systems, Minneapolis, MN) as described previously [15, 160]. The staining was quantified with ImageJ [143, 144]. Immunohistochemistry on BAL cell-spots and cryosections was performed as described previously [47, 111, 130, 180] using anti-CD11b (101202, clone M1/70 BioLegend) to detect blood and inflammatory macrophages, anti-CD11c (M100-3, clone 223H7, MBL International, Woburn, MA) to detect alveolar macrophages and dendritic cells, anti-CD45 (103102, clone 30-F11, BioLegend) for total leukocytes, anti-Ly-6G (127602, clone 1A8, BioLegend) to detect neutrophils, and anti-Ly-6C (128001, clone HK1.4, BioLegend) to detect a variety of inflammatory immune system cells, and with isotype-matched irrelevant antibodies (BioLegend) as controls. SDS-PAGE analysis of BAL, and nanodrop protein assays, were performed as described previously [14, 160, 180].

4.3.11. Hydroxyproline assay

Hydroxyproline assays were performed as described previously [180] with the exception that approximately half lobes of lungs frozen in OCT were cut off in three pieces, thawed, and washed three times with 0.5 ml PBS to remove OCT by centrifugation at 2000 × g for 5 minutes in pre-weighed Eppendorf tubes. After the last centrifugation, the tubes were kept inverted for 5 minutes to allow PBS to blot onto blotting paper, and the tissue was then weighed. Tissues were then processed using a hydroxyproline quantification kit (MAK008-1KT, Sigma-Aldrich) following the manufacturer's directions.

4.3.12. Statistical analysis

Data were analyzed by t-test or ANOVA using Prism 7 (GraphPad, La Jolla, CA). Significance was defined as $p < 0.05$. IC_{50} curves for enzyme assays were generated using the Dose Response - Inhibition curve fitting model with variable slope with Prism 7.

4.4. Results

4.4.1. Recombinant human NEU3 desialylates recombinant human LAP and releases active TGF-β1

Neuraminidases from influenza virus and bacteria remove sialic acid from the LAP protein, which causes the LAP to release active TGF-β1 [92, 93, 210]. To determine the effect of recombinant human sialidases on recombinant human LAP

(rhLAP), we incubated recombinant human sialidases (made in HEK293 cells) or *C. perfringens* neuraminidase [47] with rhLAP. Western blots of the rhLAP were stained with *Sambucus nigra* lectin to detect sialic acids [36, 245]. NEU3, NEU4, and *C. perfringens* neuraminidase significantly decreased sialic acid on rhLAP (Figures 31 a and b).

We previously found that the addition of recombinant human NEU3 (rhNEU3) to human immune cells, pulmonary fibroblasts, and small airway epithelial cells causes them to upregulate extracellular and intracellular TGF-β1 [160]. To determine if NEU3 causes recombinant human latent TGF-β1 (rhL-TGF-β1) to release active TGF-β1, we incubated rhL-TGF-β1 with rhNEU3, and measured released active TGF-β1. rhNEU3 did cause a release of active TGF-β (Figure 31 c). Together, these results suggest that NEU3 removes sialic acid from the LAP protein and releases active TGF-β1 from rhL-TGF-β1.

The standard assay for sialidases is cleavage of the fluorogenic substrate 2′-(4-Methylumbelliferyl)-α-D-N-acetylneuraminic acid (4MU-NANA) [134]. At concentrations of rhNEU3 up to 100 ng/ml (1.94 nM), and using 4MU-NANA with no enzyme as a control, we were unable to detect statistically significant activity of rhNEU3 on 4MU-NANA. Compared to commercially available HEK-293 cell-synthesized rhNEU3, we were able to purify much higher amounts of a bacterially expressed fusion of the 42 kDa maltose binding protein with the 51 kDa human NEU3

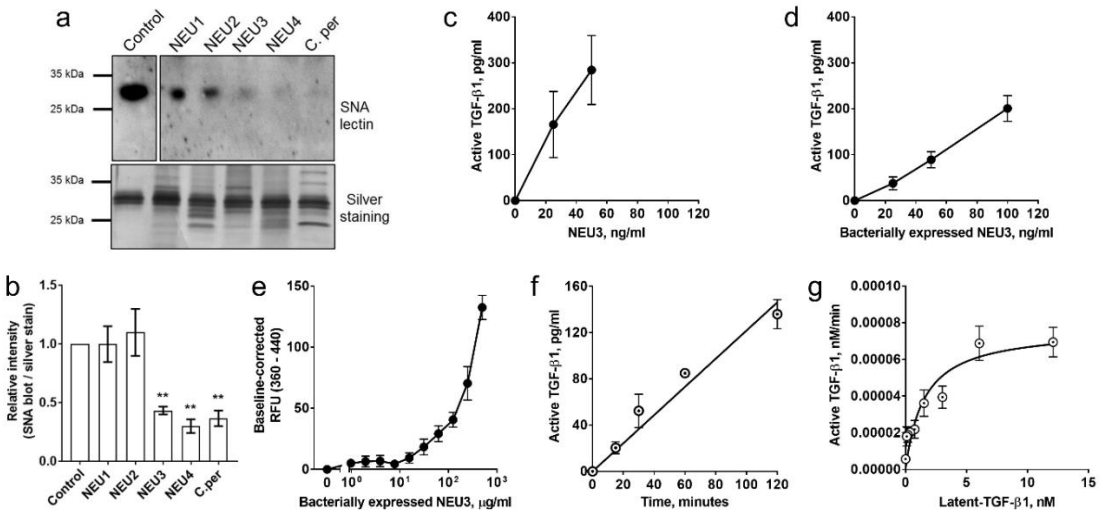

Figure 31. Recombinant human NEU3 releases active TGF-β1 by desialylating recombinant human latency associated protein (LAP).
(a) Recombinant human LAP protein was incubated with or without recombinant human sialidases NEU 1 – 4 or *C. perfringens* neuraminidase, and a western blot was stained with *Sambucus nigra* lectin (SNA) (top panel), to detect sialic acids on glycoconjugates. Black bands are the LAP protein. Silver staining (bottom panel) was done as a loading control. Blots and silver staining are representative of three independent experiments. Degradation products from the sialidases are also visible in the silver stained gel in addition to the LAP protein. **(b)** The western blots from (A) were quantified for *Sambucus nigra* staining of LAP protein. Values are mean ± SEM, n = 3. ** $p \leq 0.01$ (1-way ANOVA, Bonferroni's test compared to control). **(c)** An ELISA assay, specific for active TGF-β1, was performed on recombinant human latent-TGF-β1 (rhL-TGF-β1) treated with the indicated concentrations of recombinant human NEU3. Values are mean ± SEM, n = 6. Purified bacterially expressed recombinant human MBP-NEU3 was assayed for effects on **(d)** rhL-TGF-β1 and **(e)** hydrolysis of the substrate 4MU-NANA to release fluorophore 4MU. Values are mean ± SEM, $n \geq 3$. **(f)** Release of active TGF-β1 as a function of time by 1.94 nM recombinant human NEU3 from 3 nM rhL-TGF-β1. Values are mean ± SEM, n = 4. **(g)** Kinetics of recombinant human NEU3 activity in the TGF-β1 release assay. Values are mean ± SEM, n = 4.

(brhNEU3; Figure 32 a and b). The ~93 kDa brhNEU3 contained a contaminant band that stained weakly for NEU3 on western blots (Supplemental Figure 1A and B), so the concentration of bhrNEU3 was estimated by comparison of the ~93 kDa band to BSA standards on silver-stained gels. The brhNEU3 caused a release of active TGF-β1 from

rhL-TGF-β1, albeit with somewhat lower efficacy than rhNEU3 (Figures 31 c and d). Compared to rhL-TGF-β1 as a substrate, a much higher concentration of brhNEU3 was required to obtain detectable cleavage of 4MU-NANA (Figures 31 c, d, and e).

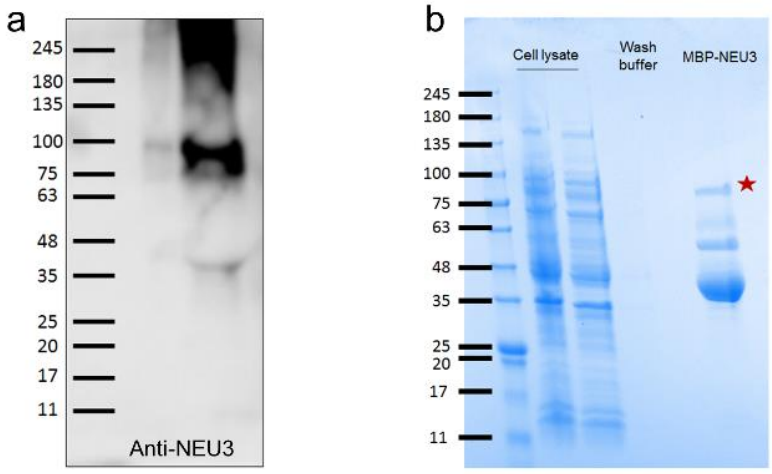

Figure 32. Recombinant human NEU3 purified from bacteria.
(a) A western blot of purified MBP-NEU3 was stained with anti-NEU3 antibodies, showing a band at the expected molecular mass of ~93 kDa, (**b)** A gel of the indicated fractions was stained with Coomassie. The desired MBP-NEU3 is marked with a star (★).

A previous study with 4MU-NANA as the substrate for NEU3 reported a K_m of 45 ± 3 μM and a k_{cat} of 0.33 ± 0.02 min^{-1} and thus a catalytic efficiency k_{cat} / K_m of 0.007 ± 0.006 μM^{-1} min^{-1} [241]. Using rhL-TGF-β1 as the substrate for rhNEU3, and, measuring the rate of TGF-β1 release for different concentrations of rhL-TGF-β1 (Figures 31 f and g), we observed a K_m of 1.5 ± 0.5 nM and a k_{cat} of (4.0 ± 0.4) x 10^{-5} min^{-1} (both mean ± SEM, n = 4), and thus a k_{cat} / K_m of 0.026 ± 0.008 μM^{-1} min^{-1}. The lower K_m and higher k_{cat} / K_m for rhL-TGF-β1 compared to 4MU-NANA suggest a

higher affinity of NEU3 for rhL-TGF-β1 compared to 4MU-NANA as a substrate. Together, these results suggest that rhL-TGF-β1 can be used as a better substrate than 4MU-NANA for a more sensitive assay to determine NEU3 activity.

4.4.2. Design of NEU3 inhibitors

We designed possible inhibitors of human NEU3 based in part on the structure of 2,3-didehydro-2-deoxy-N-acetyl-neuraminic acid (DANA) (Figure 33 a), a known inhibitor of NEU3 (K_i = 30 μM) [239]. DANA contains a double bond, of which the sp^2-hybridized carbon-2 (circled) may be a structural mimic of the putative oxacarbenium ion intermediate (OCI) (Figure 33, a and b) of the chemical mechanism of enzymatic catalysis [241]. As DANA lacks the positive charge of the OCI, a better mimic of this putative reaction intermediate is likely afforded by the tetrahydropyridine-1-ium-2-carboxylate (THPC) (Figure 33 c) which provides the positive charge, but at the expense of sp^2-hybridized carbon-2. Consequently, we pursued substituted picolinic acids, which contain both a cationic nitrogen atom and sp^2-hybridization at carbon-2 (Figure 33 d), as well as a substituted pipecolinic acid (compounds 3-5 in Table 3).

4.4.3. Compounds 3 – 5 from Table 3 inhibit NEU3 release of TGF-β1

To test the hypothesis that compounds 3-5 inhibit NEU3, we assayed their effects in the rhNEU3 - rhL-TGF-β1 release of active TGF-β1 reaction (Table 3 and Figure 34). Picolinates like 2-acetyl pyridine (2AP) and methyl picolinate

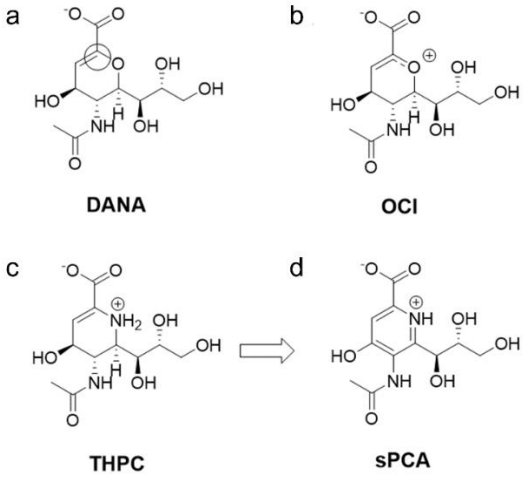

Figure 33. Schematic representation of the rationale for design of NEU3 inhibitors.
Structures of **(a)** 2,3-didehydro-2-deoxy-N-acetyl-neuraminic acid (DANA), **(b)** the predicted oxacarbenium ion intermediate (OCI), **(c)** tetrahydropyridine-1-ium-2-carboxylate (THPC), and **(d)** a substituted picolinic acid analogue of OCI (sPCA).

Table 3. Compounds used in NEU3 activity assays.
List of commercially available compounds used in the NEU3 induced release of active TGF-β1 assay and the cell-based NEU3-induced upregulation of IL-6 assay to determine IC50. The IC50 values are mean ± SEM, n ≥ 3.

No.	Compound Name	Compound structure	IC_{50}, μM	
			TGF-β1 assay	IL-6 assay
1	2,3-didehydro-2-deoxy-N-acetyl-neuraminic acid (DANA)	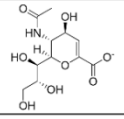	> 100	7.4 ± 3.7
2	Oseltamivir phosphate (Tamiflu)	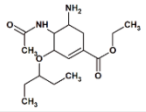	0.51 ± 0.34	0.020 ± 0.001
3	2-acetyl pyridine (2AP)	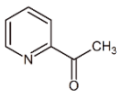	0.040 ± 0.006	0.05 ± 0.03
4	Methyl picolinate (MP)	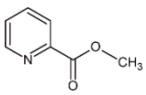	< 0.002	0.47 ± 0.08
5	4-amino-1-methyl-2-piperidine carboxylic acid (AMPCA)	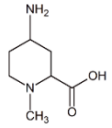	< 0.002	< 0.002

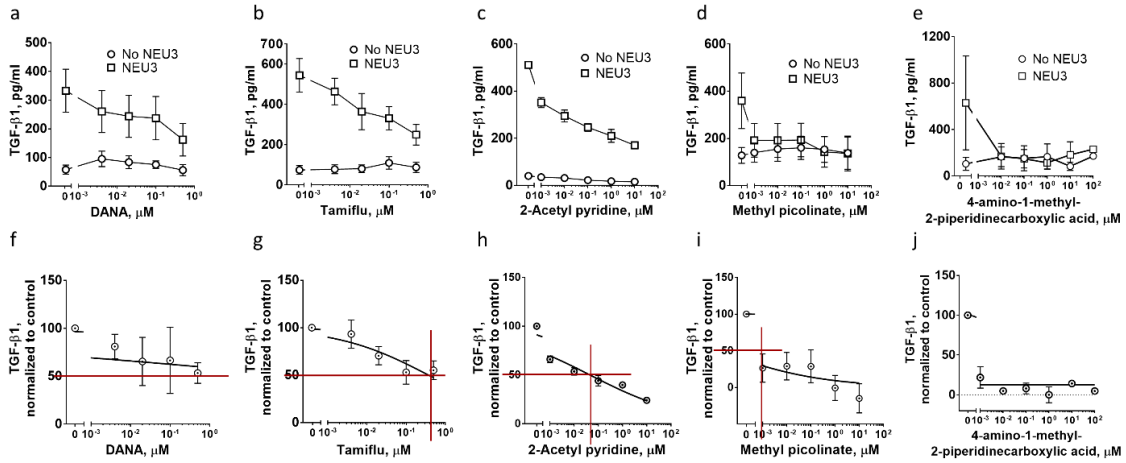

Figure 34. Inhibition of recombinant human NEU3-catalyzed release of active TGF-β1 by compounds from Table 3.
Compounds labelled on the X-axis of graphs **(a)** to **(e)** were incubated at the indicated concentrations with and without recombinant human NEU3 in PBS pH 6.9. rhL-TGF-β1 was added as substrate, and the release of active TGF-β1 was quantified by an ELISA kit. Values are mean ± SEM, n ≥ 3. The NEU3-catalyzed release of active TGF-β1 was determined by subtracting active TGF-β1 values in the absence of NEU3 from active TGF-β1 values in the presence of NEU3 in the data from (a – e). The baseline corrected values were normalized to the percent of active TGF-β1 in the absence of the compound (0 μM of inhibitor). **(f)** – **(g)** IC_{50} values (red lines) were determined from the normalized values by non-linear regression curve fitting. Values are mean ± SEM, n ≥ 3.

(MP) had higher potencies of inhibiting rhNEU3 activity compared to DANA and oseltamivir phosphate (Tamiflu) (Table 3, Figure 34 a – d and f – i), which supported our rationale for potential NEU3 inhibitors. The fully-saturated pipecolinic acid compound, 4-amino-1-methyl-2-piperidine carboxylic acid (AMPCA), was also a very potent inhibitor of NEU3 (Table 3, Figure 34 e and j) despite its lack of an adjacent sp^2-hybridized carbon as in the case of the picolinate inhibitors. These results suggest the cationic nitrogen and an adjacent keto or carboxylate group provided the essential structural elements to effect potent inhibition of rhNEU3, possibly via mimicry of the

enzymatic transition state structure, and that these inhibitors are significantly improved over DANA and oseltamivir when rhL-TGF-β1 is the substrate.

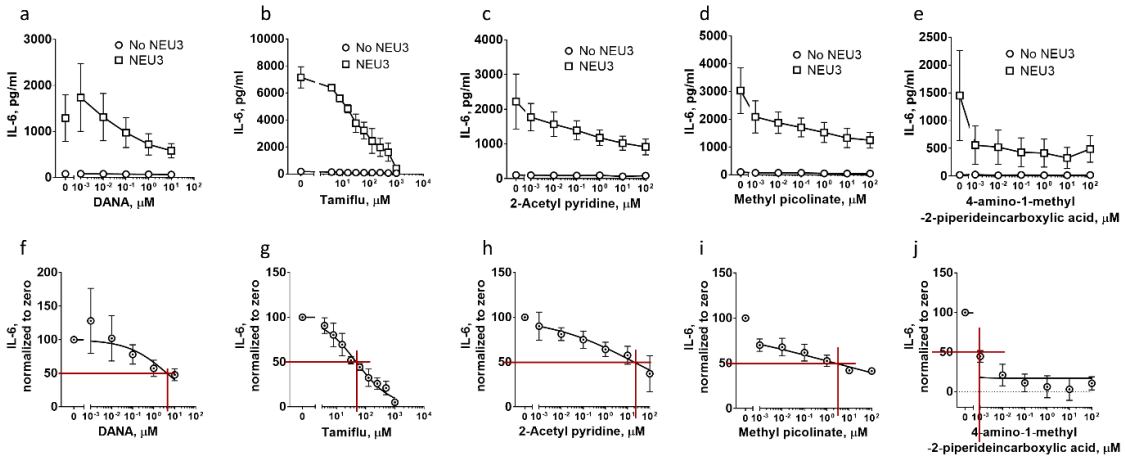

Figure 35. Inhibition by compounds from Table 3 of recombinant human NEU3-induced extracellular accumulation of IL-6 from human PBMCs.
Compounds labelled on the X-axis of graphs **(a)** to **(e)** were incubated at the indicated concentrations with and without recombinant human NEU3 in serum free media. After 30 minutes, human PBMCs were added and incubated at 37 °C, 5% CO_2. 48 hours later media supernatants were assayed for IL-6. Values are mean ± SEM, n ≥ 3. The NEU3-induced extracellular accumulation of IL-6 was determined by subtracting IL-6 values in the absence of NEU3 from IL-6 values in the presence of NEU3 in the data from (a – e). The baseline corrected values were normalized to the percent of IL-6 value in the absence of the compound (0 μM of inhibitor). **(f) – (j)**. IC_{50} values (red lines) were determined from the normalized values by non-linear regression curve fitting. Values are mean ± SEM, n ≥ 3.

4.4.4. Compounds 3-5 inhibit NEU3-induced extracellular accumulation of IL-6 by human immune cells

rhNEU3 upregulates extracellular accumulation of IL-6 from human PBMC [180]. We also measured the effects of inhibitors in a NEU3-induced IL-6 release by human immune cells assay (Table 3 and Figure 35). DANA, Tamiflu, 2AP, and MP all inhibited rhNEU3 in the cell-based NEU3-induced IL-6 release assay (Table 3, Figures

35 a – d and f – i). Compared to the other compounds, the pipecolinate AMPCA had an increased inhibition potency (Table 3, Figure 34 e and j). These results suggest that some picolinates and a pipecolinate can be used as inhibitors against NEU3 in cell-based or *in-vivo* assays. The differences in inhibition potencies in the cell-based extracellular IL-6 accumulation assay and *in-vitro* TGF-β1 based assay may be due to the presence or absence of factors that interact with NEU3 and/or the inhibitors in the cell-based IL-6 assay compared to the buffer-based TGF-β1 release assay.

4.4.5. NEU3 inhibitors inhibit mouse NEU3

To determine if compounds 3-5 would be effective in mice, we tested them against recombinant mouse NEU3 in the NEU3-induced release of active TGF-β1 assay. The IC_{50} of 2AP was 0.8 ± 1.7 μM, MP was 3.2 ± 1.6 nM, and AMPCA was less than 1 nM (Figure 36 A – F). These results suggest that the three selected NEU3 inhibitors are inhibitors of mouse NEU3.

4.4.6. AMPCA attenuates weight loss of mice after bleomycin treatment

To determine if NEU3 inhibitors affect bleomycin-induced pulmonary fibrosis, C57BL/6 mice were treated with an oropharyngeal aspiration of saline or bleomycin and then starting 10 days after saline or bleomycin, mice were given daily intraperitoneal injections of 1 mg/kg 2AP or MP, or 0.1 mg/kg AMPCA. As previously observed, compared to saline treated-control mice, bleomycin-treated control mice had lower body weights at day 21 after bleomycin aspiration (Figure 37 a). In saline-treated mice, 2AP,

MP, and AMPCA did not significantly affect body weights. AMPCA attenuated the bleomycin-induced weight loss (Figure 37 a). 2AP, MP, and AMPCA did not significantly affect liver, heart, kidneys, spleen, white fat or brown fat weights as percent of total body weight (Figure 38 a – f). Together these results suggest that AMPCA attenuates bleomycin-induced weight loss in mice.

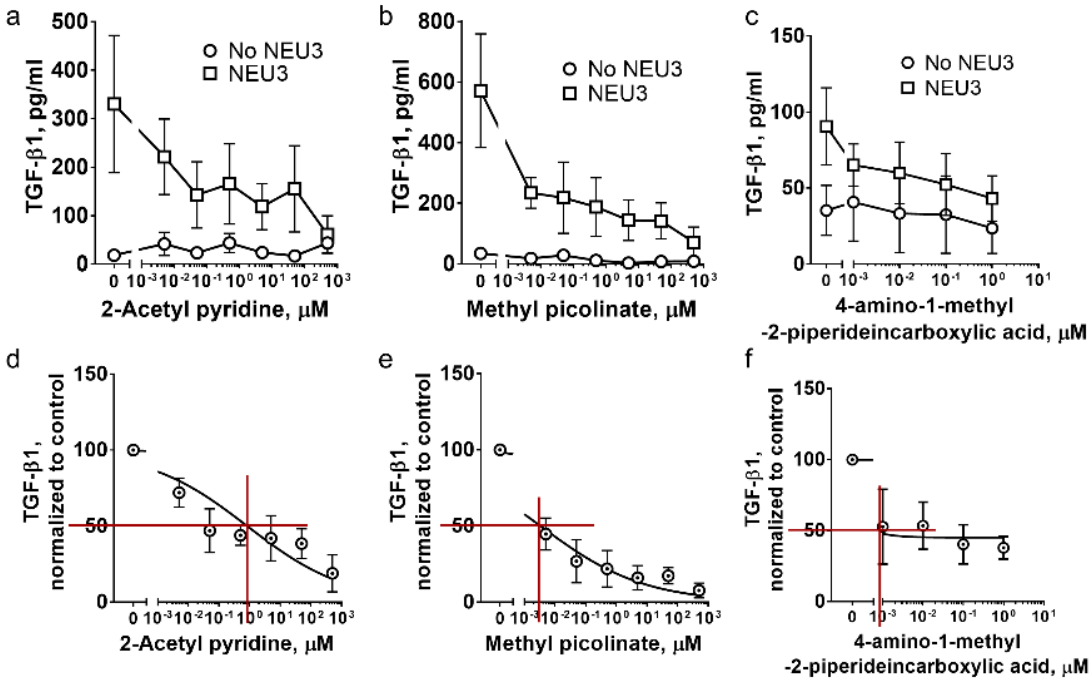

Figure 36. NEU3 inhibitors inhibit recombinant mouse NEU3-catalyzed release of active TGF-β1.
(a – c) The indicated compounds were incubated with and without recombinant mouse NEU3. rhL-TGF-β1 was added as a substrate, and the release of active TGF-β1 was quantified. Values are mean ± SEM, n ≥ 3. **(d – f)** IC_{50} values were determined as described for Figure E4. Values are mean ± SEM, n ≥ 3.

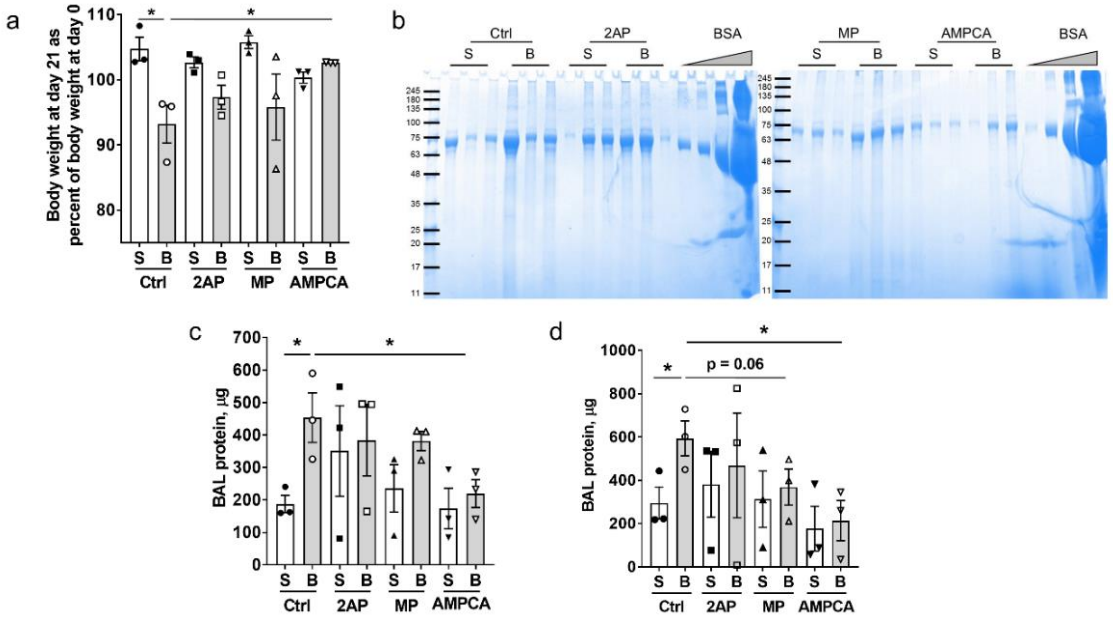

Figure 37. AMPCA attenuates bleomycin-induced decline in body weight and protein increase in the BAL fluid at day 21 after bleomycin treatment.
(a) Percent change in body weight after saline (S) or bleomycin (B) treatment at day 0, and then at day 10 starting daily intraperitoneal injections of PBS (Ctrl), 2 acetyl pyridine (2AP), Methyl picolinate (MP), or 4-amino-1-methyl-2-piperidie carboxylic acid (AMPCA). Values are mean ± SEM, n = 3. * $p \leq 0.05$ (t test). BAL fluid was collected at day 21 following saline or bleomycin (bleo) treatment and 2AP, MP, or AMPCA i.p. injections. **(b)** BAL fluids from the indicated mice were analyzed by PAGE gels stained with Coomassie. Molecular mass markers in kDa are at left and in the center. Bovine serum albumin (BSA) at 0.01, 0.1, 1.0, and 10.0 µg was loaded at right on each gel. **(c)** Quantification of protein by densitometry in lanes from panel a, using the BSA band densities as standards, and then for each mouse multiplying by the BAL volume to obtain total BAL protein. S indicates saline and B indicates bleomycin. **(d)** Quantification of protein from BAL as in panel b, using a nanodrop assay to obtain BAL protein concentrations and then for each mouse multiplying by the BAL volume to obtain total BAL protein. S indicates saline and B indicates bleomycin. For b and c, values are mean ± SEM, n = 3. * $p < 0.05$ (t test).

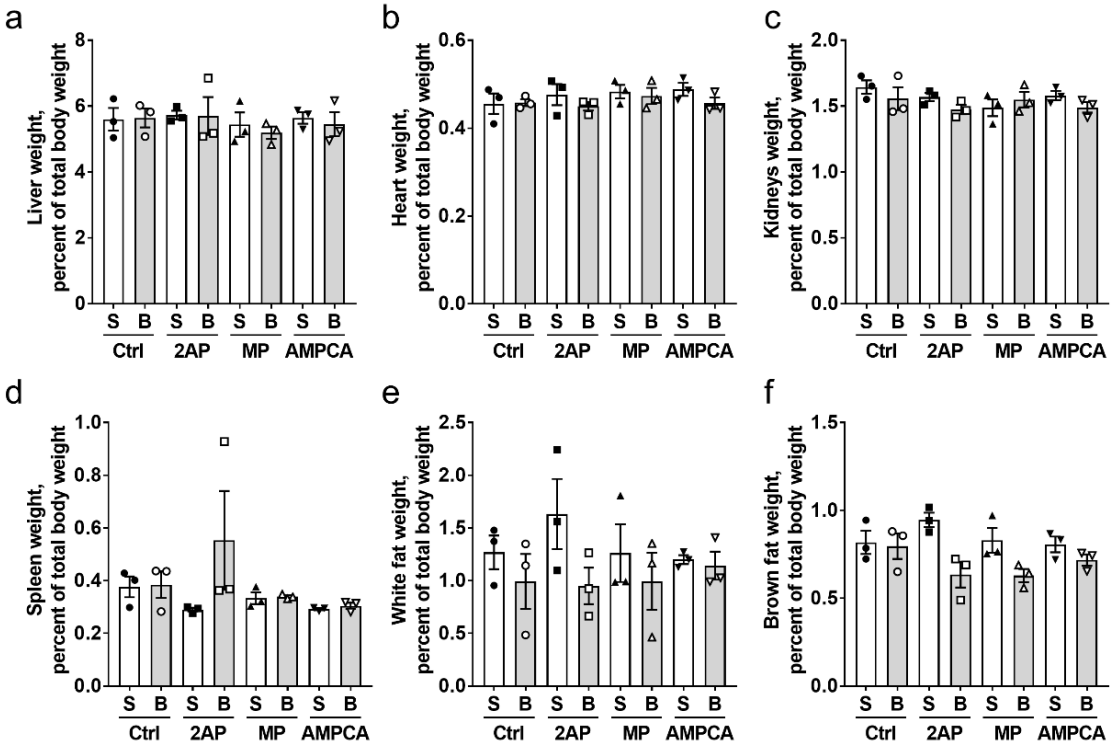

Figure 38. Injections of 2AP, MP, or AMPCA from day 10 after bleomycin treatment had no significant effect on organ weights.
Weights of **(a)** Liver, **(b)** Heart, **(c)** Kidneys, **(d)** Spleen, **(e)** White fat, and **(f)** Brown fat as percent of total body weight at day 21 after saline (S) or bleomycin (B) treatment. Values are mean ± SEM, n = 3. There were no significant changes (1way ANOVA, Bonferroni's test).

4.4.7. AMPCA attenuates protein increase in the BAL fluid at day 21 after bleomycin treatment

Bleomycin causes an increase in protein levels in the bronchoalveolar lavage fluid (BAL) from mouse lungs [111, 188, 189]. To determine if inhibiting NEU3 affects these BAL protein levels, we measured the protein in the BAL as a measure of lung tissue damage post bleomycin treatment. As observed previously [111, 180, 188, 189], at day 21, compared to saline-treated control mice, bleomycin-treated control mice showed

upregulated BAL protein levels (Figure 37 b – d). Compared to saline-treated control, the saline-treated 2AP, MP, or AMPCA injected mice had no significant difference in the levels of proteins in the BAL as assayed by either gel densitometry (Figure 37 b – c) or nanodrop (Figure 37 c). AMPCA treatment significantly attenuated the bleomycin-induced increase of protein levels in the BAL (Figure 37 b – d). Although 2AP and MP seemed to decrease BAL protein levels in bleomycin-treated mice, the effect was not statistically significant. We previously observed that Tamiflu treatment, but not DANA treatment, attenuated bleomycin-induced increased protein levels in the BAL [160]. Together, these results suggest that some NEU3 inhibitors can attenuate bleomycin-induced upregulation of protein levels in the BAL.

4.4.8. NEU3 inhibitors attenuate the increased number of inflammatory cells in the BAL at day 21 after bleomycin treatment

Bleomycin aspiration also causes an upregulation of inflammatory cells in the BAL at day 21 [47, 107, 111, 130]. Compared to saline-treated control mice, the bleomycin- treated control mice showed upregulated BAL cell counts (Figure 39 a). The saline-treated control mice and saline-treated and 2AP, MP, or AMPCA injected mice showed similar BAL cell counts (Figure 39 a). Compared to saline-treated mice, bleomycin-treated and MP or AMPCA injected mice showed upregulated BAL cell counts, but these were significantly less compared to bleomycin-treated control mice (Figure 39 a). In the BAL

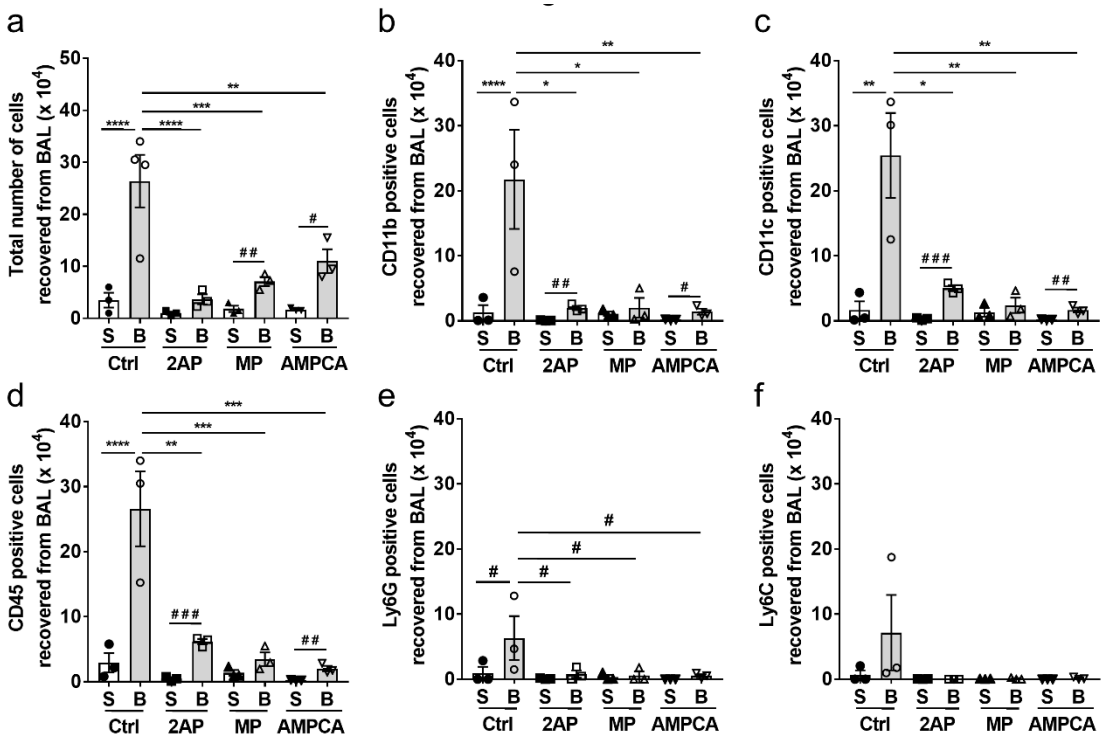

Figure 39. 2AP, MP, or AMPCA from day 10 after bleomycin treatment decrease BAL cells.

(a) The total number of cells in mouse BAL after the indicated treatment. S indicates saline and B indicates bleomycin. Values are mean ± SEM, n ≥ 3 mice per group. ** $p < 0.01$, *** $p < 0.001$, and **** $p < 0.0001$ (1way ANOVA, Bonferroni's test). # $p < 0.05$ and ## $p < 0.01$ (t-test). BAL cell-spots at day 21 were stained for the markers **(b)** CD11b, **(c)** CD11c, **(d)** CD45, **(e)** Ly6G, and **(f)** Ly6C. The percent of cells stained was determined in 5 randomly chosen fields of 100-150 cells, and the percentage was multiplied by the total number of BAL cells for that mouse to obtain the total number of BAL cells staining for the marker. Values are mean ± SEM, n = 3. * $p < 0.05$, *** $p < 0.001$, **** $p < 0.0001$ (1-way ANOVA, Bonferroni's test), # $p < 0.05$, ## $p < 0.01$, and ### $p < 0.001$ (t-test).

resident alveolar macrophages (Figure 39 c), CD45 positive leukocytes (Figure 39 d), and Ly6G positive cells (Figure 39 e). Significant differences were not observed for Ly6C positive cells (Figure 39 f). The BAL of saline-treated control mice, and saline-treated and 2AP, MP, or AMPCA treated mice, showed similar counts of the above cell

types (Figure 39 b – f). Compared to BAL from saline-treated mice, bleomycin-treated 2AP or AMPCA injected mice showed upregulated counts of CD11b positive cells (Figure 39 b), CD11c positive cells (Figure 39 c), and CD45 positive cells (Figure 39 d) in the BAL, but these counts were significantly less compared to bleomycin-treated control mice. The MP injected mice did not show significantly increased counts of the above cell types in the BAL of saline-treated or bleomycin-treated mice (Figure 39 b – f). Together, these data suggest that NEU3 inhibitors attenuate the bleomycin-induced increase of inflammatory cell counts in the BAL.

Lung sections were also stained to detect inflammatory cells. As previously observed [180], bleomycin increased the counts of CD11b+, CD11c+, and CD45+ cells remaining in the lungs after BAL (Figure 40 a – c), but did not affect the counts of Ly6G+ or Ly6C+ cells (Figure 40 d – e). 2AP, MP, or AMPCA did not affect the counts of CD11b+ and CD11c+ cells (Figure 40 a – b), but 2AP and MP significantly counteracted the increase in CD45+ cells in the lungs after BAL at day 21 (Figure 40 c). Together, these results suggest that some NEU3 inhibitors attenuate the upregulation of some leukocytes remaining in the lungs after BAL at day 21 post bleomycin treatment.

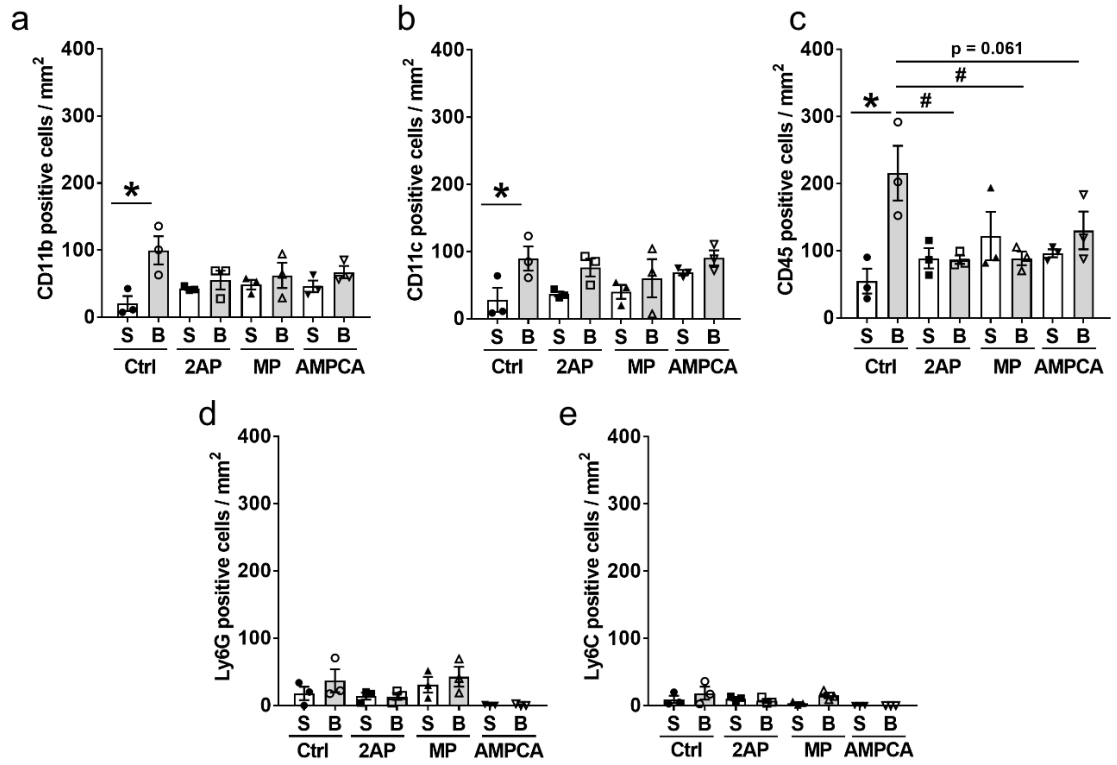

Figure 40. Remaining immune cells in lungs post BAL.
Cryosections of mouse lungs were stained for **(a)** CD11b, **(b)** CD11c, **(c)** CD45, **(d)** Ly6G, and **(e)** Ly6C, and cells in 5 randomly chosen 0.45 mm diameter fields of view were counted, and the number was then calculated to number per mm^2. Values are mean ± SEM, n = 3. * $p < 0.05$ (1-way ANOVA, Bonferroni's test). # $p < 0.05$ (t-test).

4.4.9. NEU3 inhibitors decrease fibrosis

To determine if inhibiting NEU3 can decrease bleomycin-induced fibrosis, lung sections were stained with hematoxylin and eosin to detect tissue, picrosirius red to detect total collagen, and hydroxyproline levels were measured in the lung tissue lysates. As previously observed [182, 198-200], bleomycin treatment caused fibrosis in the

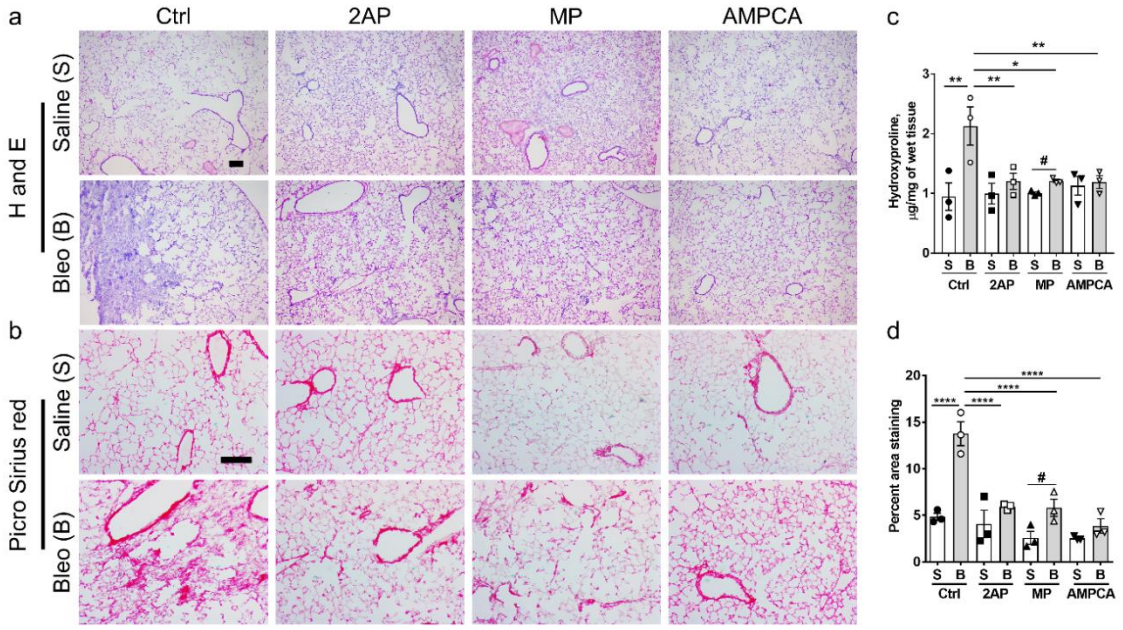

Figure 41. 2AP, MP, or AMPCA injections starting at day 10 after bleomycin attenuate fibrosis.
Sections of lung tissue from mice treated with saline or bleomycin, and then injected daily with control or 2AP or MP or AMPCA starting at day 10 after bleomycin, and then euthanized at day 21, were stained with **(a)** H&E, and **(b)** picrosirius red to show collagen content. All images are representative of 3 mice per group. In both (a) and (b), Bar is 200 µm. **(c)** Hydroxyproline in lungs. Values are mean ± SEM, n = 3. * $p < 0.05$ and ** $p < 0.01$ (1-way ANOVA, Bonferroni's test). # $p < 0.05$ (t-test). **(d)** Picrosirius red quantification analyzed by selecting 5 random fields of view of the sizes shown in (B) for each mouse, and the average percent area of the field of view showing staining for each mouse was measured. Values are mean ± SEM, n = 3. **** $p < 0.0001$ (1-way ANOVA, Bonferroni's test). # $p < 0.05$ (t-test).

mouse lungs at day 21 (Figure 41 a – d and Figure 42). Compared to saline treatment, lungs from mice exposed to bleomycin and then treated with MP showed increased Sirius red staining and hydroxyproline levels at day 21 (Figure 41 b – d). The Sirius red staining and hydroxyproline levels from bleomycin treated and then 2AP, MP, or AMPCA treated mice was significantly less than the bleomycin-treated control mice (Figure 41 c – d and Figure 42). The bleomycin-treated and then 2AP or MP or AMPCA

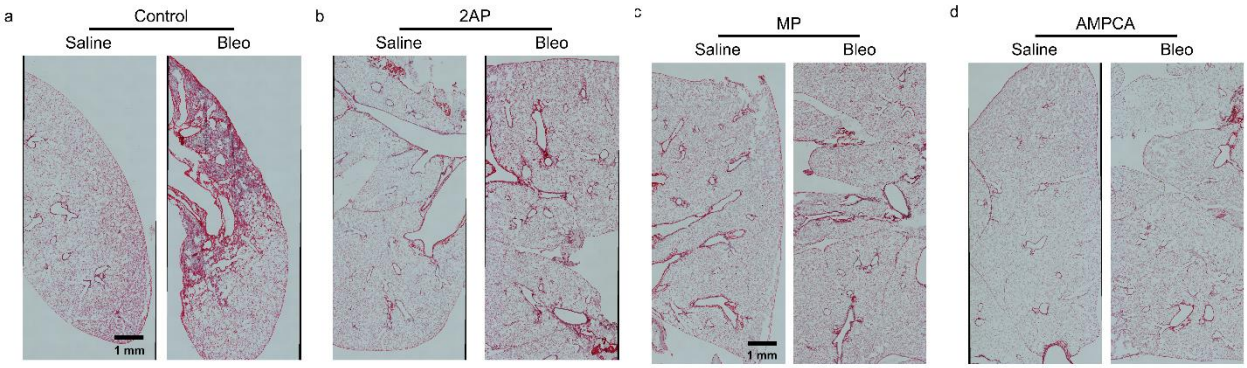

Figure 42. Picrosirius red staining of lung cryosections.
Representative mosaic images of mouse lung cryosections stained with Sirius red. Images are representative of 3 mice aspirated with saline or bleomycin and injected with (**a**) PBS as control, (**b**) 2-acetyl pyridine (2AP), (**c**) Methyl picolinate (MP), or (**d**) 4-amino-1-methyl-2-piperidine carboxylic acid (AMPCA).

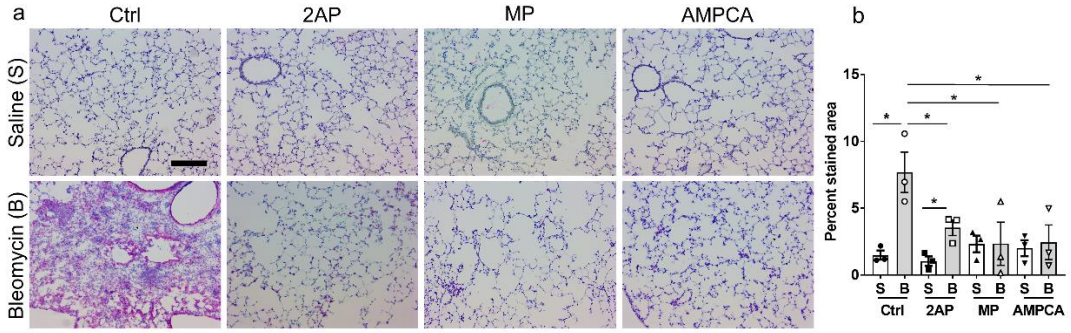

Figure 43. 2AP, MP, or AMPCA injections starting at day 10 after bleomycin reduces TGF-β1 staining.
(a) Sections of lung tissue from mice treated with saline or bleomycin, and then injected daily with control or 2AP or MP or AMPCA starting at day 10 after bleomycin, and then euthanized at day 21, were stained with antibodies against TGF-β1. All images are representative of 3 mice per group. Pink is staining, blue is counterstain. Bar is 200 μm.
(b) Quantification of staining analyzed by selecting 3 random fields of view of the sizes shown in (A) for each mouse, and the average percent area of the field of view showing staining for each mouse was measured. Values are mean ± SEM, n = 3. * $p < 0.05$ (t-test).

treatment showed reduced staining for active TGF-β1 in the lung sections compared to bleomycin-treated control mice (Figures 43 a – b). These results suggest that NEU3 inhibitors reduce bleomycin-induced fibrosis and TGF-β1 upregulation in mouse lungs.

4.5. Discussion

In this report, we observed that the human sialidase NEU3 desialylates human LAP and causes release of active TGF-β1. This is in agreement with the observation that LAP desialylation by viral and bacterial sialidases [93, 210] causes a conformational modification of the LAP which results in disruption of the interaction between LAP and active TGF-β1, releasing active TGF-β1 [211]. Compared to the more conventional mechanism of a cell sensing a signal, and activating a gene expression pathway to make and secrete a responding signal, the desialylation of LAP and release of active TGF-β1 is a much more rapid response. This then suggests that fibrosis is associated with a mechanism that originally evolved to rapidly respond to an insult such as a sialidase-expressing pathogen, with the extracellular NEU3 mimicking and thus amplifying the pathogen signal.

NEU1 may also be involved in potentiating pulmonary fibrosis [37], but this sialidase did not significantly desialylate LAP, suggesting that it may act by other mechanisms to promote fibrosis. NEU4 did desialylate LAP, but since this sialidase is present in lysosomes [157] or mitochondria and endoplasmic reticulum [246, 247], it either does not normally desialylate LAP, or NEU4 from necrotic or otherwise lysed cells may normally desialylate LAP.

We used a predicted reaction intermediate from the NEU3 reaction mechanism [239, 241] to test the idea that picolinic acid-like compounds containing a cationic

nitrogen replacing the putative positively-charged oxygen of the reaction intermediate could act as NEU3 inhibitors. In both the TGF-β1 release from LAP and the IL-6 production by PBMC assays, we observed significantly improved inhibition potency of AMPCA compared to DANA or oseltamivir (Table 1). Since some tumors have upregulated NEU3 [55-57, 248], and since mice lacking Neu3 are resistant to colitis-associated colon tumor formation [178], AMPCA or similar compounds may useful to treat NEU3-associated tumors.

NEU1 and NEU2 do not significantly desialylate LAP, and thus this assay was incompatible for determining inhibition potencies of our compounds against NEU1 and NEU2. The extracellular pH of lesions in lung fibrosis ranges from 6.45 to 6.95 [158]. Our repeated efforts to assay NEU1, NEU2, and NEU4 in this pH range with the substrate 4MU-NANA were unsuccessful. Thus, it is unclear if our compounds inhibit sialidases other than NEU3.

As with AMPCA, DANA and Tamiflu attenuated bleomycin-induced protein upregulation in the BAL at day 21 [160]. However, 2AP or MP did not significantly attenuate bleomycin-induced protein upregulation in BAL at day 21. These disparate results may be due to dose effects, or due to effects that DANA, Tamiflu, 2AP, MP, and AMPCA have on targets other than NEU3.

We previously observed that NEU3 is upregulated in the mouse bleomycin model, and that inhibition of sialidases with DANA or oseltamivir, or loss of NEU3, attenuate bleomycin induced pulmonary fibrosis in mice [160, 180]. The human and mouse NEU3 inhibitors 2AP, MP, and AMPCA all inhibited pulmonary inflammation, levels of active TGF-β1 in the lungs, and pulmonary fibrosis in the mouse bleomycin model. The Uniprot sequences P01137 for human L-TGF-β1 and P04202 for mouse L-TGF-β1 show 90% amino acid sequence similarity and conserved glycosylation sites [249-252]. A reasonable explanation for the ability of NEU3 inhibitors to decrease bleomycin-induced increased levels of active TGF-β1 is that mouse NEU3 also desialylates mouse LAP to release mouse TGF-β1. Together, these results support the hypothesis that a positive feedback loop where NEU3 desialylates LAP to release active TGF-β1, and the active TGF-β1 causes lung epithelial cells to increase translation of *NEU3* mRNA and decrease degradation of NEU3 protein [231], contributes to pulmonary fibrosis, and suggest that NEU3 inhibitors are potential therapeutics for pulmonary fibrosis.

5. CONCLUSIONS AND FUTURE DIRECTIONS

5.1. Conclusions

Overall, my dissertation has focused on understanding the contributions of sialidases to the pathophysiology of IPF and designing potential therapeutic interventions to halt IPF progression in patients. Over the years, a great amount of research has been conducted to understand the pathophysiology of IPF with the objectives of developing potential therapeutics to inhibit IPF progression. However, these studies have failed to determine a single protein or factor that causes the progression of IPF. Currently, there are only two FDA approved therapeutics which slow down, but not inhibit the progression of IPF.

Previous data from our lab had indicated that a serum protein called serum amyloid P, (SAP), attenuated fibrosis-associated cell differentiation and could be used as a potential therapeutic to inhibit IPF progression [15, 111, 253]. When SAP is sialylated, it can attenuate fibrosis-associated cell differentiation, but when SAP is desialylated, it loses the ability to inhibit the fibrosis-associated cell differentiation [17]. This desialylation is carried out by sialidases. There are 4 different types of sialidases present in mammals, NEU1 – 4 [52].

We first sought to identify which sialidases among NEU1 – 4 are responsible for the progression of IPF. To this end, I report that there is upregulation of at least two

sialidases, NEU2 and NEU3, in both human lung fibrotic lesions and in a bleomycin-induced pulmonary fibrosis mouse model. In support of the previously reported effects of desialylated SAP [17], I show that treatment with recombinant human NEU2 or NEU3 counteracts SAP's ability to inhibit of fibrosis-associated cell differentiation. In addition, sialidase NEU3 was upregulated in the bronchoalveolar lavage (BAL) lung fluid of a fibrotic mouse lung. In a cell-based in-vitro study, human PBMC's incubated with recombinant human NEU3 upregulated the levels of active TGF-β1, which is one of the many reported factors promoting IPF development [84, 88]. Conversely, different lung cell types incubated with active TGF-β1 showed upregulated sialidases expression, and this upregulation was primarily made up of NEU3. Thus, in these studies, I found that sialidase NEU3 is upregulated in the fibrotic lesions of the lung, and that NEU3 potentiates the upregulation of active TGF-β1 levels.

Many studies strongly imply that active TGF-β1 plays an important role in the development of IPF [84, 88, 91]. The sequestration protein LAP keeps TGF-β1 in its inactive form [89]. Both LAP and TGF-β1 exists as a complex of dimers called latent-TGF-β1 [86, 90]. In this complex, LAP exists as a glycoconjugate which when desialylated, releases the active TGF-β1 [22, 92, 93, 96, 212]. Although a considerable amount is known about the release of TGF-β1 from its sequestering protein LAP [84, 91, 221, 254, 255], relatively little is known about the release of TGF-β1 from its inactive latent form at the fibrotic lesion site within the lungs. In this dissertation, I report a mechanism which supports NEU3-induced activation of TGF-β1 from its latent inactive

form in lung fibrosis. I report that recombinant human NEU–3 acts on recombinant human latent-TGF-β1 and desialylates LAP, which leads to the release and eventually, the upregulation of active TGF-β1. This suggests that upregulated levels of NEU3 in fibrotic lesions plays an important role in activating TGF-β1. All of these results suggest there is a positive feedback loop, where high levels of sialidase NEU3 increase active TGF-β1 levels, and upregulated active TGF-β1 increases sialidases in different lung cell types and primarily at the active site of a fibrotic lesion.

Subsequently, we sought to validate this hypothesis in mouse models. We wanted to see if we could prevent the progression of pulmonary fibrosis when NEU3 is not present. To this end, we used NEU3 knockout mice [178] to validate the role of NEU3 in the pulmonary fibrosis positive feedback loop. Compared to wild-type mice, mice lacking NEU3 have significantly less bleomycin-induced pulmonary fibrosis, and attenuated levels of upregulated TGF-β1 in the lungs. In addition, mice lacking NEU3 have reduced protein leakage, cell infiltration, and IL-6 levels in the BAL lung fluid, which are recognized as some of the hallmark features of bleomycin-induced pulmonary fibrosis in a mouse model. These results provide genetic evidence that NEU3 plays a role in pulmonary fibrosis progression in mice. Taken together, these results suggest that inhibiting sialidases could be useful strategy to break the positive feedback loop and attenuate pulmonary fibrosis progression.

Burmeister et al. and Kim et al. showed two small molecules, DANA and oseltamivir phosphate (Tamiflu) can be used as sialidase inhibitors [155, 238, 239, 256, 257]. In addition, I show that both DANA and Tamiflu strongly attenuate sialidase-induced upregulation of fibrosis-associated signals like TGF-β1 and IL-6 in *in-vitro* cell-based studies. In the bleomycin-induced pulmonary fibrosis mouse model, daily intraperitoneal injections of either DANA or oseltamivir at 10 mg/kg, starting from day 10 after bleomycin assault, strongly attenuated pulmonary fibrosis at day 21. However, DANA and oseltamivir (Tamiflu) only work well on viral and mouse sialidases [159]. Both DANA and oseltamivir (Tamiflu) work poorly on human sialidases [155, 159, 238]. Hence, we designed a new class of small molecule NEU3 inhibitors based on DANA as the parent molecule [239-241]. Some of the designed inhibitors have nanomolar – picomolar potency for inhibition of recombinant human NEU3-induced release of active TGF-β1 from the recombinant human latent TGF-β1. Three of these small molecule inhibitors, 2-acetyl pyridine (2AP), methyl picolinate (MP), and 4-amino-1-methyl-2-piepridine carboxylic acid (AMPCA), were given as daily 0.1 mg/kg or 1 mg/kg injections starting on day 10 and strongly attenuated most of the pulmonary fibrosis-associated characteristics on day 21 in the bleomycin-induced fibrosis mouse model. Together, these results suggest that sialidase NEU3 potentiates fibrosis, and that NEU3 could be a useful target to treatment fibrosis.

Thus, I can summarize my dissertation as containing major contributions to the identification of an uncontrolled positive feedback loop involving NEU3 – pulmonary

fibrosis – NEU3 in IPF progression, the elucidation of a possible mechanism for NEU3 induced activation of TGF-β1 in pulmonary fibrosis, the identification of existing sialidase inhibitors for off-label uses as a stand-alone therapy against pulmonary fibrosis, and finally, the invention and validation of new class of inhibitors against sialidase NEU3 as potential therapeutics for pulmonary fibrosis, which can also be studied as therapeutics for other NEU3-induced diseases.

5.2. Future directions

5.2.1. Structural studies of the NEU3 with novel inhibitors

One possible future direction for this project is the study of the crystal structure of NEU3 complexed with some of our proposed novel inhibitors. There is an urgent need to have a crystal structure of NEU3, which can help us understand any structural differences between the different isoforms of mammalian sialidases. Such studies can help us to better understand the substrate specificities and rationale of the different substrate recognition by NEU3. Also, such studies can provide useful insights into efficient structure-based design for specific inhibitors for the different mammalian sialidases.

5.2.2. Study the inhibition potency of our sialidase inhibitors on other sialidase isoforms

An immediate continuation for this project is to study the inhibition potency of our novel inhibitors on sialidases other than NEU3. Our repeated efforts to assay NEU1,

NEU2, or NEU4 in a physiological pH range of 6.45 to 7.0 with a commonly used fluorogenic sialidase substrate, 4MU-NANA, were inconclusive. One possible explanation could be that the reported optimal pH for NEU1, NEU2, or NEU4 assays is from pH 4.4 to 6.0 [52]. A cell culture-based assay to study sialidase activity or sialidase inhibition would be more useful. One such sialidase activity through a cellular response has been reported with Jurkat T-cells lines, which when incubated with NEU1, upregulated interleukin-4 (IL-4) levels [34]. This property of Jurkat T-cells acting in response to NEU1 can be utilized to study the inhibition efficiency and specificity of our sialidase inhibitors against NEU1. A carefully designed dosing study of the inhibitors can help avoid initiating a NEU1-deficient pathological condition called sialidosis. A few studies report NEU1 upregulation in pulmonary fibrosis and other inflammatory diseases [34, 53, 123, 126]. Thus, detailed and thorough studies on the inhibition potencies of our new class of sialidase inhibitors on sialidases other than NEU3 can help develop potential therapeutics for diseases caused by the upregulation of a specific sialidase.

5.2.3. Development of potential therapeutics from the proposed sialidase NEU3 inhibitors

The work of my dissertation has guided us to single out one sialidase, NEU3, which when inhibited has a significant effect in attenuating pulmonary fibrosis in mouse model studies. A future direction for this project is to promote our NEU3 inhibitors as anti-fibrotics, either as a stand-alone therapy or in combination with other therapeutics.

Our studies show that the daily administration of sialidase inhibitors like DANA, Tamiflu, 2AP, MP, or AMPCA, showed no discernable effects on the normal mouse physiological conditions in the animal model studies. This suggests that the aforementioned inhibitors can be promoted for clinical trials and we should continue efforts to establish them as potential therapeutics against pulmonary fibrosis. Many other studies report that upregulated NEU3 helps cancer cells to evade apoptosis and thus, NEU3 potentiates their survival [52, 55-57, 248]. An exciting new future direction would be a study of NEU3 inhibitors and their effects on cancer cell apoptosis to determine if NEU3 inhibitors can contribute to the development of therapeutics for NEU3-induced cancers.

The growing evidence of sialidase/ neuraminidase involvement in human diseases emphasizes the need of further studies to determine the overall activity of sialidases, and the potential usefulness of sialidase inhibitors, in human diseases.

REFERENCES

1. Duffield, J.S., et al., *Host responses in tissue repair and fibrosis.* Annu Rev Pathol, 2013. **8**: p. 241-76.

2. Wynn, T.A. and T.R. Ramalingam, *Mechanisms of fibrosis: therapeutic translation for fibrotic disease.* Nat Med, 2012. **18**(7): p. 1028-40.

3. Wynn, T.A., *Common and unique mechanisms regulate fibrosis in various fibroproliferative diseases.* The Journal of Clinical Investigation. **117**(3): p. 524-529.

4. Borthwick, L.A., T.A. Wynn, and A.J. Fisher, *Cytokine mediated tissue fibrosis.* Biochim Biophys Acta, 2013. **1832**(7): p. 1049-60.

5. Wynn, T.A., *Fibrotic disease and the T(H)1/T(H)2 paradigm.* Nat Rev Immunol, 2004. **4**(8): p. 583-94.

6. Zisman, D.A., et al., *Pulmonary fibrosis.* Methods in molecular medicine, 2005. **117**: p. 3-44.

7. Hubbard, R., et al., *Occupational exposure to metal or wood dust and aetiology of cryptogenic fibrosing alveolitis.* Lancet, 1996. **347**(8997): p. 284-9.

8. Baumgartner, K.B., et al., *Occupational and environmental risk factors for idiopathic pulmonary fibrosis: a multicenter case-control study. Collaborating Centers.* Am J Epidemiol, 2000. **152**(4): p. 307-15.

9. Thannickal, V.J., et al., *Fibrosis: ultimate and proximate causes.* The Journal of Clinical Investigation, 2014. **124**(11): p. 4673-4677.

10. Martinez, F.J., et al., *Idiopathic pulmonary fibrosis.* Nature Reviews Disease Primers, 2017. **3**: p. 17074.

11. Raghu, G., et al., *Diagnosis of Idiopathic Pulmonary Fibrosis. An Official ATS/ERS/JRS/ALAT Clinical Practice Guideline.* Am J Respir Crit Care Med, 2018. **198**(5): p. e44-e68.

12. Raghu, G., et al., *An official ATS/ERS/JRS/ALAT statement: idiopathic pulmonary fibrosis: evidence-based guidelines for diagnosis and management.* Am J Respir Crit Care Med, 2011. **183**(6): p. 788-824.

13. Raghu, G. and M. Selman, *Nintedanib and pirfenidone. New antifibrotic treatments indicated for idiopathic pulmonary fibrosis offer hopes and raises questions.* Am J Respir Crit Care Med, 2015. **191**(3): p. 252-4.

14. Pilling, D., et al., *Inhibition of fibrocyte differentiation by serum amyloid P.* J Immunol, 2003. **171**(10): p. 5537-46.

15. Pilling, D., et al., *Reduction of bleomycin-induced pulmonary fibrosis by serum amyloid P.* J Immunol, 2007. **179**(6): p. 4035-44.

16. Gomer, R.H., et al., *A serum amyloid P-binding hydrogel speeds healing of partial thickness wounds in pigs.* Wound Repair Regen, 2009. **17**(3): p. 397-404.

17. Cox, N., Pilling, D., Gomer, R. H., *DC-SIGN activation mediates the differential effects of SAP and CRP on the innate immune system and inhibits fibrosis in mice* Proceedings of the National Academy of Sciences, 2015. **112**(27): p. 8385-90.

18. Pshezhetsky, A.V. and L.I. Ashmarina, *Desialylation of surface receptors as a new dimension in cell signaling.* Biochemistry (Mosc), 2013. **78**(7): p. 736-45.

19. Miyagi, T., et al., *Sialidase significance for cancer progression.* Glycoconj J, 2012. **29**(8-9): p. 567-77.

20. Razonable, R.R., *Antiviral drugs for viruses other than human immunodeficiency virus.* Mayo Clin Proc, 2011. **86**(10): p. 1009-26.

21. Soong, G., et al., *Bacterial neuraminidase facilitates mucosal infection by participating in biofilm production.* J Clin Invest, 2006. **116**(8): p. 2297-2305.

22. Gratz, N., et al., *Pneumococcal neuraminidase activates TGF-β signalling.* Microbiology, 2017. **163**(8): p. 1198-1207.

23. Bonten, E., et al., *Characterization of human lysosomal neuraminidase defines the molecular basis of the metabolic storage disorder sialidosis.* Genes Dev, 1996. **10**(24): p. 3156-69.

24. Pshezhetsky, A.V., et al., *Cloning, expression and chromosomal mapping of human lysosomal sialidase and characterization of mutations in sialidosis.* Nat Genet, 1997. **15**(3): p. 316-20.

25. Lillehoj, E.P., et al., *NEU1 sialidase expressed in human airway epithelia regulates epidermal growth factor receptor (EGFR) and MUC1 protein signaling.* J Biol Chem, 2012. **287**(11): p. 8214-31.

26. D'Avila, F., et al., *Identification of lysosomal sialidase NEU1 and plasma membrane sialidase NEU3 in human erythrocytes.* Journal of Cellular Biochemistry, 2013. **114**(1): p. 204-211.

27. Monti, E., et al., *Sialidases in Vertebrates: A Family Of Enzymes Tailored For Several Cell Functions*, in *Adv Carbohydr Chem Biochem*, H. Derek, Editor. 2010, Academic Press. p. 403-479.

28. Smutova, V., et al., *Structural Basis for Substrate Specificity of Mammalian Neuraminidases.* PLOS ONE, 2014. **9**(9).

29. Zanchetti, G., et al., *Sialidase NEU3 is a peripheral membrane protein localized on the cell surface and in endosomal structures.* Biochem J, 2007. **408**(2): p. 211-9.

30. Liang, F., et al., *Monocyte differentiation up-regulates the expression of the lysosomal sialidase, Neu1, and triggers its targeting to the plasma membrane via major histocompatibility complex class II-positive compartments.* J Biol Chem, 2006. **281**(37): p. 27526-38.

31. Amith, S.R., et al., *Dependence of pathogen molecule-induced toll-like receptor activation and cell function on Neu1 sialidase.* Glycoconj J, 2009. **26**(9): p. 1197-212.

32. Amith, S.R., et al., *Neu1 desialylation of sialyl alpha-2,3-linked beta-galactosyl residues of TOLL-like receptor 4 is essential for receptor activation and cellular signaling.* Cell Signal, 2010. **22**(2): p. 314-24.

33. Stamatos, N.M., et al., *LPS-induced cytokine production in human dendritic cells is regulated by sialidase activity.* J Leukoc Biol, 2010. **88**(6): p. 1227-39.

34. Wang, P., et al., *Induction of lysosomal and plasma membrane-bound sialidases in human T-cells via T-cell receptor.* Biochem J, 2004. **380**(Pt 2): p. 425-33.

35. Sakarya, S., et al., *Mobilization of neutrophil sialidase activity desialylates the pulmonary vascular endothelial surface and increases resting neutrophil adhesion to and migration across the endothelium.* Glycobiology, 2004. **14**(6): p. 481-94.

36. Feng, C., et al., *Neuraminidase reprograms lung tissue and potentiates lipopolysaccharide-induced acute lung injury in mice.* J Immunol, 2013. **191**(9): p. 4828-37.

37. Luzina, I.G., et al., *Elevated expression of NEU1 sialidase in idiopathic pulmonary fibrosis provokes pulmonary collagen deposition, lymphocytosis, and fibrosis.* Am J Physiol Lung Cell Mol Physiol, 2016. **310**(10): p. L940-54.

38. Lambré, C.R., et al., *Sialidase activity and antibodies to sialidase-treated autologous erythrocytes in bronchoalveolar lavages from patients with idiopathic pulmonary fibrosis or sarcoidosis.* Clin Exp Immunol, 1988. **73**(2): p. 230-5.

39. Varki, A., et al., *Symbol Nomenclature for Graphical Representations of Glycans.* Glycobiology, 2015. **25**(12): p. 1323-4.

40. Spiro, R.G., *Glycoproteins.* Adv Protein Chem, 1973. **27**: p. 349-467.

41. Varki, A., et al., in *Essentials of Glycobiology*. 2009, Cold Spring Harbor Laboratory Press, Copyright © 2009, The Consortium of Glycobiology Editors, La Jolla, California.: Cold Spring Harbor (NY).

42. Schwab, I. and F. Nimmerjahn, *Intravenous immunoglobulin therapy: how does IgG modulate the immune system?* Nat Rev Immunol, 2013. **13**(3): p. 176-89.

43. Freire-de-Lima, L., et al., *Sialic acid: a sweet swing between mammalian host and Trypanosoma cruzi.* Front Immunol, 2012. **3**: p. 356.

44. Varki, A. and P. Gagneux, *Multifarious roles of sialic acids in immunity.* Ann N Y Acad Sci, 2012. **1253**: p. 16-36.

45. Varki, N.M. and A. Varki, *Diversity in cell surface sialic acid presentations: implications for biology and disease.* Laboratory Investigation, 2007. **87**(9): p. 851-857.

46. Varki, A., *Sialic acids in human health and disease.* Trends in molecular medicine, 2008. **14**(8): p. 351-360.

47. Cox, N., D. Pilling, and R.H. Gomer, *DC-SIGN activation mediates the differential effects of SAP and CRP on the innate immune system and inhibits fibrosis in mice.* Proc Natl Acad Sci U S A, 2015. **112**(27): p. 8385-90.

48. Lewis, A.L. and W.G. Lewis, *Host sialoglycans and bacterial sialidases: a mucosal perspective.* Cellular Microbiology, 2012. **14**(8): p. 1174-1182.

49. Fanzani, A., et al., *Implications for the mammalian sialidases in the physiopathology of skeletal muscle.* Skelet Muscle, 2012. **2**(1): p. 23.

50. Pshezhetsky, A.V. and M. Ashmarina, *Keeping it trim: roles of neuraminidases in CNS function.* Glycoconjugate Journal, 2018. **35**(4): p. 375-386.

51. Monti, E., et al., *Sialidases in vertebrates: a family of enzymes tailored for several cell functions.* Adv Carbohydr Chem Biochem, 2010. **64**: p. 403-79.

52. Miyagi, T. and K. Yamaguchi, *Mammalian sialidases: Physiological and pathological roles in cellular functions.* Glycobiology, 2012. **22**(7): p. 880-896.

53. Katoh, S., et al., *A crucial role of sialidase Neu1 in hyaluronan receptor function of CD44 in T helper type 2-mediated airway inflammation of murine acute asthmatic model.* Clin Exp Immunol, 2010. **161**(2): p. 233-41.

54. Sieve, I., et al., *A positive feedback loop between IL-1beta, LPS and NEU1 may promote atherosclerosis by enhancing a pro-inflammatory state in monocytes and macrophages.* Vascul Pharmacol, 2018. **103-105**: p. 16-28.

55. Kakugawa, Y., et al., *Up-regulation of plasma membrane-associated ganglioside sialidase (Neu3) in human colon cancer and its involvement in apoptosis suppression.* Proceedings of the National Academy of Sciences, 2002. **99**(16): p. 10718-10723.

56. Ueno, S., et al., *Plasma membrane-associated sialidase is up-regulated in renal cell carcinoma and promotes interleukin-6-induced apoptosis suppression and cell motility.* J Biol Chem, 2006. **281**(12): p. 7756-64.

57. Nomura, H., et al., *Expression of NEU3 (plasma membrane-associated sialidase) in clear cell adenocarcinoma of the ovary: its relationship with T factor of pTNM classification.* Oncol Res, 2006. **16**(6): p. 289-97.

58. Kawamura, S., et al., *Plasma membrane-associated sialidase (NEU3) regulates progression of prostate cancer to androgen-independent growth through modulation of androgen receptor signaling.* Cell Death And Differentiation, 2011. **19**: p. 170.

59. Knudsen, L. and M. Ochs, *The micromechanics of lung alveoli: structure and function of surfactant and tissue components.* Histochem Cell Biol, 2018. **150**(6): p. 661-676.

60. Varon, J., P.E. Marik, and Z.D. Bisbal, *CHAPTER 1 - Restrictive Diseases*, in *Mechanical Ventilation*, P.J. Papadakos, B. Lachmann, and L. Visser-Isles, Editors. 2008, W.B. Saunders: Philadelphia. p. 3-10.

61. Kendall, R.T. and C.A. Feghali-Bostwick, *Fibroblasts in fibrosis: novel roles and mediators.* Front Pharmacol, 2014. **5**(123).

62. Allard, B., A. Panariti, and J.G. Martin, *Alveolar Macrophages in the Resolution of Inflammation, Tissue Repair, and Tolerance to Infection.* Frontiers in Immunology, 2018. **9**(1777).

63. Autissier, P., et al., *Evaluation of a 12-color flow cytometry panel to study lymphocyte, monocyte, and dendritic cell subsets in humans.* Cytometry A, 2010. **77**(5): p. 410-9.

64. Pilling, D. and R.H. Gomer, *Differentiation of circulating monocytes into fibroblast-like cells.* Methods in molecular biology (Clifton, N.J.), 2012. **904**: p. 191-206.

65. Reilkoff, R.A., R. Bucala, and E.L. Herzog, *Fibrocytes: emerging effector cells in chronic inflammation.* Nat Rev Immunol, 2011. **11**(6): p. 427-35.

66. Chambers, R.C. and P.F. Mercer, *Mechanisms of alveolar epithelial injury, repair, and fibrosis.* Ann Am Thorac Soc, 2015. **12 Suppl 1**(Suppl 1): p. S16-20.

67. Chambers, R.C., *Abnormal wound healing responses in pulmonary fibrosis: focus on coagulation signalling.* European Respiratory Review, 2008. **17**(109): p. 130.

68. Roh, J.S. and D.H. Sohn, *Damage-associated molecular patterns in inflammatory diseases.* Immune Netw, 2018. **18**(4): p. e27.

69. Betensley, A., R. Sharif, and D. Karamichos, *A systematic review of the role of dysfunctional wound healing in the pathogenesis and treatment of idiopathic pulmonary fibrosis.* Journal of clinical medicine, 2016. **6**(1): p. 2.

70. Gonzalez, A.C.d.O., et al., *Wound healing - A literature review.* Anais brasileiros de dermatologia, 2016. **91**(5): p. 614-620.

71. Schultz, G., et al., *Wound healing and TIME; new concepts and scientific applications.* Wound Repair and Regeneration, 2005. **13**(s4): p. S1-S11.

72. Acloque, H., et al., *Epithelial-mesenchymal transitions: the importance of changing cell state in development and disease.* J Clin Invest, 2009. **119**(6): p. 1438-49.

73. Jolly, M.K., et al., *Epithelial-mesenchymal transition, a spectrum of states: Role in lung development, homeostasis, and disease.* Dev Dyn, 2018. **247**(3): p. 346-358.

74. Moore, M.W. and E.L. Herzog, *Regulation and Relevance of Myofibroblast Responses in Idiopathic Pulmonary Fibrosis.* Current pathobiology reports, 2013. **1**(3): p. 199-208.

75. King, T.E., Jr., et al., *Idiopathic pulmonary fibrosis: relationship between histopathologic features and mortality.* Am J Respir Crit Care Med, 2001. **164**(6): p. 1025-32.

76. Herrera, J., C.A. Henke, and P.B. Bitterman, *Extracellular matrix as a driver of progressive fibrosis.* The Journal of Clinical Investigation, 2018. **128**(1): p. 45-53.

77. Booth, A.J., et al., *Acellular normal and fibrotic human lung matrices as a culture system for in vitro investigation.* Am J Respir Crit Care Med, 2012. **186**(9): p. 866-76.

78. Clarke, D.L., et al., *Matrix regulation of idiopathic pulmonary fibrosis: the role of enzymes.* Fibrogenesis & Tissue Repair, 2013. **6**(1): p. 20.

79. Organ, L.A., et al., *Biomarkers of collagen synthesis predict progression in the PROFILE idiopathic pulmonary fibrosis cohort.* Respir Res, 2019. **20**(1): p. 148.

80. Specks, U., et al., *Increased expression of type VI collagen in lung fibrosis.* Am J Respir Crit Care Med, 1995. **151**(6): p. 1956-64.

81. Zhang, K. and S.H. Phan, *Cytokines and pulmonary fibrosis.* Biol Signals, 1996. **5**(4): p. 232-9.

82. Agostini, C. and C. Gurrieri, *Chemokine/Cytokine Cocktail in Idiopathic Pulmonary Fibrosis.* Proceedings of the American Thoracic Society, 2006. **3**(4): p. 357-363.

83. Thannickal, V.J., et al., *Mechanisms of pulmonary fibrosis.* Annu Rev Med, 2004. **55**: p. 395-417.

84. Yue, X., B. Shan, and J.A. Lasky, *TGF-β: Titan of Lung Fibrogenesis.* Current enzyme inhibition, 2010. **6**(2): p. 10.2174/10067.

85. Roberts, A.B. and M.B. Sporn, *Physiological actions and clinical applications of transforming growth factor-beta (TGF-beta).* Growth Factors, 1993. **8**(1): p. 1-9.

86. Robertson, I.B. and D.B. Rifkin, *Regulation of the Bioavailability of TGF-beta and TGF-beta-Related Proteins.* Cold Spring Harb Perspect Biol, 2016. **8**(6).

87. Wahl, S.M., J. Wen, and N. Moutsopoulos, *TGF-β: a mobile purveyor of immune privilege.* Immunol Rev, 2006. **213**(1): p. 213-227.

88. Sheppard, D., *Transforming growth factor beta: a central modulator of pulmonary and airway inflammation and fibrosis.* Proceedings of the American Thoracic Society, 2006. **3**(5): p. 413-417.

89. Hinck, A.P., T.D. Mueller, and T.A. Springer, *Structural Biology and Evolution of the TGF-beta Family.* Cold Spring Harb Perspect Biol, 2016. **8**(12).

90. Moremen, K.W., M. Tiemeyer, and A.V. Nairn, *Vertebrate protein glycosylation: diversity, synthesis and function.* Nat Rev Mol Cell Biol, 2012. **13**(7): p. 448-62.

91. Travis, M.A. and D. Sheppard, *TGF-beta activation and function in immunity.* Annu Rev Immunol, 2014. **32**: p. 51-82.

92. Schultz-Cherry, S. and V.S. Hinshaw, *Influenza virus neuraminidase activates latent transforming growth factor beta.* J Virol, 1996. **70**(12): p. 8624-9.

93. Carlson, C.M., et al., *Transforming growth factor-beta: activation by neuraminidase and role in highly pathogenic H5N1 influenza pathogenesis.* PLoS Pathog, 2010. **6**(10): p. e1001136.

94. Grillet, F., et al., *Acute pulmonary embolism associated with COVID-19 pneumonia detected by pulmonary ct angiography.* Radiology. **0**(0): p. 201544.

95. Sha, X., et al., *Transforming growth factor beta 1: importance of glycosylation and acidic proteases for processing and secretion.* Mol Endocrinol, 1989. **3**(7): p. 1090-8.

96. Miyazono, K. and C.H. Heldin, *Role for carbohydrate structures in TGF-beta 1 latency.* Nature, 1989. **338**(6211): p. 158-60.

97. Wynn, T.A. and K.M. Vannella, *Macrophages in Tissue Repair, Regeneration, and Fibrosis.* Immunity, 2016. **44**(3): p. 450-462.

98. Salton, F., M.C. Volpe, and M. Confalonieri, *Epithelial–Mesenchymal Transition in the Pathogenesis of Idiopathic Pulmonary Fibrosis.* Medicina (Kaunas, Lithuania), 2019. **55**(4): p. 83.

99. Kasai, H., et al., *TGF-beta1 induces human alveolar epithelial to mesenchymal cell transition (EMT).* Respir Res, 2005. **6**(1): p. 56-56.

100. Sheppard, D., *Transforming Growth Factor β: A central modulator of pulmonary and airway inflammation and fibrosis.* Proc Am Thorac Soc, 2006. **3**(5): p. 413-7.

101. Fernandez, I.E. and O. Eickelberg, *The Impact of TGF-β on Lung Fibrosis.* Proceedings of the American Thoracic Society, 2012. **9**(3): p. 111-116.

102. Datta, A., C.J. Scotton, and R.C. Chambers, *Novel therapeutic approaches for pulmonary fibrosis.* Br J Pharmacol, 2011. **163**(1): p. 141-72.

103. Wolters, P.J., H.R. Collard, and K.D. Jones, *Pathogenesis of Idiopathic Pulmonary Fibrosis.* Annu Rev Pathol, 2014. **9**: p. 157-79.

104. Barnes, P.J., *Immunology of asthma and chronic obstructive pulmonary disease.* Nat Rev Immunol, 2008. **8**(3): p. 183-92.

105. Friedman, S.L., et al., *Therapy for Fibrotic Diseases: Nearing the Starting Line.* Science Translational Medicine, 2013. **5**(167): p. 167sr1.

106. Castaño, A.P., et al., *Serum Amyloid P Inhibits Fibrosis Through FcγR-Dependent Monocyte-Macrophage Regulation in Vivo.* Science Translational Medicine, 2009. **1**(5): p. 5ra13.

107. Murray, L.A., et al., *Serum Amyloid P Therapeutically Attenuates Murine Bleomycin-Induced Pulmonary Fibrosis via Its Effects on Macrophages.* PLOS ONE, 2010. **5**(3): p. e9683.

108. Murray, L.A., et al., *TGF-beta driven lung fibrosis is macrophage dependent and blocked by Serum amyloid P.* Int J Biochem Cell Biol, 2011. **43**(1): p. 154-62.

109. Verna, E.C., et al., *Novel association between serum pentraxin-2 levels and advanced fibrosis in well-characterised patients with non-alcoholic fatty liver disease.* Alimentary Pharmacology & Therapeutics, 2015. **42**(5): p. 582-590.

110. Zhang, Y.M., et al., *Role of serum amyloid P in skin graft survival and wound healing in burned patients receiving skin grafts.* Clin Chim Acta, 2011. **412**: p. 227-229.

111. Pilling, D. and R.H. Gomer, *Persistent Lung Inflammation and Fibrosis in Serum Amyloid P Component (Apcs-/-) Knockout Mice.* PLOS ONE, 2014. **9**(4): p. e93730.

112. Tennent, G.A. and M.B. Pepys, *Glycobiology of the pentraxins.* Biochemical Society Transactions, 1994. **22**(1): p. 74-79.

113. Li, Z.I., et al., *C-reactive protein promotes acute renal inflammation and fibrosis in unilateral ureteral obstructive nephropathy in mice.* Lab Invest, 2011. **91**(6): p. 837-51.

114. Crawford, J.R., D. Pilling, and R.H. Gomer, *FcγRI mediates serum amyloid P inhibition of fibrocyte differentiation.* Journal of Leukocyte Biology, 2012. **92**(4): p. 699-711.

115. Cox, N., D. Pilling, and R.H. Gomer, *Distinct Fcγ receptors mediate the effect of Serum Amyloid P on neutrophil adhesion and fibrocyte differentiation.* J Immunol, 2014. **193**(4): p. 1701-8.

116. Nimmerjahn, F. and J.V. Ravetch, *Anti-inflammatory actions of intravenous immunoglobulin.* Annu Rev Immunol, 2008. **26**: p. 513-33.

117. Anthony, R.M., F. Wermeling, and J.V. Ravetch, *Novel roles for the IgG Fc glycan.* Ann N Y Acad Sci, 2012. **1253**: p. 170-80.

118. Anthony, R.M., et al., *Recapitulation of IVIG anti-inflammatory activity with a recombinant IgG Fc.* Science, 2008. **320**(5874): p. 373-6.

119. Kaneko, Y., F. Nimmerjahn, and J.V. Ravetch, *Anti-inflammatory activity of immunoglobulin G resulting from Fc sialylation.* Science, 2006. **313**(5787): p. 670-3.

120. Abdulkhalek, S. and M.R. Szewczuk, *Neu1 sialidase and matrix metalloproteinase-9 cross-talk regulates nucleic acid-induced endosomal TOLL-like receptor-7 and -9 activation, cellular signaling and pro-inflammatory responses.* Cell Signal, 2013. **25**(11): p. 2093-105.

121. Cross, A.S., et al., *Recruitment of murine neutrophils in vivo through endogenous sialidase activity.* J Biol Chem, 2003. **278**(6): p. 4112-20.

122. Nan, X., I. Carubelli, and N.M. Stamatos, *Sialidase expression in activated human T lymphocytes influences production of IFN-gamma.* J Leukoc Biol, 2007. **81**(1): p. 284-96.

123. Chen, G.Y., et al., *Amelioration of sepsis by inhibiting sialidase-mediated disruption of the CD24-SiglecG interaction.* Nat Biotechnol, 2011. **29**(5): p. 428-35.

124. Chang, Y.C., et al., *Leukocyte inflammatory responses provoked by pneumococcal sialidase.* MBio, 2012. **3**(1).

125. Naraparaju, V.R. and N. Yamamoto, *Roles of beta-galactosidase of B lymphocytes and sialidase of T lymphocytes in inflammation-primed activation of macrophages.* Immunol Lett, 1994. **43**(3): p. 143-8.

126. Chen, X.P., E.Y. Enioutina, and R.A. Daynes, *The control of IL-4 gene expression in activated murine T lymphocytes: a novel role for neu-1 sialidase.* J Immunol, 1997. **158**(7): p. 3070-80.

127. Pilling, D., V. Vakil, and R.H. Gomer, *Improved serum-free culture conditions for the differentiation of human and murine fibrocytes.* J Immunol Methods, 2009. **351**(1-2): p. 62-70.

128. Pilling, D., et al., *Identification of markers that distinguish monocyte-derived fibrocytes from monocytes, macrophages, and fibroblasts.* PLOS ONE, 2009. **4**(10): p. e7475.

129. Shao, D.D., et al., *Pivotal Advance: Th-1 cytokines inhibit, and Th-2 cytokines promote fibrocyte differentiation.* J Leukoc Biol, 2008. **83**(6): p. 1323-33.

130. Pilling, D., et al., *Fibroblasts secrete Slit2 to inhibit fibrocyte differentiation and fibrosis.* Proc Natl Acad Sci U S A, 2014. **111**(51): p. 18291-6.

131. Daubeuf, F. and N. Frossard, *Performing Bronchoalveolar Lavage in the Mouse.* Curr Protoc Mouse Biol, 2012. **2**(2): p. 167-75.

132. Giri, S.N., *Pharmacokinetics, subcellular distribution, and covalent binding of [3H]bleomycin in hamsters after intratracheal administration.* Exp Mol Pathol, 1986. **45**(2): p. 207-20.

133. Svennerholm, L., *Quantitive estimation of sialic acids.* Biochimica et Biophysica Acta, 1957. **24**: p. 604-611.

134. Potier, M., et al., *Fluorometric assay of neuraminidase with a sodium (4-methylumbelliferyl-alpha-D-N-acetylneuraminate) substrate.* Anal Biochem, 1979. **94**(2): p. 287-96.

135. Marathe, B.M., et al., *Determination of Neuraminidase Kinetic Constants Using Whole Influenza Virus Preparations and Correction for Spectroscopic Interference by a Fluorogenic Substrate.* PLOS ONE, 2013. **8**(8).

136. Herlihy, S.E., et al., *Dipeptidyl Peptidase IV Is a Human and Murine Neutrophil Chemorepellent.* The Journal of Immunology, 2013. **190**(12): p. 6468-6477.

137. Klein, E., et al., *Properties of the K562 cell line, derived from a patient with chronic myeloid leukemia.* Int J Cancer, 1976. **18**(4): p. 421-31.

138. Sundstrom, C. and K. Nilsson, *Establishment and characterization of a human histiocytic lymphoma cell line (U-937).* Int J Cancer, 1976. **17**(5): p. 565-77.

139. Tsuchiya, S., et al., *Establishment and characterization of a human acute monocytic leukemia cell line (THP-1).* Int J Cancer, 1980. **26**(2): p. 171-6.

140. Ziegler-Heitbrock, H.W., et al., *Establishment of a human cell line (Mono Mac 6) with characteristics of mature monocytes.* Int J Cancer, 1988. **41**(3): p. 456-61.

141. Hurwitz, R., et al., *Characterization of a leukemic cell line of the pre-B phenotype.* Int J Cancer, 1979. **23**(2): p. 174-80.

142. Xu, X., et al., *The genomic sequence of the Chinese hamster ovary (CHO)-K1 cell line.* Nat Biotechnol, 2011. **29**(8): p. 735-41.

143. Jensen, E.C., *Quantitative Analysis of Histological Staining and Fluorescence Using ImageJ.* The Anatomical Record, 2013. **296**(3): p. 378-381.

144. Schneider, C.A., W.S. Rasband, and K.W. Eliceiri, *NIH Image to ImageJ: 25 years of image analysis.* Nat Methods, 2012. **9**(7): p. 671-5.

145. Li, Y. and X. Chen, *Sialic acid metabolism and sialyltransferases: natural functions and applications.* Appl Microbiol Biotechnol, 2012. **94**(4): p. 887-905.

146. Takashima, S., *Characterization of Mouse Sialyltransferase Genes: Their Evolution and Diversity.* Bioscience, Biotechnology, and Biochemistry, 2008. **72**(5): p. 1155-1167.

147. Harduin-Lepers, A., et al., *The animal sialyltransferases and sialyltransferase-related genes: a phylogenetic approach.* Glycobiology, 2005. **15**(8): p. 805-17.

148. Stamatos, N.M., et al., *Differential expression of endogenous sialidases of human monocytes during cellular differentiation into macrophages.* FEBS J, 2005. **272**(10): p. 2545-56.

149. Lillehoj, E.P., et al., *Human airway epithelia express catalytically active NEU3 sialidase.* Am J Physiol Lung Cell Mol Physiol, 2014. **306**(9): p. L876-86.

150. Moore, B.B. and C.M. Hogaboam, *Murine models of pulmonary fibrosis.* American Journal of Physiology - Lung Cellular and Molecular Physiology, 2008. **294**(2): p. L152-L160.

151. Blackwell, T.S., et al., *Future Directions in Idiopathic Pulmonary Fibrosis Research. An NHLBI Workshop Report.* American Journal of Respiratory and Critical Care Medicine, 2013. **189**(2): p. 214-222.

152. Neurohr, C., S.L. Nishimura, and D. Sheppard, *Activation of Transforming Growth Factor-β by the Integrin αvβ8 Delays Epithelial Wound Closure.* Am J Respir Cell Mol Biol, 2006. **35**(2): p. 252-9.

153. Kim, J.H., et al., *Transforming growth factor beta1 induces epithelial-to-mesenchymal transition of A549 cells.* J Korean Med Sci, 2007. **22**(5): p. 898-904.

154. Kasabova, M., et al., *Regulation of TGF-β1-driven Differentiation of Human Lung Fibroblasts: EMERGING ROLES OF CATHEPSIN B AND CYSTATIN C.* Journal of Biological Chemistry, 2014. **289**(23): p. 16239-16251.

155. Cairo, C.W., *Inhibitors of the human neuraminidase enzymes.* MedChemComm, 2014. **5**(8): p. 1067-1074.

156. Miyagi, T., *Aberrant expression of sialidase and cancer progression.* Proc Jpn Acad Ser B Phys Biol Sci, 2008. **84**(10): p. 407-18.

157. Seyrantepe, V., et al., *Neu4, a novel human lysosomal lumen sialidase, confers normal phenotype to sialidosis and galactosialidosis cells.* J Biol Chem, 2004. **279**(35): p. 37021-9.

158. Jones, K.M., et al., *Measuring Extracellular pH in a Lung Fibrosis Model with acidoCEST MRI.* Mol Imaging Biol, 2015. **17**(2): p. 177-84.

159. Magesh, S., et al., *Design, synthesis, and biological evaluation of human sialidase inhibitors. Part 1: selective inhibitors of lysosomal sialidase (NEU1).* Bioorg Med Chem Lett, 2008. **18**(2): p. 532-7.

160. Karhadkar, T.R., et al., *Sialidase inhibitors attenuate pulmonary fibrosis in a mouse model.* Scientific Reports, 2017. **7**(1): p. 15069.

161. Nance, T., et al., *Transcriptome Analysis Reveals Differential Splicing Events in IPF Lung Tissue.* PLOS ONE, 2014. **9**(3): p. e92111.

162. Chaudhury, A., et al., *TGF-beta-mediated phosphorylation of hnRNP E1 induces EMT via transcript-selective translational induction of Dab2 and ILEI.* Nat Cell Biol, 2010. **12**(3): p. 286-93.

163. Bonten, E.J., I. Annunziata, and A. d'Azzo, *Lysosomal multienzyme complex: pros and cons of working together.* Cell Mol Life Sci, 2014. **71**(11): p. 2017-32.

164. Weiss, N.G., et al., *Examining serum amyloid P component microheterogeneity using capillary isoelectric focusing and MALDI-MS.* PROTEOMICS, 2011. **11**(1): p. 106-113.

165. Pepys, M.B., et al., *Human serum amyloid P component is an invariant constituent of amyloid deposits and has a uniquely homogeneous glycostructure.* Proc.Natl.Acad.Sci.U.S.A, 1994. **91**(12): p. 5602.

166. Kiernan, U.A., et al., *Proteomic characterization of novel serum amyloid P component variants from human plasma and urine.* PROTEOMICS, 2004. **4**(6): p. 1825-9.

167. Korfei, M., et al., *Comparative proteome analysis of lung tissue from patients with idiopathic pulmonary fibrosis (IPF), non-specific interstitial pneumonia (NSIP) and organ donors.* Journal of Proteomics, 2013. **85**: p. 109-128.

168. Verstovsek, S., et al., *Role of neoplastic monocyte-derived fibrocytes in primary myelofibrosis.* J Exp Med, 2016. **213**(9): p. 1723-40.

169. Uhal, B.D., *The role of apoptosis in pulmonary fibrosis.* European Respiratory Review, 2008. **17**(109): p. 138-144.

170. Fielding, C.A., et al., *Interleukin-6 signaling drives fibrosis in unresolved inflammation.* Immunity, 2014. **40**(1): p. 40-50.

171. Diefenderfer, A.J., *Principles of Electronic Instrumentation*. 1972, Philadelphia: WB Saunders.

172. Pilling, D. and R.H. Gomer, *The Development of Serum Amyloid P as a Possible Therapeutic.* Front Immunol, 2018. **9**: p. 2328.

173. Bucala, R., et al., *Circulating fibrocytes define a new leukocyte subpopulation that mediates tissue repair.* Mol Med, 1994. **1**(1): p. 71-81.

174. Bucala, R., *Review Series – Inflammation & FibrosisFibrocytes and fibrosis.* QJM: An International Journal of Medicine, 2012. **105**(6): p. 505-508.

175. Li, S.C., et al., *Degradation of G(M1) and G(M2) by mammalian sialidases.* Biochem J, 2001. **360**(Pt 1): p. 233-7.

176. Wada, T., et al., *Cloning, expression, and chromosomal mapping of a human ganglioside sialidase.* Biochem Biophys Res Commun, 1999. **261**(1): p. 21-7.

177. Kato, K., et al., *Plasma-membrane-associated sialidase (NEU3) differentially regulates integrin-mediated cell proliferation through laminin- and fibronectin-derived signalling.* Biochemical Journal, 2006. **394**(3): p. 647-656.

178. Yamaguchi, K., et al., *Reduced Susceptibility to Colitis-Associated Colon Carcinogenesis in Mice Lacking Plasma Membrane-Associated Sialidase.* PLOS ONE, 2012. **7**(7): p. e41132.

179. Strauss, W.M., *Preparation of Genomic DNA from Mammalian Tissue.* Current Protocols in Molecular Biology, 1998. **42**(1): p. 2.2.1-2.2.3.

180. Karhadkar, T.R., W. Chen, and R.H. Gomer, *Attenuated pulmonary fibrosis in sialidase-3 knockout (Neu3−/−) mice.* American Journal of Physiology-Lung Cellular and Molecular Physiology, 2020. **318**(1): p. L165-L179.

181. Izbicki, G., et al., *Time course of bleomycin-induced lung fibrosis.* Int J Exp Pathol, 2002. **83**(3): p. 111-9.

182. Izbicki, G., et al., *Bleomycin-induced lung fibrosis in IL-4-overexpressing and knockout mice.* American Journal of Physiology-Lung Cellular and Molecular Physiology, 2002. **283**(5): p. L1110-L1116.

183. Arndt, C., et al., *Native polyacrylamide gels.* Methods Mol Biol, 2012. **869**: p. 49-53.

184. Gilhodes, J.-C., et al., *Quantification of Pulmonary Fibrosis in a Bleomycin Mouse Model Using Automated Histological Image Analysis.* PLOS ONE, 2017. **12**(1): p. e0170561-e0170561.

185. Yamauchi, K., et al., *Attenuation of lung inflammation and fibrosis in CD69-deficient mice after intratracheal bleomycin.* Respir Res, 2011. **12**: p. 131.

186. Voltz, J.W., et al., *Male sex hormones exacerbate lung function impairment after bleomycin-induced pulmonary fibrosis.* American journal of respiratory cell and molecular biology, 2008. **39**(1): p. 45-52.

187. Gharaee-Kermani, M., et al., *Gender-based differences in bleomycin-induced pulmonary fibrosis.* The American journal of pathology, 2005. **166**(6): p. 1593-1606.

188. Parker, J.C. and M.I. Townsley, *Evaluation of lung injury in rats and mice.* Am J Physiol Lung Cell Mol Physiol, 2004. **286**(2): p. L231-46.

189. Kulkarni, A.A., et al., *The Triterpenoid CDDO-Me Inhibits Bleomycin-Induced Lung Inflammation and Fibrosis.* PLOS ONE, 2013. **8**(5): p. e63798.

190. Izbicki, G., et al., *Time course of bleomycin-induced lung fibrosis.* Int J Exp Pathol, 2002. **83**(3): p. 111-9.

191. Ji, W.J., et al., *Spironolactone attenuates bleomycin-induced pulmonary injury partially via modulating mononuclear phagocyte phenotype switching in circulating and alveolar compartments.* PLOS ONE, 2013. **8**(11): p. e81090.

192. Sundararaj, K., et al., *Neuraminidase activity mediates IL-6 production by activated lupus-prone mesangial cells.* Am J Physiol Renal Physiol, 2018. **314**(4): p. F630-f642.

193. Miyagi, T., T. Wada, and K. Yamaguchi, *Roles of plasma membrane-associated sialidase NEU3 in human cancers.* Biochimica et Biophysica Acta (BBA) - General Subjects, 2008. **1780**(3): p. 532-537.

194. Taooka, Y., et al., *Effects of Neutrophil Elastase Inhibitor on Bleomycin-Induced Pulmonary Fibrosis in Mice.* American Journal of Respiratory and Critical Care Medicine, 1997. **156**(1): p. 260-265.

195. Monnier, J. and B.A. Zabel, *Anti-asialo GM1 NK cell depleting antibody does not alter the development of bleomycin induced pulmonary fibrosis.* PLOS ONE, 2014. **9**(6): p. e99350.

196. Kim, M.S., et al., *Changes in expression of cytokines in polyhexamethylene guanidine-induced lung fibrosis in mice: Comparison of bleomycin-induced lung fibrosis.* Toxicology, 2018. **393**: p. 185-192.

197. Massaro, G.D., J.P. Mortola, and D. Massaro, *Sexual dimorphism in the architecture of the lung's gas-exchange region.* Proceedings of the National Academy of Sciences, 1995. **92**(4): p. 1105-1107.

198. Moore, B.B., et al., *Animal Models of Fibrotic Lung Disease.* American journal of respiratory cell and molecular biology, 2013. **49**(2): p. 167-179.

199. Adamson, I.Y. and D.H. Bowden, *The pathogenesis of bleomycin-induced pulmonary fibrosis in mice.* Am J Pathol, 1974. **77**(2): p. 185-97.

200. Walters, D.M. and S.R. Kleeberger, *Mouse models of bleomycin-induced pulmonary fibrosis.* Curr Protoc Pharmacol, 2008. **Chapter 5**: p. Unit 5.46.

201. Sullivan, N.J., et al., *Interleukin-6 induces an epithelial-mesenchymal transition phenotype in human breast cancer cells.* Oncogene, 2009. **28**(33): p. 2940-7.

202. Jiang, G., et al., *Interleukin-6 induces epithelial-mesenchymal transition in human intrahepatic biliary epithelial cells.* Mol Med Rep, 2016. **13**(2): p. 1563-9.

203. Borthwick, L.A., *The IL-1 cytokine family and its role in inflammation and fibrosis in the lung.* Semin Immunopathol, 2016. **38**(4): p. 517-34.

204. van de Vlekkert, D., et al., *Excessive exosome release is the pathogenic pathway linking a lysosomal deficiency to generalized fibrosis.* Sci Adv, 2019. **5**(7): p. eaav3270.

205. Frankish, A., et al., *Ensembl 2018.* Nucleic Acids Research, 2017. **46**(D1): p. D754-D761.

206. Manzoni, M., et al., *Molecular cloning and biochemical characterization of sialidases from zebrafish (Danio rerio).* Biochem J, 2007. **408**(3): p. 395-406.

207. Rodriguez-Walker, M. and J.L. Daniotti, *Human Sialidase Neu3 is S-Acylated and Behaves Like an Integral Membrane Protein.* Scientific Reports, 2017. **7**(1): p. 4167.

208. Cross, A.S., et al., *NEU1 and NEU3 sialidase activity expressed in human lung microvascular endothelia: NEU1 restrains endothelial cell migration, whereas NEU3 does not.* J Biol Chem, 2012. **287**(19): p. 15966-80.

209. Reyfman, P.A., et al., *Single-Cell Transcriptomic Analysis of Human Lung Provides Insights into the Pathobiology of Pulmonary Fibrosis.* Am J Respir Crit Care Med, 2018.

210. Gratz, N., et al., *Pneumococcal neuraminidase activates TGF-beta signalling.* Microbiology, 2017.

211. Biernacka, A., M. Dobaczewski, and N.G. Frangogiannis, *TGF-beta signaling in fibrosis.* Growth Factors, 2011. **29**(5): p. 196-202.

212. Miyazono, K., et al., *A role of the latent TGF-beta 1-binding protein in the assembly and secretion of TGF-beta 1.* The EMBO Journal, 1991. **10**(5): p. 1091-1101.

213. Alsaffar, H., et al., *Interleukin-6 promotes a sustained loss of endothelial barrier function via Janus kinase-mediated STAT3 phosphorylation and de novo protein synthesis.* American Journal of Physiology-Cell Physiology, 2018. **314**(5): p. C589-C602.

214. Desai, T.R., et al., *Interleukin-6 causes endothelial barrier dysfunction via the protein kinase C pathway.* J Surg Res, 2002. **104**(2): p. 118-23.

215. Didion, S.P., *Cellular and Oxidative Mechanisms Associated with Interleukin-6 Signaling in the Vasculature.* International journal of molecular sciences, 2017. **18**(12): p. 2563.

216. Pedroza, M., et al., *Interleukin-6 Contributes to Inflammation and Remodeling in a Model of Adenosine Mediated Lung Injury.* PLOS ONE, 2011. **6**(7): p. e22667.

217. Gabay, C., *Interleukin-6 and chronic inflammation.* Arthritis research & therapy, 2006. **8 Suppl 2**(Suppl 2): p. S3-S3.

218. Rincon, M., *Interleukin-6: from an inflammatory marker to a target for inflammatory diseases.* Trends in Immunology, 2012. **33**(11): p. 571-577.

219. Lewandrowski, U., et al., *Elucidation of N-glycosylation sites on human platelet proteins: a glycoproteomic approach.* Mol Cell Proteomics, 2006. **5**(2): p. 226-33.

220. Crawford, S.E., et al., *Thrombospondin-1 is a major activator of TGF-beta1 in vivo.* Cell, 1998. **93**(7): p. 1159-70.

221. Munger, J.S., et al., *The integrin alpha v beta 6 binds and activates latent TGF beta 1: a mechanism for regulating pulmonary inflammation and fibrosis.* Cell, 1999. **96**(3): p. 319-28.

222. Jenkins, G., *The role of proteases in transforming growth factor-beta activation.* Int J Biochem Cell Biol, 2008. **40**(6-7): p. 1068-78.

223. Lyons, R.M., J. Keski-Oja, and H.L. Moses, *Proteolytic activation of latent transforming growth factor-beta from fibroblast-conditioned medium.* J Cell Biol, 1988. **106**(5): p. 1659-65.

224. Jobling, M.F., et al., *Isoform-specific activation of latent transforming growth factor beta (LTGF-beta) by reactive oxygen species.* Radiat Res, 2006. **166**(6): p. 839-48.

225. Pociask, D.A., P.J. Sime, and A.R. Brody, *Asbestos-derived reactive oxygen species activate TGF-beta1.* Lab Invest, 2004. **84**(8): p. 1013-23.

226. Zhou, X., G. Yang, and F. Guan, *Biological Functions and Analytical Strategies of Sialic Acids in Tumor.* Cells, 2020. **9**(2).

227. Anthony, R.M. and J.V. Ravetch, *A novel role for the IgG Fc glycan: the anti-inflammatory activity of sialylated IgG Fcs.* J Clin Immunol, 2010. **30 Suppl 1**: p. S9-14.

228. Mozzi, A., et al., *NEU3 activity enhances EGFR activation without affecting EGFR expression and acts on its sialylation levels.* Glycobiology, 2015. **25**(8): p. 855-68.

229. Kopitz, J., C. Oehler, and M. Cantz, *Desialylation of extracellular GD1a-neoganglioprotein suggests cell surface orientation of the plasma membrane-bound ganglioside sialidase activity in human neuroblastoma cells.* FEBS Lett, 2001. **491**(3): p. 233-6.

230. van de Vlekkert, D., et al., *Excessive exosome release is the pathogenic pathway linking a lysosomal deficiency to generalized fibrosis.* Sci Adv, 2019. **5**(7): p. eaav - 3270.

231. Chen, W., T.M. Lamb, and R.H. Gomer, *TGF-β1 increases sialidase 3 expression in human lung epithelial cells by decreasing its degradation and upregulating its translation.* Experimental Lung Research, 2020. **46**(3-4): p. 75-80.

232. Cutroneo, K.R., et al., *Therapies for bleomycin induced lung fibrosis through regulation of TGF-beta1 induced collagen gene expression.* J Cell Physiol, 2007. **211**(3): p. 585-9.

233. von Itzstein, M., *The war against influenza: discovery and development of sialidase inhibitors.* Nat Rev Drug Discov, 2007. **6**(12): p. 967-74.

234. Moscona, A., *Neuraminidase Inhibitors for Influenza.* New England Journal of Medicine, 2005. **353**(13): p. 1363-1373.

235. Hayden, F.G., et al., *Efficacy and Safety of the Neuraminidase Inhibitor Zanamivir in the Treatment of Influenzavirus Infections.* New England Journal of Medicine, 1997. **337**(13): p. 874-880.

236. Monto, A.S., et al., *Efficacy and Safety of the Neuraminidase Inhibitor Zanamivir in the Treatment of Influenza A and B Virus Infections.* The Journal of Infectious Diseases, 1999. **180**(2): p. 254-261.

237. Mäkelä, M.J., et al., *Clinical efficacy and safety of the orally inhaled neuraminidase inhibitor zanamivir in the treatment of influenza: a randomized, double-blind, placebo-controlled European study.* J Infect, 2000. **40**(1): p. 42-8.

238. Hata, K., et al., *Limited inhibitory effects of oseltamivir and zanamivir on human sialidases.* Antimicrob Agents Chemother, 2008. **52**(10): p. 3484-91.

239. Albohy, A., et al., *Inhibitor selectivity of a new class of oseltamivir analogs against viral neuraminidase over human neuraminidase enzymes.* Bioorg Med Chem, 2011. **19**(9): p. 2817-22.

240. Zou, Y., et al., *Inhibition of human neuraminidase 3 (NEU3) by C9-triazole derivatives of 2,3-didehydro-N-acetyl-neuraminic acid.* Bioorg Med Chem Lett, 2010. **20**(24): p. 7529-33.

241. Albohy, A., et al., *Insight into substrate recognition and catalysis by the human neuraminidase 3 (NEU3) through molecular modeling and site-directed mutagenesis.* Glycobiology, 2010. **20**(9): p. 1127-38.

242. Guo, T., et al., *Selective Inhibitors of Human Neuraminidase 3.* Journal of Medicinal Chemistry, 2018. **61**(5): p. 1990-2008.

243. Magesh, S., et al., *Homology modeling of human sialidase enzymes NEU1, NEU3 and NEU4 based on the crystal structure of NEU2: hints for the design of selective NEU3 inhibitors.* J Mol Graph Model, 2006. **25**(2): p. 196-207.

244. Morrissey, J.H., *Silver stain for proteins in polyacrylamide gels: a modified procedure with enhanced uniform sensitivity.* Anal Biochem, 1981. **117**(2): p. 307-10.

245. Shibuya, N., et al., *The elderberry (Sambucus nigra L.) bark lectin recognizes the Neu5Ac(alpha 2-6)Gal/GalNAc sequence.* J Biol Chem, 1987. **262**(4): p. 1596-601.

246. Yamaguchi, K., et al., *Evidence for mitochondrial localization of a novel human sialidase (NEU4).* Biochem J, 2005. **390**(Pt 1): p. 85-93.

247. Bigi, A., et al., *Human sialidase NEU4 long and short are extrinsic proteins bound to outer mitochondrial membrane and the endoplasmic reticulum, respectively.* Glycobiology, 2010. **20**(2): p. 148-57.

248. Kawamura, S., et al., *Plasma membrane-associated sialidase (NEU3) regulates progression of prostate cancer to androgen-independent growth through modulation of androgen receptor signaling.* Cell Death Differ, 2012. **19**(1): p. 170-9.

249. Areström, I., et al., *Measurement of human latent Transforming Growth Factor-β1 using a latency associated protein-reactive ELISA.* J Immunol Methods, 2012. **379**(1-2): p. 23-9.

250. Pruitt, K.D., T. Tatusova, and D.R. Maglott, *NCBI reference sequences (RefSeq): a curated non-redundant sequence database of genomes, transcripts and proteins.* Nucleic Acids Res, 2007. **35**(Database issue): p. D61-5.

251. Consortium, T.U., *UniProt: a worldwide hub of protein knowledge.* Nucleic Acids Research, 2018. **47**(D1): p. D506-D515.

252. Doğan, T., et al., *UniProt-DAAC: domain architecture alignment and classification, a new method for automatic functional annotation in UniProtKB.* Bioinformatics (Oxford, England), 2016. **32**(15): p. 2264-2271.

253. Pilling, D., et al., *The kinetics of interaction between lymphocytes and magnetic polymer particles.* J Immunol Methods, 1989. **122**: p. 235-241.

254. Henderson, N.C. and D. Sheppard, *Integrin-mediated regulation of TGFβ in fibrosis.* Biochim Biophys Acta, 2013. **1832**(7): p. 891-6.

255. Jullien, P., T.M. Berg, and D.A. Lawrence, *Acidic cellular environments: Activation of latent tgf-β and sensitization of cellular responses to tgf-β and egf.* Int J Cancer, 1989. **43**(5): p. 886-891.

256. Burmeister, W.P., et al., *Influenza B virus neuraminidase can synthesize its own inhibitor.* Structure, 1993. **1**(1): p. 19-26.

257. Kim, C.U., X. Chen, and D.B. Mendel, *Neuraminidase inhibitors as anti-influenza virus agents.* Antivir Chem Chemother, 1999. **10**(4): p. 141-54.